

Statistical inference for radially-stable generalised Pareto distributions and return level-sets in geometric extremes

Ioannis Papastathopoulos ^{*1}, Lambert De Monte ^{†1}, Ryan Campbell ^{‡2}, and Håvard Rue ^{§3}

¹School of Mathematics and Maxwell Institute, University of Edinburgh, Edinburgh, EH9 3FD, Scotland

²Department of Mathematics and Statistics, Lancaster University, Lancaster, LA1 4YF, England

³Statistics Program, King Abdullah University of Science and Technology, Thuwal 23955-6900, Saudi Arabia

Abstract

We use a functional analogue of the quantile function for probability measures admitting a continuous Lebesgue density on \mathbb{R}^d to characterise the class of non-trivial limit distributions of radially recentered and rescaled multivariate exceedances. A new class of multivariate distributions is identified, termed *radially-stable generalised Pareto distributions*, and is shown to admit certain stability properties that permit extrapolation to extremal sets along any direction in cones such as \mathbb{R}^d and \mathbb{R}_+^d . Leveraging the limit Poisson point process likelihood of the point process of radially renormalised exceedances, we develop parsimonious statistical models that exploit theoretical links between structural star-bodies and are amenable to Bayesian inference. Our framework sharpens statistical inference by suitably including additional information from the angular directions of the geometric exceedances and facilitates efficient computations in dimensions $d = 2$ and $d = 3$. Additionally, it naturally leads to the notion of return level-set, which is a canonical quantile set expressed in terms of its average recurrence interval, and a geometric analogue of the uni-dimensional return level. We illustrate our methods with a simulation study showing superior predictive performance of probabilities of rare events, and with two case studies, one associated with river flow extremes, and the other with oceanographic extremes.

Keywords: Bayesian inference, limit set, Poisson process, quantile set, multivariate regular variation, radial function, radially-stable distributions, return level-set, multivariate threshold exceedances, starshaped set

1 Introduction

The multivariate nature of extreme events casts a shadow of potentially devastating consequences upon ecosystems, infrastructures, as well as financial, economic, and insurance sectors. Knowledge of the frequency and magnitude of extreme events is crucial in enhancing planning strategies and adaptation efforts. The statistical properties of univariate extremes are well-established ([Balkema & de Haan 1974](#), [Pickands 1975](#), [Davison & Smith 1990](#)), but statistical inference for multivariate random processes is much more intricate: one must analyse how random processes interact with and influence each other. A common way to describe the extremal dependence structure of a real-valued random vector $\mathbf{X} = (X_1, \dots, X_d)$ is through the coefficient of tail dependence defined by

$$\chi_q(A) = \mathbb{P} \left[\bigcap_{j \in A} \{F_j(X_j) > q\} \right] / (1 - q), \quad q \in (0, 1), \quad A \subseteq \{1, \dots, d\}, |A| > 1, \quad (1)$$

^{*}i.papastathopoulos@ed.ac.uk

[†]l.demonte@ed.ac.uk

[‡]r.campbell3@lancaster.ac.uk

[§]haavard.rue@kaust.ed.sa

where F_j is the cumulative distribution function of X_j . When $\lim_{q \rightarrow 1} \chi_q(A) = 0$, the variables in A are unlikely to grow large together and we say that they exhibit asymptotic independence. Conversely, when $\lim_{q \rightarrow 1} \chi_q(A) > 0$, the variables in A are likely to grow large together and the variables in A exhibit asymptotic dependence. The different dependence structures that can be present within subgroups of the marginal variables of \mathbf{X} can make inference for rare events challenging and extrapolation inaccurate.

Classical approaches to multivariate extreme events often rely on the framework of multivariate regular variation (MRV) (de Haan & Resnick 1977), which posits that the point processes of exceedances of a random vector over a high threshold, when suitably renormalised, converge in distribution to a non-degenerate non-homogenous Poisson point process (de Haan 1984). This provides a framework for understanding the joint behaviour of extreme observations and leads to meaningful limit distributions that can be used for statistical inference of multivariate extremes. A major development in this context is the class of multivariate max-stable (de Haan & Resnick 1977) and multivariate generalised Pareto (Rootzén & Tajvidi 2006) distributions. These distributions emerge as the unique non-trivial limit distributions of renormalised componentwise maxima, and of renormalised exceedances. However, in practical implementations, MRV is applied in a way that does not adequately describe relationships among asymptotically independent random variables (Nolde & Wadsworth 2021), which is the scenario that is of most practical interest. This is due to the type of the renormalisation that is employed: given a random sample of n d -dimensional observations, all components are normalised by the same amount. This leads to considering the dependence structure only in a single direction in \mathbb{R}^d (see Figure 1 and Section 2.1). If the extremal dependence properties between the components of the random vector are strong, that is, if $\chi_q(\{1, \dots, d\}) > 0$ for all sufficiently large q , then MRV provides with a rich description of the extremal dependence structure of asymptotically dependent random variables. If this is not the case, then MRV as a practical assumption for statistical inference of multivariate extremes may be inappropriate.

Another drawback of statistical methods based on MRV is the limited set of directions in the multivariate space in which one can extrapolate the model. In particular, under MRV, the probability of lying in an extremal set is estimated by shifting the extremal set and performing empirical probability estimation on the translated set. When the translated set does not contain observations from the initial dataset, then this leads to an inability to estimate the probability of interest. To correct the joint rate of tail decay in the case of weaker extremal dependence, the notion of HRV was introduced in Ledford & Tawn (1996, 1997), Maulik & Resnick (2004). However, HRV also suffers from the same extrapolation drawbacks as MRV since it does not allow extrapolation along directions where not all variables are simultaneously large. To extrapolate to a wider range of directions, the frameworks of conditional extremes (Heffernan & Tawn 2004) and angular dependence (Wadsworth & Tawn 2013) have been introduced to extrapolate to a wider range of extremal regions with a wider array of dependence structures, but statistical methodology based on these frameworks comes with some drawbacks. Despite its wide applicability and widespread adoption, the conditional extremal inference method of Heffernan & Tawn (2004) is based on composite likelihood methods and on gluing post-fit separate models, making statistical inference and computations unwieldy. While the angular dependence method of Wadsworth & Tawn (2013) permits extrapolation in regions where variables are not simultaneously extreme, it is only useful for joint survival regions. The directions of extrapolation of the above described frameworks in multivariate extreme value theory (MEVT) are shown in Figure 1.

Recently, a characterisation of extremal dependence through the limiting geometry of suitably rescaled sample clouds—or observations from \mathbf{X} —has become of interest. The limit set, with boundary arising as the limiting hull of appropriately scaled sample clouds, provides insight into the extremal dependence structure of \mathbf{X} . The so-called *gauge function*, whose unit level set is in one-to-one correspondence with the boundary of the limit set, has been shown to connect several known coefficients describing extremal dependence of known copulas (Nolde 2014, Nolde & Wadsworth 2021). Wadsworth & Campbell (2022) proposed a new framework for performing statistical inference for multivariate extremes using this geometric approach. Using a radial-angular decomposition, this framework treats the gauge function evaluated at angles as a rate parameter of a left-truncated gamma model for the distribution of radii conditioned

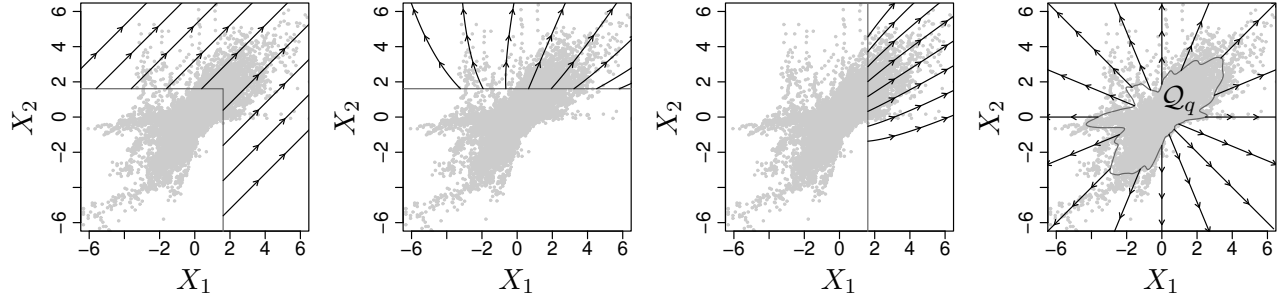


Figure 1: Directions along which MEVT frameworks allow extrapolation to tail regions: (a) MRV, (b) and (c) conditional extremes given X_2 and X_1 are large, respectively, and (d) geometric extremes, with \mathcal{Q}_q illustrating the posterior mean of the quantile set ($q = 0.95$). The support of the distribution of multivariate exceedances is inscribed by the region containing the arrows.

on angles on the unit simplex. Inference for the gauge function and its associated limit set is based on parametric models derived from known copulas in d -dimensions and in standard exponential margins, and a maximum likelihood approach is implemented within the rate parameter of the truncated Gamma distribution. This is the first work that uses the geometric approach to propose a new statistical inference method in estimating extremal probabilities with superior performance relative to state-of-the-art methods in multivariate extremes. Also in exponential margins, but in a bivariate setting, [Simpson & Tawn \(2022\)](#) model the conditional distribution of the excess radii given angles on the simplex via the generalised Pareto (GP) distribution ([Pickands 1975](#)). In this framework, the gauge function is seen as a rate parameter of the GP distribution and is modelled via generalised additive models ([Wood 2017](#)). [Majumder et al. \(2023\)](#) also propose a statistical method to estimate the bivariate gauge function and the shape of its associated limit set using Bézier splines.

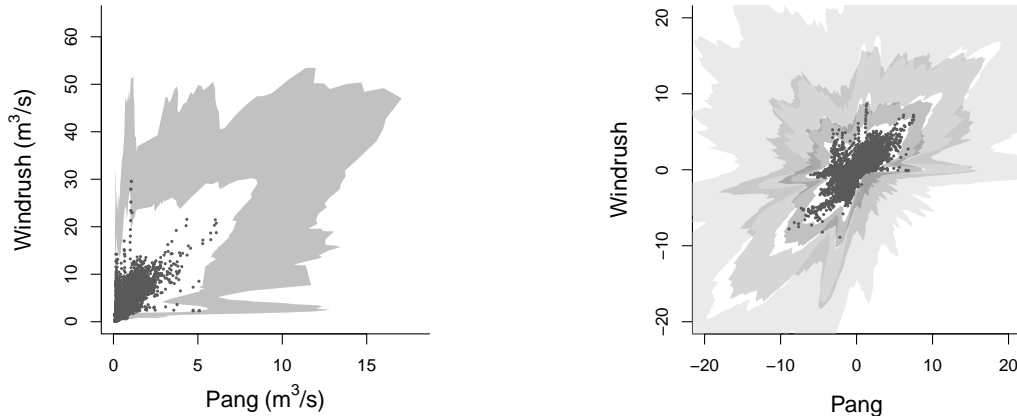


Figure 2: 0.95 prediction intervals for the boundary of river flow return level-sets of the Pang and Windrush tributaries. *Left*: original margins, return period of $T = 10^3$ days. *Right*: standard Laplace margins, return periods from dark to light grey, $T = 10^3$, 10^5 , and $T = 10^9$ days.

In this paper, we develop a framework beyond the cone \mathbb{R}_+^d by exploiting the structure of weak limits found in suitably radially renormalised multivariate exceedances. Multivariate exceedances are samples that lie in the complement of a quantile set, a compact subset of \mathbb{R}^d containing the origin. The boundary of the quantile set can be interpreted as a canonical quantile in \mathbb{R}^d , allowing to bypass complications experienced in multivariate extreme value theory due to the lack of natural ordering in \mathbb{R}^d , see for example ([Barnett 1976](#)). By specifying an appropriate sequence of quantile sets, we show under mild conditions that, not

only can the framework of MRV be suitably extended to the cone $\mathbb{R}^d \setminus \{0\}$, but that similar extensions are also available for light-tailed and bounded multivariate distributions. A key property of our framework is that it is applicable to any $d \geq 1$. In the multivariate setting ($d > 1$), our framework enables the modelling of the entire joint tail, accommodating scenarios where subsets of components are extreme. This approach can capture behaviours across the entire spectrum of multivariate space and reveal hidden dependencies, thereby bridging the gap between theory and practice. Using radially recentred and rescaled exceedances over high quantile sets, we characterise non-trivial limit distributions on $\mathbb{R}^d \setminus \{0\}$, termed *radially-stable distributions*. The radial stability properties of these families of distributions permit extrapolation beyond the range of observed data along any direction (Figure 1, right) and lead to the notion of a canonical *return level-set* in \mathbb{R}^d . The return level-set is a geometric extension of the uni-dimensional (upper-tail) return level (Coles 2001). Specifically, it is a quantile of the multivariate distribution expressed in terms of its average recurrence interval. This gives a clear and interpretable way to communicate the risk associated with extreme multivariate events which in turn, allows decision-makers, policymakers, and the general public to understand the likelihood of experiencing impact from *joint extreme events* within, for example, a specified scale frame. Figure 2 shows predictive intervals of return level-set boundaries associated with different return periods of daily river flow (m^3/s) at the rivers Pang and Windrush, in England, previously analysed by Keef et al. (2013).

Section 2 provides background on univariate extreme value theory and multivariate regular variation, and introduces the main results, which include the weak convergence of radially recentred and rescaled exceedances to a Poisson point process on $\mathbb{R}^d \setminus \{0\}$. Our findings lead to a novel class of limit multivariate distributions that are presented in Section 2.5 and to novel return level-sets presented in Section 2.6. Section 3 details methodology for statistical inference of $d = 2$ and $d = 3$ dimensional extremes using hierarchical Bayesian models with latent Gaussian random effects on Euclidean spheres. Section 3.4 discusses sampling from the joint posterior distribution of the latent parameters and rare event probability estimation. Last, in Section 4 we illustrate the merits of our approach on 2- and 3-dimensional data sets of extreme flow in the rivers Pang and Windrush, both tributaries to the Thames in England, and of extreme sea levels in Newlyn, England.

2 Theory

2.1 Univariate extremes

When focusing on the upper right tail (\mathbf{R}) of a random variable $X \in \mathbb{R}$, prevailing approaches primarily rely on the fundamental assumption of extended regular variation (de Haan 1970). This assumption postulates the existence of sequences of norming scalars, $a_n \in \mathbb{R}_+$, and $b_n \in \mathbb{R}$, $n = 1, 2, \dots$, satisfying

$$n\mathbb{P}[\{X - b_n\}/a_n \in \cdot] \xrightarrow{\mathbf{v}} \Lambda_{\mathbf{R}}(\cdot) \quad \text{in } M_+((-\infty, \infty]), \quad \text{as } n \rightarrow \infty, \quad (2)$$

where

$$\Lambda_{\mathbf{R}}((z, \infty]) := (1 + \xi_{\mathbf{R}} z)_+^{-1/\xi_{\mathbf{R}}}, \quad z \in \mathbb{R},$$

for some $\xi_{\mathbf{R}} \in \mathbb{R}$ and $(x)_+ = \max(x, 0)$. Here, $\xrightarrow{\mathbf{v}}$ is interpreted as vague convergence in the space $M_+((-\infty, \infty])$ of nonnegative Radon measures on Borel subsets of $(-\infty, \infty]$, see also Appendix A.1 for a definition. The significance of this convergence becomes particularly pronounced when examining its interplay with classical limit theorems governing univariate extreme events, as it encompasses two central statistical methods that have been developed to model the univariate extremes. The first method relates to the appropriately renormalised maxima, a concept often harnessed within the statistical methodology based on block maxima. Within this context, the convergence (2) leads to the well-known generalized extreme value (GEV) distribution, which stands as a foundational model for the limiting behaviour of maxima over long time intervals or blocks. The sequences of norming factors and translation constants, which feature in the analysis of block maxima, are effectively absorbed into the limit GEV distribution

as part of the inference process. As a result, the GEV distribution acquires distinct location, scale and shape parameters $\mu_R \in \mathbb{R}$, $\sigma_R > 0$, $\xi_R \in \mathbb{R}$, respectively, and its cumulative distribution function takes the form

$$G_R(x) = \exp \left[- \left\{ 1 + \xi_R \left(\frac{z - \mu_R}{\sigma_R} \right) \right\}_+^{-1/\xi} \right] = \exp \{ -\Lambda_R(z; \theta_R) \},$$

where $\theta_R = (\mu_R, \sigma_R, \xi_R)$. The GEV distribution has max-stability, a cornerstone trait that underpins its utility in modelling extreme events across diverse contexts.

The second method emanating from convergence (2) relates to the distribution of threshold exceedances. This method aligns with the peaks over threshold approach, which focuses on modelling the distribution of extreme values that exceed a predefined high threshold level. In this case, the convergence leads to the generalized Pareto (GP) distribution function given by

$$H_R(y) = 1 - \left\{ 1 + \xi_R \left(\frac{z}{\sigma_R} \right) \right\}_+^{-1/\xi},$$

which offers a robust framework for analyzing extreme events that exceed a prespecified threshold. By facilitating the modelling of these exceedances, the GP provides a statistical method that is more efficient than the block-maxima approach for estimating tail probabilities and assessing risks associated with extreme events. These limit distributions provide insights into the behaviour of extreme values in the upper right tail. When interest is in the lower left tail (**L**) of the distribution of X , the convergence condition is rewritten with X replaced by $-X$, and with a different sequence of norming constants so as to allow flexibility on the shape parameter. Thus, in this case, we typically assume that there exist sequences of norming constants $\alpha_n > 0$ and $\beta_n \in \mathbb{R}$ such that

$$n\mathbb{P}[\{-X - \beta_n\}/\alpha_n > z] \xrightarrow{v} \Lambda_L(\cdot) \quad \text{in } M_+((-\infty, \infty]), \quad (3)$$

where

$$\Lambda_L((z, \infty]) := (1 + \xi_L z)_+^{-1/\xi_L}, \quad z \in \mathbb{R},$$

for some $\xi_L \in \mathbb{R}$. When interest is in both left and right tails, the convergence assumptions (2) and (3) can be unified under a single theme. To describe this unification, we introduce our first assumption below which explicitly uses the directions along which extremes occur.

Assumption 1. *Suppose that $X \in \mathbb{R}$ is an absolutely continuous random variable with probability density function f . Let $S = \{x \in \mathbb{R} : f(x) > 0\}$ and assume that $0 \in S$.*

There exist constants $a_{n,R} > 0$ and $b_{n,R} \in \mathbb{R}$, for $n = 1, 2, \dots$, such that

$$n\mathbb{P}[\{X - b_{n,R}\}/a_{n,R} \in \cdot \mid X > 0] \xrightarrow{v} \Lambda_R(\cdot) \quad \text{in } M_+((-\infty, \infty]), \quad \text{as } n \rightarrow \infty, \quad (4)$$

and constants $a_{n,L} > 0$ and $b_{n,L} \in \mathbb{R}$, for $n = 1, 2, \dots$,

$$n\mathbb{P}[-\{X - b_{n,L}\}/a_{n,L} \in \cdot \mid X \leq 0] \xrightarrow{v} \Lambda_L(\cdot) \quad \text{in } M_+((-\infty, \infty]), \quad \text{as } n \rightarrow \infty. \quad (5)$$

Perhaps not surprisingly, if Assumption 1 holds true, then we can construct sequences of norming functions $r_n^a : \mathbb{S}^0 \rightarrow \mathbb{R}_+$ and $r_n^b : \mathbb{S}^0 \rightarrow \mathbb{R}$, $n = 1, 2, \dots$, that are functions of the direction $X/|X| \in \mathbb{S}^0$, where $\mathbb{S}^0 = \{-1, 1\}$, along which extremes occur, such that

$$n\mathbb{P} \left[\frac{X - r_n^a(X/|X|)}{r_n^b(X/|X|)} \in \cdot \right] \xrightarrow{v} \Lambda(\cdot) \quad \text{in } M_+((-\infty, \infty] \times (-\infty, \infty]), \quad \text{as } n \rightarrow \infty, \quad (6)$$

where

$$\Lambda((z_L, \infty] \times (z_R, \infty]) = (1 - \pi)(1 - \xi_L z_L)_+^{-1/\xi_L} + \pi(1 + \xi_R z_R)_+^{-1/\xi_R}, \quad \pi = \mathbb{P}(X/|X| = 1), \quad \xi_L, \xi_R \in \mathbb{R}. \quad (7)$$

Convergence (6) implies domain of attraction properties for the distribution of univariate extremes. In particular, as $n \rightarrow \infty$, the joint distribution of the appropriately renormalised minima and maxima of a random sample (X_1, \dots, X_n) from X , converges weakly to a non-degenerate distribution. This is described in Proposition 1.

Proposition 1. *Suppose that Assumption 1 holds true. Let $m_n = \min_{i=1, \dots, n}(X_i)$ and $M_n = \max_{i=1, \dots, n}(X_i)$. Then*

$$\mathbb{P}\left(-\frac{m_n - b_{n,L}}{a_{n,L}} \leq z_L, \frac{M_n - b_{n,R}}{a_{n,R}} \leq z_R\right) \xrightarrow{w} G(z_L, z_R),$$

where $G(z_L, z_R) = \exp(-\Lambda((z_L, \infty] \times (z_R, \infty]))$ and Λ is defined by expression (7).

A proof is given in Appendix C.2. It can be seen that the limit distribution in Proposition 1 satisfies a min – max stability property, that is, for any $t > 0$, $G(z_L, z_R)^t$ is, up to location and scale, of the same type as G . This intriguing stability property, evident from the form of Λ in equation (7), might be aptly termed *radial stability*. However, while the term min – max *stable distribution* could be tempting for G , it might not comprehensively convey the unique characteristics of this distribution, especially when extended to the multivariate setting, which is the focus of this paper. In the multivariate context, extremes cannot be solely described by component-wise maxima or minima, but rather involve intricate dependencies among components. This naming convention underscores the distinct behaviour of the limit distribution in capturing extreme events across both left and right tails while respecting the inherent relationships among components. Remarkably, the unifying convergence assumption (6), overlooked in the literature until now, presents a substantial departure from traditional approaches to extreme value modelling.

2.2 Multivariate regular variation

To understand radial stability properties in a d -dimensional setup, we revisit classical multivariate extreme value theory through consideration of multivariate regular variation (MRV), as it is still a key extremal dependence assumption invoked in a wide range of statistical methods including multivariate max-stable and multivariate generalised Pareto distributions. Under the choice of exponential margins, a random vector \mathbf{X} is multivariate regularly varying on the cone $\mathcal{E} = [-\infty, \infty]^d \setminus \{-\infty\}$ if there exists a limit measure ν_{MRV} such that for any relatively compact set $B \subset \mathcal{E}$,

$$r\mathbb{P}[\mathbf{X} - (\log r)\mathbf{1} \in B] \rightarrow \nu_{\text{MRV}}(B), \quad \text{as } r \rightarrow \infty, \quad (8)$$

with $\nu_{\text{MRV}}(\partial B) = 0$. A consequence of convergence (8) is that $\nu_{\text{MRV}}(t\mathbf{1} + B) = \exp(-t)\nu_{\text{MRV}}(B)$. This stability property implies domain of attraction properties for the distribution of \mathbf{X} . For example, after appropriate recentering, the distribution function of the componentwise maxima converges weakly to

$$\mathbb{P}(\mathbf{M}_n - (\log n)\mathbf{1} \leq \mathbf{z}) = \mathbb{P}\{\mathbf{X}_i - (\log n)\mathbf{1} \in [-\infty, \mathbf{z}] : i = 1, \dots, n\} \xrightarrow{w} \exp[-\Lambda_{\text{MRV}}([-\infty, \mathbf{z}])],$$

where $\Lambda_{\text{MRV}}(B) = \nu_{\text{MRV}}(B')$. The measure Λ_{MRV} is in one-to-one correspondence with a Radon measure H_{MRV} on the unit-simplex $\Delta_+^{d-1} = \{\boldsymbol{\omega} \in \mathbb{R}_+^d : \|\boldsymbol{\omega}\|_1 = 1\}$, where $\|\mathbf{x}\|_p = (\sum_{i=1}^d |x_i|^p)^{1/p}$ for $\mathbf{x} = (x_1, \dots, x_d) \in \mathbb{R}^d$, termed the spectral measure, satisfying the mass-moment constraint $H(\Delta_+^{d-1}) = d$ and

$\int_{\Delta_+^{d-1}} w_i H(d\mathbf{w}) = 1$, for $i = 1, \dots, d$. The correspondence is given by

$$\Lambda_{\text{MRV}}(B) = \int_{\Delta_+^{d-1}} \max[\mathbf{w} \exp(-\mathbf{x})] H_{\text{MRV}}(d\mathbf{w}),$$

where vector algebra is interpreted component-wise. Similarly, the vector of renormalised threshold exceedances converges in distribution to a multivariate Pareto distribution, that is,

$$\lim_{r \rightarrow \infty} \mathbb{P}[\mathbf{X} - r\mathbf{1} \in [-\infty, \mathbf{x}] \mid \max \mathbf{X} > r] = \frac{\Lambda_{\text{MRV}}(\mathbf{x} \wedge \mathbf{0}) - \Lambda_{\text{MRV}}(\mathbf{x})}{\Lambda_{\text{MRV}}(\mathbf{0})},$$

at continuity points $\mathbf{x} \in \mathcal{E}$ of the limit distribution function of the multivariate generalised Pareto distribution, where $\Lambda_{\text{MRV}}(\mathbf{x}) = \nu_{\text{MRV}}([-\infty, \mathbf{x}']')$. Multivariate generalised Pareto distributions arise as the only non-trivial limit distributions when renormalised multivariate exceedances are considered (Rootzén & Tajvidi 2006). These distributions possess several appealing theoretical and practical properties Engelke & Hitz (2020). Crucially, they are often thought to be the multivariate analogue of the generalised Pareto distribution Pickands (1975) by being the only threshold-stable multivariate distributions (Kiriliouk et al. 2019). The practical importance of their threshold-stability lies in the preservation of the model’s distributional type at higher levels, which is advantageous for extrapolation into the joint tail region of the distribution.

Both component-wise maxima and multivariate threshold exceedance approaches can be unified under a single theme. Let r_q be the q -th quantile of the distribution of $\|\mathbf{X}\|_1$. Then the overarching assumption that unifies these approaches is that as $q \rightarrow 1$, the point process of recentered exceedances $\mathbf{X}_i - r_q\mathbf{1} \mid \|\mathbf{X}_i\|_1 > r_q$, converges in distribution to Poisson point process on $(0, \infty] \times \Delta_+^{d-1}$ with mean measure

$$\lim_{q \rightarrow 1} \mathbb{P} \left[\|\mathbf{X}\|_1 - r_q > z, \frac{\mathbf{X}}{\|\mathbf{X}\|_1} \in B \mid \|\mathbf{X}\|_1 > r_q \right] = \exp(-z) H_{\text{MRV}}(B), \quad z > 0, B \subset \Delta_+^{d-1}. \quad (9)$$

In practice, the convergence (9) is typically assumed to hold with H_{MRV} placing mass in the interior $(\Delta_+^{d-1})^\circ := \{\boldsymbol{\omega} \in \mathbb{R}_+^d : \min_i \omega_i > 0, \|\boldsymbol{\omega}\|_1 = 1\}$ of the unit-simplex Δ_+^{d-1} . Although useful for theoretical investigations, H_{MRV} placing mass in $(\Delta_+^{d-1})^\circ$ as a *dependence assumption* is inadequate in practice since it imposes a strong form of dependence in the joint tail, see for example Section 4.2. The strength of this dependence, known as asymptotic dependence (see Section 1), is necessary so that the mass of the distribution of \mathbf{X} does not rapidly diffuse along the sequence of joint tail regions described by events of the form $\|\mathbf{X}\|_1 > r_q$, as q increases. Although elegant as an assumption, this limitation has been appreciated by a broad range of theoretical and practical studies.

2.3 Multivariate quantiles and weak convergence to Poisson point process

In this section, we consider a novel point process of multivariate exceedances over suitably chosen star-shaped sets. In what follows, we say that $\mathcal{A} \in \star \subset \mathcal{K}$ and call \mathcal{A} a star-body whenever \mathcal{A} is starshaped at 0 and $0 \in (\ker \mathcal{A})^\circ$, see Appendix A.2 for background information on starshaped sets. Because \mathcal{A} is compact and $0 \in (\ker G)^\circ$, then the radial function $r_{\mathcal{A}}(\mathbf{x}) = \sup\{\lambda > 0 : \lambda\mathbf{x} \in \mathcal{A}\}$ of \mathcal{A} is a Lipschitz continuous (-1) -homogeneous function on $\mathbb{R}^d \setminus \{0\} \cong \mathbb{S}^{d-1}$, that is $r_{\mathcal{A}}(\mathbf{x}) = \|\mathbf{x}\|^{-1} r_{\mathcal{A}}(\mathbf{x}/\|\mathbf{x}\|)$, $\mathbf{x} \in \mathbb{R}^d \setminus \{0\}$. The reciprocal of the radial function $g_{\mathcal{A}} := 1/r_{\mathcal{A}}$ is known as the gauge function of \mathcal{A} . The simplest star-body, perhaps, is the ball of radius ℓ centred about 0, denoted $B_\ell(0)$: its radial function given by $r_{B_\ell(0)}(\mathbf{x}) = \ell/\|\mathbf{x}\|$. The algebraic structure on \star (see Appendix A.3) enables operations between star-bodies over the field of scalars in a coherent and systematic manner, much like in a familiar algebraic structure over a field. The space of compact star-bodies \star is endowed with the operations $+$ and \cdot of radial addition and multiplication respectively. The radial addition operation combines two compact star-bodies G_1 and G_2 by adding their radial functions. It is commutative, associative, and has an identity

element (the empty set), which are properties akin to addition in a ring. Similarly, the radial multiplication combines two compact star bodies by multiplying their radial functions. The radial multiplication \cdot is distributive over $+$ and also associative. These operations are illustrated through examples of simple star-bodies in Figure 3.

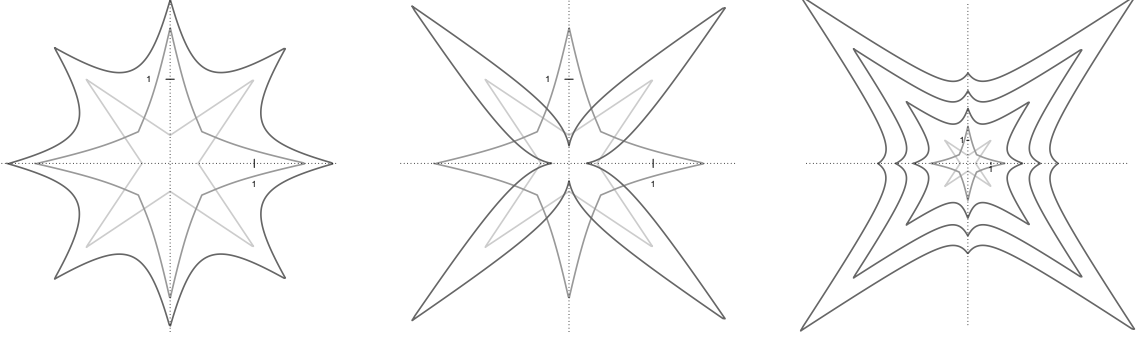


Figure 3: Left: $\mathcal{M} + \mathcal{G}$. Centre: \mathcal{M}/\mathcal{G} . Right: $\mathcal{M} + B_{-\log(1-q)}(0) \cdot \mathcal{G}$, for $B_r(\mathbf{x})$ the ball of radius r centred at \mathbf{x} , and $q \in \{0.9, 0.99, 0.999\}$. \mathcal{M} in lightest grey, \mathcal{G} in mid grey, result of operations in dark grey.

Multivariate exceedances are no longer defined with respect to $\|\mathbf{X}\|_p$ exceeding a high quantile relative to the distribution of $F_{\|\mathbf{X}\|_p}$. Instead, multivariate exceedances are understood as observations \mathbf{X}_i hitting the complement of an (inter-)quantile set $\mathcal{Q}_q \in \star$ in \mathbb{R}^d . Henceforth, we define the polar transformation given by $R = \|\mathbf{X}\|$ and $\mathbf{W} = \mathbf{X}/R$, where $\|\mathbf{X}\| = \|\mathbf{X}\|_2$.

Definition 1. Let $r_{\mathcal{Q}_q}(\mathbf{w}) = \sup\{r \in \mathbb{R} : F_{R|\mathbf{W}}(r | \mathbf{w}) \leq q\}$ be the conditional quantile function of the distribution of $R | \mathbf{W} = \mathbf{w}$. The q -th quantile set of the distribution of $\mathbf{X} = R\mathbf{W}$ is

$$\mathcal{Q}_q := \bigcup_{\mathbf{w} \in \mathbb{S}^{d-1}} [0 : r_{\mathcal{Q}_q}(\mathbf{w}) \mathbf{w}], \quad q \in (0, 1),$$

where $[0 : r_{\mathcal{Q}_q}(\mathbf{w}) \mathbf{w}]$ denotes the closed line segment from the origin to $r_{\mathcal{Q}_q}(\mathbf{w}) \mathbf{w}$.

The conditional quantile function $r_{\mathcal{Q}_q}$ is in one-to-one correspondence with $\mathcal{Q}_q \in \star$ in the sense that $r_{\mathcal{Q}_q}$ is the radial function of \mathcal{Q}_q . From total probability, the quantile function satisfies the property

$$\mathbb{P}[\mathbf{X} \in \mathcal{Q}_q] = q. \quad (10)$$

Remarkably, the quantile function can be interpreted as a quantile both conditionally and unconditionally, that is, for any fixed $q \in (0, 1)$, the quantile function \mathcal{Q}_q is one of the class of values of a variate that divides the total mass of a probability measure on $\mathbb{R}^d \setminus \{0\}$ into two parts, one that is visited by any single observation $\mathbf{X}_i \in \mathbb{R}^d$ with probability q and the other with probability $(1 - q)$. Thus, under random sampling, the set \mathcal{Q}'_q can be interpreted as a set that is expected to be visited on average once in $1/(1 - q)$ observations. This observation leads to the notion of return set \mathcal{Q}'_q , which is a geometric analogue of the return level in univariate extreme value analysis. Details on return level sets are given in Section 2.6.

We now motivate our first main result via an assumption that

Assumption 2. There exist $\xi := \log r_{\Xi}$ with $\Xi \in \star$ and a sequence $\{\mathcal{G}_q : \mathcal{G}_q \in \star, q \in (0, 1)\}$ such that

$$\lim_{q \rightarrow 1} \frac{\partial}{\partial z} \mathbb{P} \left[\frac{R - r_{\mathcal{Q}_q}(\mathbf{w})}{r_{\mathcal{G}_q}(\mathbf{w})} \leq z \mid \{R > r_{\mathcal{Q}_q}(\mathbf{w})\}, \mathbf{W} = \mathbf{w} \right] = \{1 + \xi(\mathbf{w})z\}_+^{-1-1/\xi(\mathbf{w})}, \quad \mathbb{P} - a.s.,$$

for $\mathbf{w} \in \mathbb{S}^{d-1}$, where $\{x\}_+ := \max(x, 0)$.

Theorem 1. Let $\{\mathbf{X}_i : i = 1, \dots, n\}$ be a random sample from \mathbf{X} satisfying Assumption 2, $q_{n,k} = 1 - k/n$ where $1 \leq k < n$, and consider the sequence of point processes

$$P_n = \left\{ \left(\frac{\|\mathbf{X}_i\| - r_{\mathcal{Q}_{q_{n,k}}}(\mathbf{X}_i/\|\mathbf{X}_i\|)}{r_{\mathcal{G}_{q_{n,k}}}(\mathbf{X}_i/\|\mathbf{X}_i\|)}, \mathbf{X}_i/\|\mathbf{X}_i\| \right) : i = 1, \dots, n \right\}, \quad n = 1, 2, \dots \quad (11)$$

Then, as n approaches ∞ ,

$$P_n \xrightarrow{w} P \quad \text{in } M_p((-\infty, \infty] \times \mathbb{S}^{d-1}), \quad (12)$$

where P is a Poisson point process defined on $(-\infty, \infty] \times \mathbb{S}^{d-1}$ with intensity measure given by $k(1 + \xi(\mathbf{w})r)^{-1-1/\xi(\mathbf{w})} dr F_{\mathbf{X}/\|\mathbf{X}\|}(d\mathbf{w})$, and $M_p((-\infty, \infty] \times \mathbb{S}^{d-1})$ denotes the collection of all Radon point measures on $(-\infty, \infty] \times \mathbb{S}^{d-1}$.

A proof is given in Appendix C.4. Convergence can be alternatively casted as

$$n\mathbb{P} \left[\frac{\mathbf{X} - r_{\mathcal{Q}_{1-(1/n)}}(\mathbf{X}/\|\mathbf{X}\|)(\mathbf{X}/\|\mathbf{X}\|)}{r_{\mathcal{G}_{1-(1/n)}}(\mathbf{X}/\|\mathbf{X}\|)} \in B \right] \xrightarrow{v} \nu_{\mathcal{G}}(B), \quad \text{in } M_+(\mathcal{E}), \quad (13)$$

where $\nu_{\mathcal{G}}$ is a Radon measure on \mathcal{E} . Convergence (13) implies domain of attraction properties for the random vector \mathbf{X} . For example, an analogue of convergence (13) in the geometric setting is that for any compact neighbourhood B of the origin 0, the appropriately renormalised sample cloud converges weakly to a non-degenerate limit distribution, that is,

$$\mathbb{P} \left[\frac{\mathbf{X}_i - r_{\mathcal{Q}_{1-(1/n)}}(\mathbf{X}_i/\|\mathbf{X}_i\|)(\mathbf{X}_i/\|\mathbf{X}_i\|)}{r_{\mathcal{G}_{1-(1/n)}}(\mathbf{X}_i/\|\mathbf{X}_i\|)} \in B : i = 1, \dots, n \right] \xrightarrow{w} \exp\{-\Lambda_G(B)\}, \quad (14)$$

where $\Lambda_G(B) = \nu_{\mathcal{G}}(B')$. The survival measure Λ_G admits the spectral decomposition given by

$$\Lambda_G(B) = \int_{\mathbb{S}^{d-1}} \int_{]0 : \mathbf{w}) \cap B'} \{1 + \xi(\mathbf{w})r\}_+^{-1-1/\xi(\mathbf{w})} dr F_{\mathbf{X}/\|\mathbf{X}\|}(d\mathbf{w}), \quad B \in \mathbb{R}^d \setminus \{0\}, \quad (15)$$

where $F_{\mathbf{X}/\|\mathbf{X}\|}$ is a probability measure on \mathbb{S}^{d-1} and $]0 : \mathbf{w})$ denotes the open half-line in the direction of \mathbf{w} . The limit probability in convergence (14) is the void probability of a Poisson random variable with rate Λ_G . The void probability is interpreted as the probability that no point from a recentred and rescaled sample cloud fall outside a set B as $n \rightarrow \infty$. This explains why the integral of the intensity measure is over the complement of B . The outer integral is with respect to $d\mathbf{w} = \mu(d\mathbf{w})$, where μ is the spherical Lebesgue measure and the inner integral is with respect to the 1-dimensional Lebesgue measure on $]0 : \mathbf{w}) \cap A$. Representation (17) suggests that $F_{\mathbf{X}/\|\mathbf{X}\|}$ has similar interpretation to the spectral measure H_{MRV} (de Haan & Resnick 1977). This is further discussed in Section 2.4.

Conditioning on the event that \mathbf{X} exceeds the (continuous) boundary $r_{\mathcal{Q}_q}(\mathbf{X}/\|\mathbf{X}\|)$ of the quantile set \mathcal{Q}_q , is remarkably informative for the joint tail region \mathcal{Q}'_q . An equivalent formulation of convergence (13) is through the polar transform which gives

$$\lim_{q \rightarrow 1} \mathbb{P} \left[\frac{\|\mathbf{X}\| - r_{\mathcal{Q}_q}(\mathbf{X}/\|\mathbf{X}\|)}{r_{\mathcal{G}_q}(\mathbf{X}/\|\mathbf{X}\|)} > z, \frac{\mathbf{X}}{\|\mathbf{X}\|} \in B \mid \|\mathbf{X}\| > r_{\mathcal{Q}_q}(\mathbf{X}/\|\mathbf{X}\|) \right] = [1 + \xi z]_+^{-1/\xi} F_{\mathbf{X}/\|\mathbf{X}\|}(B), \quad (16)$$

where $z > 0$, which implies that for any relatively compact set $A \subset \mathbb{R}^d \setminus \{0\}$, convergence (16) implies that the appropriately renormalised *multivariate threshold exceedances* satisfy

$$\mathbb{P}[\mathbf{Z} \in A] := \lim_{q \rightarrow 1} \mathbb{P} \left[\frac{\mathbf{X} - r_{\mathcal{Q}_q}(\mathbf{X}/\|\mathbf{X}\|)(\mathbf{X}/\|\mathbf{X}\|)}{r_{\mathcal{G}_q}(\mathbf{X}/\|\mathbf{X}\|)} \in A \mid \|\mathbf{X}\| > r_{\mathcal{Q}_q}(\mathbf{X}/\|\mathbf{X}\|) \right] = \Lambda_G(A). \quad (17)$$

The distribution of the limiting random vector \mathbf{Z} is defined through $F_{\mathbf{X}/\|\mathbf{X}\|}$ and due to the stability property of the generalised Pareto distribution, it enjoys certain threshold stability properties. These are described in Section 2.5.

Next, we give simple sufficient conditions subject to which Assumption 2 holds for the cases of bounded ($\xi < 0$), light-tailed ($\xi = 0$) and heavy-tailed ($\xi > 0$) distributions. We remark that for the light-tailed case, our assumption guarantees that a suitable sequence of scaling constants r_n can be found so that the random point-set $N_n = \{\mathbf{X}_1/r_n, \dots, \mathbf{X}_n/r_n\}$ converges in probability onto a limit set \mathcal{G} (Nolde & Wadsworth 2021) whereas for the heavy tailed-case, our assumption is in a similar spirit to de Haan & Resnick (1987) and guarantees that the distribution of \mathbf{X} is multivariate regularly varying on $\mathbb{R}^d \setminus \{0\}$. The corresponding assumption for the case $\xi < 0$ is equivalent to the case $\xi > 0$ after a suitable transformation, which is illustrated in Figure 4. A proof of Proposition 2 is given in Appendix C.3.

Proposition 2. *Suppose that the random vector \mathbf{X} has a Lebesgue density $f_{\mathbf{X}}$ on \mathbb{R}^d and let $\mathcal{G} \in \star$ be a star-body described by continuous gauge function $g_{\mathcal{G}} : \mathbb{R}^d \setminus \{0\} \rightarrow \mathbb{R}_+$. Suppose that one of the following conditions holds:*

- (i) *The limit $\mathcal{Q}_1 := \lim_{q \rightarrow 1} \mathcal{Q}_q$ exists in \star , $f_{\mathbf{X}}(\mathbf{x}) > 0$ when $\mathbf{x} \in \mathcal{G}^\circ$, $f_{\mathbf{X}}(\mathbf{x}) = 0$ when $\mathbf{x} \in \mathcal{G}'$, and there exists $\psi_{\mathcal{B}} : \mathbb{R}_+ \rightarrow \mathbb{R}_+$, and a $\xi < 0$ such that as $t \rightarrow \infty$,*

$$\frac{f_{\mathbf{X}}[\{1 - (\|t\mathbf{y}\|)^{-1}\}r(t\mathbf{y})(t\mathbf{y})]}{\psi_{\mathcal{B}}(t)} \rightarrow g_{\mathcal{G}}(\mathbf{y})^{1/\xi+1}, \quad \mathbf{y} \in \mathbb{R}^d \setminus \{0\}. \quad (18)$$

- (ii) *There exists $\psi_{\mathcal{L}} : \mathbb{R}_+ \rightarrow \mathbb{R}_+$, and a $\rho > 0$ such that as $t \rightarrow \infty$,*

$$-\frac{\log f_{\mathbf{X}}(t\mathbf{y})}{\psi_{\mathcal{L}}(t)} \rightarrow g_{\mathcal{G}}(\mathbf{y})^\rho, \quad \mathbf{y} \in \mathbb{R}^d \setminus \{0\}. \quad (19)$$

- (iii) *There exists $\psi_{\mathcal{H}} : \mathbb{R}_+ \rightarrow \mathbb{R}_+$, and $\xi > 0$, such that as $t \rightarrow \infty$,*

$$\frac{f_{\mathbf{X}}(t\mathbf{y})}{\psi_{\mathcal{H}}(t)} \rightarrow g_{\mathcal{G}}(\mathbf{y})^{-(d+\xi^{-1})}, \quad \mathbf{y} \in \mathbb{R}^d \setminus \{0\}. \quad (20)$$

If, in addition, the convergence is uniform on \mathbb{S}^{d-1} , then Assumption 2 holds, and $r_{\mathcal{G}_q}$ can be taken as

- (i) $r_{\mathcal{G}_q}(\mathbf{w}) = \xi [r_{\mathcal{Q}_1}(\mathbf{w}) - r_{\mathcal{Q}_q}(\mathbf{w})]$ when $\xi < 0$;
- (ii) $r_{\mathcal{G}_q}(\mathbf{w}) = r_{\mathcal{G}}(\mathbf{w})^\rho / \psi_{\mathcal{L}}' \{r_{\mathcal{Q}_q}(\mathbf{w})\}$ when $\xi = 0$;
- (iii) $r_{\mathcal{G}_q}(\mathbf{w}) = r_{\mathcal{G}}(\mathbf{w})(1 - q)^{-\xi/\xi}$ when $\xi > 0$.

2.4 Probability density function of angles

The framework presented in Section 2.3 has obvious advantage as it yields a limiting distribution of angles that precisely mirrors the distribution of angles found in the original variables. Proposition 3 formalises this statement and a proof is given in Appendix C.7.

Proposition 3. *Suppose that $\mathbf{X} \in \mathbb{R}^d$ admits a density $f_{\mathbf{X}}$, then for any quantile level $q \in (0, 1)$, the distribution of $\mathbf{X}/\|\mathbf{X}\| \mid \|\mathbf{X}\| > r_{\mathcal{Q}_q}(\mathbf{X}/\|\mathbf{X}\|)$ is identical to the distribution of $\mathbf{X}/\|\mathbf{X}\|$.*

Proposition 3 has meaningful implications for statistical inference as it implies that an additional source of information can be leveraged from $\mathbf{X} \mid \mathbf{X} \in \mathcal{Q}_q$ when estimating quantities related to the functionals of the distribution of $\mathbf{X} \mid \|\mathbf{X}\| > r_{\mathcal{Q}_q}(\mathbf{X}/\|\mathbf{X}\|)$. We discuss this aspect in detail in Section 3.3.

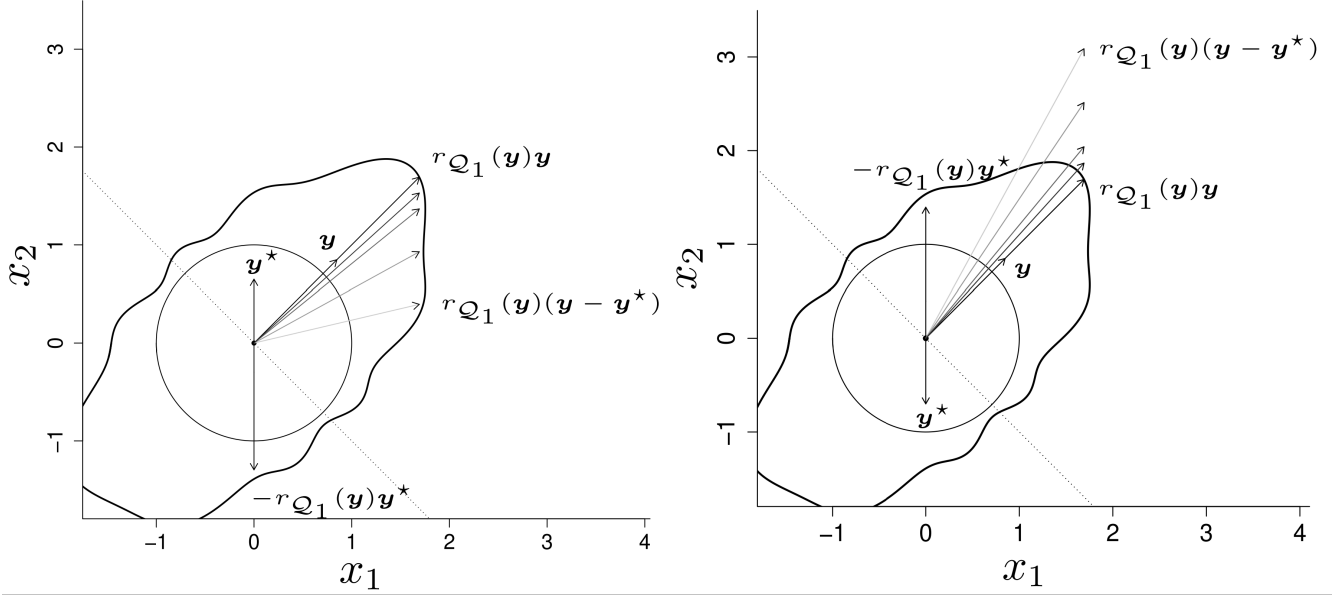


Figure 4: Illustration of the transformation $\mathbf{x} = r_{\mathcal{Q}_1}(\mathbf{y})(\mathbf{y} - \mathbf{y}^*)/t$ showing a sequence $\mathbf{x}_1, \dots, \mathbf{x}_5$ in \mathbb{R}^d approaching the boundary point $r_{\mathcal{Q}_1}(\mathbf{y})\mathbf{y}$ (arrows, $t = 1, 2, 5, 10, \infty$), from (left) a region of positive density ($\mathbf{y}^\top \mathbf{y}^* > 0$) and (right) a region of zero density ($\mathbf{y}^\top \mathbf{y}^* \leq 0$).

For many real-world applications, the assumption of an absolutely continuous distribution for $F_{\mathbf{X}/\|\mathbf{X}\|}$ is the most practical, rendering our framework highly suitable. Here, we describe further a link between $F_{\mathbf{X}/\|\mathbf{X}\|}$ and \mathcal{G} , which allows improving learning of the set \mathcal{G} through pooling information from angles. This link explains the substantial gains in uncertainty in our numerical simulations, even in cases where $F_{\mathbf{X}/\|\mathbf{X}\|}$ partially depends on \mathcal{G} partially. First, we describe a key connection between the distribution of angles $\mathbf{W} = \mathbf{X}/\|\mathbf{X}\|$ with star-bodies in \mathbb{R}^d . For simplicity, we will assume throughout that $F_{\mathbf{W}}$ is absolutely continuous with respect to the spherical Lebesgue measure. In this setting, we observe that any continuous probability density function on the sphere is in one-to-one correspondence with a strongly starshaped set \mathcal{W} defined by its radial function $r_{\mathcal{W}}(\mathbf{w}) := f_{\mathbf{W}}(\mathbf{w})$ as

$$\mathcal{W} := \bigcup_{\mathbf{w} \in \mathbb{S}^{d-1}} [0 : f_{\mathbf{W}}(\mathbf{w}) \mathbf{w}] \in \star.$$

Because $\mathcal{W} \in \star$ we see that $r_{\mathcal{W}^{1/d}}(\mathbf{w})^d = r_{\mathcal{W}}(\mathbf{w}) = f_{\mathbf{W}}(\mathbf{w})$. Thus, from the definition of the volume (A.4) given in Appendix A.2, we can verify that for $f_{\mathbf{W}}$ to be a valid density, \mathcal{W} must satisfy

$$1 = \int_{\mathbb{S}^{d-1}} f_{\mathbf{W}}(\mathbf{w}) d\mathbf{w} = d \left[\frac{1}{d} \int_{\mathbb{S}^{d-1}} r_{\mathcal{W}^{1/d}}(\mathbf{w})^d d\mathbf{w} \right] = d|\mathcal{W}^{1/d}|. \quad (21)$$

To construct any set \mathcal{W} satisfying condition (21) that $r_{\mathcal{W}}$ is a density on \mathbb{S}^{d-1} , it suffices to consider

$$\mathcal{W}^{1/d} = \mathcal{L}/(d|\mathcal{L}|)^{1/d}, \quad (22)$$

for some $\mathcal{L} \in \star$, which follows from the usual formula for the volume (A.4) in polar coordinates. Condition (22) sets the stage for the subsequent models we propose.

One a priori possibility for the form of the set \mathcal{L} in expression (22) is to have $\mathcal{L} = \mathcal{B}$ where \mathcal{B} is independent of \mathcal{G} and $\mathcal{B} \in \star$. In other words, this initial model represents the class of densities \mathcal{W} that are independent of the scaling set \mathcal{G} . A second a priori possibility is the class of probability density functions on \mathbb{R}^d which are homothetic with respect to a scaling set $\mathcal{G} \in \star$ (Balkema & Nolde 2010). In

this definition, a density is called homothetic if its level-sets that are scaled copies of a set \mathcal{G} . In this case, Proposition 4 shows that there is a one-to-one correspondence between the density of angles and \mathcal{G} .

Proposition 4. *Suppose that $f_{\mathbf{X}}(\mathbf{x}) = f_0(r_{\mathcal{G}}(\mathbf{x})^{-1})$ for a decreasing, positive, a continuous function $f_0 : [0, \infty) \rightarrow [0, \infty)$ and a (-1) -homogeneous function $r_{\mathcal{G}}$, describing a shape $\mathcal{G} \in \star$. Then $\mathcal{L} = \mathcal{G}$.*

A proof of Proposition 4 based on the integration by parts formula of Balkema & Nolde (Section 3.1, 2010) is given in Appendix C.8. Here we remark that Proposition 4 provides with a new probabilistic proof for the volume of a star-body in polar coordinates (Klain 1997). The usefulness of Proposition 4 can be seen from the ease with which one can identify the density of angles in analytic form when the density is homothetic and the joint density is known. For concreteness, consider $\mathcal{G} \in \star$ described by $r_{\mathcal{G}}(\mathbf{x}) = (\mathbf{x}^\top \mathbf{Q} \mathbf{x})^{-1/2}$ where $\mathbf{Q} = \mathbf{D}^{1/2} \Sigma^{-1} \mathbf{D}^{1/2}$, with $\mathbf{D} = \text{diag}(\Sigma)$ and Σ a positive definite matrix. Homothetic densities sharing the same homogeneous function $g_{\mathcal{G}}$ but having different density generators f_0 are given in Examples 1–3. As noted by Balkema & Nolde (2010) the rate of decay of $f_0(r)$ as $r \rightarrow \infty$ determines the properties of the margins.

Example 1. *Suppose $\mathbf{X} \sim \text{MVN}(\mathbf{0}, \mathbf{Q}^{-1})$. The margins of \mathbf{X} are standard normally distributed. The density $f_{\mathbf{X}}$ is homothetic with respect to $r_{\mathcal{G}}$ and $f_0(r) = C_1 \exp(-r^{-2}/2)$, $r > 0$, where $C_1 = [|\mathbf{Q}|^{1/2}/(2\pi)^{d/2}]$.*

Example 2. *Suppose $\mathbf{X} \sim \text{MVL}(\mathbf{0}, \mathbf{Q}^{-1})$. The margins of \mathbf{X} are standard Laplace distributed. The density $f_{\mathbf{X}}(\mathbf{x})$ is homothetic with respect to $r_{\mathcal{G}}$ and $f_0(r) = C_2 r^{-\nu} K_{\nu}(r^{-1})$, $r > 0$, where $C_2 = [|\mathbf{Q}|^{1/2}/(2\pi)^{d/2}]$, K_{ν} is the modified Bessel function of the second kind (Gradshteyn & Ryzhik 2014) and $\nu = (2 - d)/2$.*

Example 3. *Suppose $\mathbf{X} \sim t_{\nu}(\mathbf{0}, \mathbf{Q}^{-1})$. The margins of \mathbf{X} are standard Student- t_{ν} distributed. The density $f_{\mathbf{X}}(\mathbf{x})$ is homothetic with respect to $r_{\mathcal{G}}$ and $f_0(r) = C_3 (1 + r^{-2}/\nu)^{-(\nu+d)/2}$, $r > 0$, where $C_3 = [\Gamma\{(\nu + d)/2\} |\mathbf{Q}|^{1/2} / \{\Gamma(\nu/2)\}^d]$.*

Proposition 4 immediately gives the star set \mathcal{W} in analytic form for Examples 1–3. As expected from Proposition 4, the set \mathcal{W} is common to all examples and is defined by its radial function $r_{\mathcal{G}}^d/(d|\mathcal{G}|)$. Standard practice in extreme value analysis consists of removing the effect of marginal scale to studying

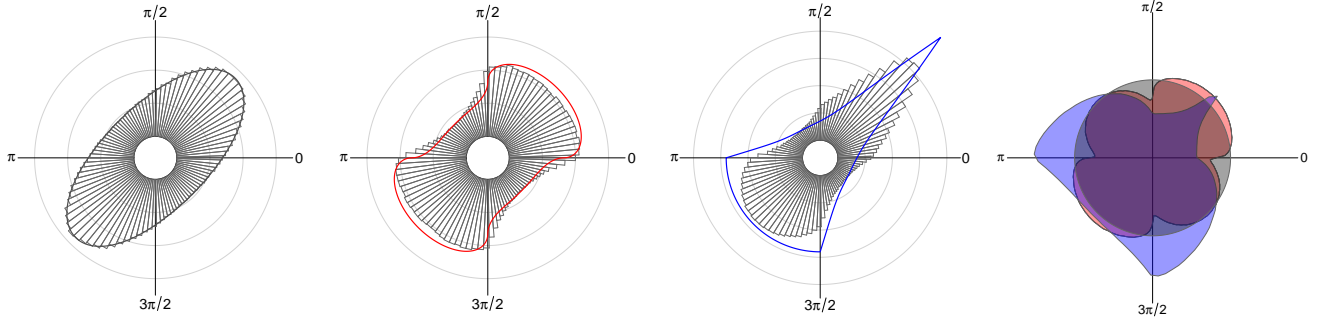


Figure 5: Left to right: Circular histogram of 10^6 angles sampled from a standard bivariate normal distribution (correlation $\rho = 0.5$) with standard normal margins, standard Laplace margins, and from a bivariate max-stable logistic distribution with Laplace margins (dependence parameter $\theta = 0.5$). A concentric circle corresponds to a leap of 0.1 in the density of angles. Solid lines correspond to the boundary of $\mathcal{G}^d/(d|\mathcal{G}|)$, for \mathcal{G} of the respective distributions. Plot 4: Sets $[\mathcal{G}^d/(d|\mathcal{G}|)] \cdot \mathcal{W}^{-1}$ corresponding to Plots 1–3.

the extremal dependence structure of \mathbf{X} . This is typically achieved by standardising the margins of \mathbf{X} to a common distribution, see Section 3.1. Consider the map $\mathbb{R}^d \ni \mathbf{x} \mapsto T(\mathbf{x}) = (\Psi^{\leftarrow}(F_{X_i}(x_i)) : i = 1, \dots, d) \in \mathbb{R}^d$ performing a transformation of the marginal distributions of \mathbf{X} , so that the i th element of

$T(\mathbf{X})$ follows Ψ where Ψ denotes a continuous cumulative distribution function on \mathbb{R} . The transformation preserves the cardinality of the set of input vectors $\mathbf{X}/\|\mathbf{X}\|$, ensuring a one-to-one correspondence with the output vector $T(\mathbf{X})/\|T(\mathbf{X})\|$. From a geometric perspective, this means that the densities of $\mathbf{X}/\|\mathbf{X}\|$ and $T(\mathbf{X})/\|T(\mathbf{X})\|$ can be defined over the same set of points. However, while the cardinality is preserved, the geometric properties of the distribution of angles may change, as for example when T introduces nonlinearities which distort the shape of the distribution of $\mathbf{X}/\|\mathbf{X}\|$. As a concrete example, suppose \mathbf{X} is a random vector distributed according to a multivariate normal distribution with zero mean and covariance matrix \mathbf{Q}^{-1} where \mathbf{Q} is such that each X_i follows the standard normal distribution. Let $\mathbf{X}_L = F_L^{-1}[\Phi(\mathbf{X})]$, where F_L and Φ denote the cumulative distribution functions of standard Laplace and standard normal random variables, respectively. Although the density of \mathbf{X} is homothetic, the density of \mathbf{X}_L is not. However, convergence (ii) of Proposition 2 holds true with $\rho = 0$ outside a set of Lebesgue measure zero with $G = \mathcal{G}_L$ determined by its radial function

$$r_{\mathcal{G}_L}(\mathbf{w}) = \left[\left\{ \text{sgn}(\mathbf{w})|\mathbf{w}|^{1/2} \right\}^\top \mathbf{Q} \left\{ \text{sgn}(\mathbf{w})|\mathbf{w}|^{1/2} \right\} \right]^{-1}, \quad \mathbf{w} \in \mathbb{S}^{d-1}. \quad (23)$$

where $\text{sgn}(x) = x/|x|$ denotes the signum function and $\text{sgn}(\mathbf{w})|\mathbf{w}|^{1/2} = (\text{sgn}(w_i)|w_i|^{1/2} : i = 1, \dots, d)$. Then, the star set \mathcal{W}_L describing the density of $\mathbf{X}_L/\|\mathbf{X}_L\|$ is no longer a constant scale multiple of \mathcal{G}_L , but instead, it is a radial product of \mathcal{G}_L with another star-body. The second panel of Figure 5 shows the true density (histogram) and $r_{\mathcal{G}_L}(\mathbf{w})^d/\{d|\mathcal{G}_L|\}$ (solid curve). The star-body is the ratio between \mathcal{W} and $\mathcal{G}_L^d/\{d|\mathcal{G}_L|\}$, and for this example, it is shown in the fourth panel of Figure 5.

The class of homothetic densities, although rich, serves at best as an idealistic setting. The analysis of the marginal transformation, however, reveals an intermediate case where \mathcal{W} can depend both on \mathcal{G} and on some additional latent star-body \mathcal{B} that is independent of \mathcal{G} . The star-body \mathcal{B} captures residual angular variation that is not explained by a homothetic density. For instance, assume that \mathbf{X} follows a bivariate max-stable logistic distribution in standard Laplace margins with density given by expression (A.5). From Figure 5, we see that $\mathcal{W} \neq \mathcal{G}^d/(d|\mathcal{G}|)$. For the practical case where both $r_{\mathcal{W}}$ and $r_{\mathcal{G}}$ are positive on \mathbb{S}^{d-1} , then $\mathcal{L} = \mathcal{B} \cdot \mathcal{G}$, $\mathcal{B}, \mathcal{G} \in \star$ with \mathcal{B} independent of \mathcal{G} . Here, the set \mathcal{B} captures the deviation of the set associated with a homothetic density of angles, \mathcal{G}^d , from the set \mathcal{W} associated with a density $f_{\mathbf{W}}$. It follows that in the specific context where $f_{[L]}$ is homothetic with respect to $r_{\mathcal{G}}$, $\mathcal{B} = B_1(0)$. Plot 4 in Figure 5 displays the sets $d|\mathcal{G}|\mathcal{W}/\mathcal{G}$ associated with the first three plots.

2.5 Multivariate radially-stable distributions

In this Section, we present the class of multivariate radially-stable (MRS) distributions. The elements of this class are the only non-trivial limits of *radially renormalised* exceedances above \mathcal{Q}_q . Due to their stability properties, MRS distributions make them suitable for extrapolation in the joint tail region. For the remainder of this section, we note that $\mathbb{R}^{d-1} \cong \mathbb{S}^{d-1}$ and $\mathbb{R}_+^{d-1} \cong \mathbb{S}_+^{d-1}$ so that integration in (17) is interpreted over the spherical domain that is congruent to the domain of the distribution. In the definitions and propositions below, we let $K \in \star$ be such that $\mathcal{M} \subseteq K$.

Definition 2 (Multivariate radially-stable exponential distributions). *A random vector \mathbf{Z} is said to follow the multivariate radially-stable exponential distribution with location $\mathcal{M} \in \star$, scale $\Sigma \in \star$, and angular component $\mathcal{W} \in \star$, $|\mathcal{W}^{1/d}| = 1/d$, if its distribution function is given by*

$$\mathbb{P}(\mathbf{Z} \leq \mathbf{z}) = 1 - \int_{\mathbb{S}_+^{d-1}} \exp \left\{ -\frac{\min(\mathbf{z}/\mathbf{w}) - r_{\mathcal{M}}(\mathbf{w})}{r_{\Sigma}(\mathbf{w})} \right\} r_{\mathcal{W}}(\mathbf{w}) \, d\mathbf{w}, \quad \mathbf{z} \in \mathbb{R}_+^d \setminus \mathcal{M}, \quad (24)$$

and if

$$\mathbb{P}[\mathbf{Z} \in K'] = \int_{\mathbb{S}^{d-1}} \exp \left\{ -\frac{r_K(\mathbf{w}) - r_{\mathcal{M}}(\mathbf{w})}{r_{\Sigma}(\mathbf{w})} \right\} r_{\mathcal{W}}(\mathbf{w}) \, d\mathbf{w}, \quad K' \subset \mathbb{R}^d \setminus \mathcal{M}. \quad (25)$$

Definition 3 (Multivariate radially-stable generalised Pareto distributions). *A random vector \mathbf{Z} is said to follow the multivariate radially-stable generalised Pareto distribution with location $\mathcal{M} \in \star$, scale $\Sigma \in \star$, and shape $\xi = \log r_{\Xi}$ for $\Xi \in \star$, and angular component $\mathcal{W} \in \star$, $|\mathcal{W}^{1/d}| = 1/d$, if its distribution function is*

$$\mathbb{P}(\mathbf{Z} \leq \mathbf{z}) = 1 - \int_{\mathbb{S}_+^{d-1}} \left\{ 1 + \xi(\mathbf{w}) \frac{\min(\mathbf{z}/\mathbf{w}) - r_{\mathcal{M}}(\mathbf{w})}{r_{\Sigma}(\mathbf{w})} \right\}_+^{-1/\xi(\mathbf{w})} r_{\mathcal{W}}(\mathbf{w}) d\mathbf{w}, \quad \mathbf{z} \in \mathbb{R}_+^d \setminus \mathcal{M}, \quad (26)$$

and if

$$\mathbb{P}[\mathbf{Z} \in K'] = \int_{\mathbb{S}^{d-1}} \left\{ 1 + \xi(\mathbf{w}) \frac{r_K(\mathbf{w}) - r_{\mathcal{M}}(\mathbf{w})}{r_{\Sigma}(\mathbf{w})} \right\}_+^{-1/\xi(\mathbf{w})} r_{\mathcal{W}}(\mathbf{w}) d\mathbf{w}, \quad K' \in \mathbb{R}^d \setminus \mathcal{M}. \quad (27)$$

Definitions 2 and 3 possess stability properties that we here detail through Propositions 5 and 6. These properties will be relevant to later Sections and provide efficient ways for extrapolating in tail regions.

Proposition 5. *Let $\mathbf{Z} \in \mathbb{R}^d$ have a MRS exponential distribution with location $\mathcal{M} \in \star$, scale $\Sigma \in \star$, and shape $\mathcal{W} \in \star$, then the quantile set \mathcal{Q}_q of \mathbf{Z} is given by*

$$\mathcal{Q}_q = \mathcal{M} + B_{-\log(1-q)}(0) \cdot \Sigma, \quad q \in [0, 1], \quad (28)$$

and \mathbf{Z} satisfies the radial memoriless property that

$$\mathbb{P}[\mathbf{Z} \in [\mathcal{M} + B_{r_1+r_2}(0) \cdot \Sigma]' \mid \mathbf{Z} \in \{\mathcal{M} + B_{r_1}(0) \cdot \Sigma\}'] = \mathbb{P}[\mathbf{Z} \in \{\mathcal{M} + B_{r_2}(0) \cdot \Sigma\}']. \quad (29)$$

Proposition 6. *Let $\mathbf{Z} \in \mathbb{R}^d$ have a MRS generalised Pareto distribution with location $\mathcal{M} \in \star$, scale $\Sigma \in \star$, tail-index $\xi = \log r_{\Xi}$ for $\Xi \in \star$ and shape $\mathcal{W} \in \star$, then the quantile set \mathcal{Q}_q of \mathbf{Z} is given by*

$$\mathcal{Q}_q = \mathcal{M} + (\log \Xi)^{-1} \{B_{1-q}(0)^{-\log \Xi} - B_1(0)\} \cdot \Sigma, \quad q \in [0, 1], \quad (30)$$

and, if $\xi \in \mathbb{R}$, \mathbf{Z} satisfies the radial stability property that

$$\mathbb{P}[\mathbf{Z} \in [\mathcal{M} + B_{r_1+r_2}(0) \cdot \Sigma]' \mid \mathbf{Z} \in \{\mathcal{M} + B_{r_1}(0) \cdot \Sigma\}'] = \mathbb{P}\left[\mathbf{Z} \in \left\{ \mathcal{M} + \frac{B_{r_2}(0) \cdot \Sigma}{B_1(0) + B_{\xi}(0) \cdot B_{r_1}(0)} \right\}'\right]. \quad (31)$$

The stability properties given in equations (29) and (31) and the expressions for the quantile set \mathcal{Q}_q of both MRS distributions in terms of their starshaped parameters provide an efficient mean of extrapolating in tail regions and proofs are given in Appendix C.5 and C.6. Note that in equation 29, the location \mathcal{M} can be replaced by any $K \in \star$ such that $\mathcal{M} \subseteq K$ on the left-hand side to yield the same result. These properties are pivotal for the following section, introducing the notion of return level-sets, as well as Section 3.5, on probability estimation.

2.6 Return level-sets

The MRS developed in Section 2.5 are central to the concept of *return level-sets* introduced in this section. Analogously to a univariate return level corresponding to a value expected to be exceeded by a random variable X once in a certain return period, return level-sets correspond to a specific set expected to be attained by a random vector \mathbf{X} once in a certain return period. Below, we detail the important properties of return level-sets, which give insight into the extremes of a random vector of interest.

For any Bernoulli experiment with probability $1 - q$ of success, a return period $T = 1/(1 - q)$ defines the expected number of experiments needed to obtain one success. Given a random vector $\mathbf{X} \in \mathbb{R}^d$ and

an arbitrary set $B \in \mathbb{R}^d$, the event $\mathbf{X} \in B$ can be interpreted as a Bernoulli experiment with some return period T . Perhaps unsurprisingly, depending on the properties of \mathbf{X} , there can be infinitely many distinct sets in \mathbb{R}^d satisfying this property. If \mathbf{X} has a Lebesgue density on \mathbb{R}^d , then we can always uniquely determine a canonical return set as in Definition 1. In particular, two open subsets $U_{1/(1-q)}$ and $V_{1/(1-q)}$ of $\mathbb{R}^d \setminus \{0\}$ are said to be equivalent with respect to a random vector \mathbf{Z} and a measure \mathbb{P} , denoted $U_{1/(1-q)} \sim^{\mathbb{P}} V_{1/(1-q)}$, if there exists $q \in (0, 1)$ such that $\mathbb{P}[\mathbf{Z} \in U_{1/(1-q)}] = 1 - q$ and $\mathbb{P}[\mathbf{Z} \in V_{1/(1-q)}] = 1 - q$.

The relation $\sim^{\mathbb{P}}$ is an equivalence relation and the collection of subsets of $\mathbb{R}^d \setminus \{0\}$, $\{U_{1/(1-q)}\}_{\sim^{\mathbb{P}}} = \{V_{1/(1-q)} \text{ open in } \mathbb{R}^d \setminus \{0\}, : V_{1/(1-q)} \sim^{\mathbb{P}} U_{1/(1-q)}\}$ is an equivalence class of $U_{1/(1-q)}$. An equivalence class $\{U_{1/(1-q)}\}_{\sim^{\mathbb{P}}}$ always contains a unique set $\mathbf{X}_{1/(1-q)}$ defined by

$$\mathbf{X}_{1/(1-q)} = \mathbb{R}^d \setminus \mathcal{Q}_q, \quad q \in (0, 1), \quad (32)$$

where \mathcal{Q}_q is the quantile set introduced in Definition 1.

Definition 4. The set \mathbf{X}_T defined by (32) is called a return level-set with return-period T .

By Definition 4, a sequence of return level-sets $\mathbf{X}_{T_1}, \dots, \mathbf{X}_{T_k}$ with $T_1 \leq \dots \leq T_k$ forms a nested sequence of open sets. It thus follows that for return periods $T_i \leq T_j$ with $1 \leq i \leq j \leq k$,

$$\mathbb{P}[\mathbf{Z} \in \mathbf{X}_{T_j} \mid \mathbf{Z} \in \mathbf{X}_{T_i}] = \mathbb{P}[\mathbf{Z} \in \mathbf{X}_{T_j}] / \mathbb{P}[\mathbf{Z} \in \mathbf{X}_{T_i}] = T_i / T_j.$$

From Section 2.3, we know that the MRS distributions described in Section 2.5 arise as limiting distributions of suitably scaled excesses of a quantile set. We here describe the geometry of the return level-sets corresponding to these distributions.

If the random vector \mathbf{Z} follows a MRS exponential distribution with location parameter \mathcal{M} and scale parameter Σ , the return level-set \mathbf{X}_{T_j} can be written in terms of another \mathbf{X}_{T_i} with $T_j \geq T_i$ via

$$\mathbf{X}_{T_j} = [\mathbf{X}'_{T_i} + B_{\{\log(T_j/T_i)\}}(0) \cdot \Sigma]'. \quad (33)$$

Similarly, if the random vector \mathbf{Z} follows a MRS generalised Pareto distribution with location parameter \mathcal{M} and scale parameter Σ and tail-index $\xi = \log r_{\Xi}$ for $\Xi \in \star$, the return level-set \mathbf{X}_{T_j} can be written in terms of another return level-set \mathbf{X}_{T_i} with $T_j \geq T_i$ as

$$\mathbf{X}_{T_j} = \left[\mathbf{X}'_{T_i} + (B_{T_j}(0)^{\log \Xi} - B_{T_i}(0)^{\log \Xi}) \cdot \Sigma / (\log \Xi) \right]'. \quad (34)$$

A classical assumption in extreme value theory, phrased in our setting, is that there exists $q \in (0, 1)$ such that suitably scaled exceedances of the quantile set \mathcal{Q}_q follow the MRS distributions exactly. Under this assumption, expressions (33) and (34) for the return sets provide a well-posed way of extrapolating far beyond $\mathbf{X}_{1/(1-q)} = \mathcal{Q}'_q$. This assumption is central to the upcoming Section 3, which details the statistical inference procedure based on the limiting results provided in Section 2.

3 Statistical inference

3.1 Standardisation of margins

Statistical inference for real data, encoded into realisations from a random sample $\{\mathbf{X}_i : i = 1, \dots, n\}$, is messy as the support and tail properties of the marginal distributions of \mathbf{X}_i may behave in wildly differing manners. It is therefore convenient, and frequently done in practice, to standardise observed data to common marginal distributions prior to statistical modelling. This is often achieved by applying the probability integral transform (PIT) to each component of the vectors in the random sample and inverting from the uniform to the desired marginal distribution. The PIT can be performed by approximating the cumulative distribution function through a semi-parametric procedure consisting in fitting a generalised

Pareto distribution to the lower, the upper, or both tails and an empirical distribution function for the remaining part of the data.

FpA convenient choice of marginal distribution is that of the standard Laplace as the density convergence of Assumption 2 is satisfied with $\xi = 0$ for a wide class of families of distributions studied in Appendix B.

3.2 Quantile regression

Quantile regression methods are typically implemented using a pinball loss function (Koenker 2005) and often without a distributional model for the density. Although Yu & Moyeed (2001) propose the use of the asymmetric Laplace distribution for the model density due to the equivalence of the negative log density of the asymmetric Laplace with the pinball loss function, naively treating the asymmetric Laplace as an adequate model for the data is precarious in a Bayesian setting. For example Waldmann et al. (2013) show that the resulting posterior prediction intervals have poor frequentist calibration properties, and this is especially pronounced for tail quantiles, which are essential in our setup. Second, the scale parameter of the asymmetric Laplace distribution is arbitrary in a Bayesian framework and even maximum likelihood based estimators are known to lead to inaccurate quantile estimates, see Fasiolo et al. (2021).

We adopt a *generalised linear model* based approach for quantile regression, requiring an adequate distributional model for the density of $R \mid \mathbf{W}$. In particular, we assume that $R \mid \mathbf{W} = \mathbf{w}$ follows a Gamma distribution and model the logarithm of conditional q -quantile $\log r_{\mathcal{Q}_q}(\mathbf{w})$ using a finite-dimensional continuously specified Gaussian process prior on \mathbb{S}^{d-1} (see Section 3.4).

There are at least two major strengths behind this choice. First, due to Proposition 8, the Gamma distribution serves as a good approximation for the density in the tail region of the distribution of $R \mid \mathbf{W}$. Since estimators of high quantiles are not influenced by the bulk of the distribution, a likely misspecification between our choice and the true density of $R \mid \mathbf{W}$ in the body of the distribution is not of concern. Second, our choice exploits the form of the decay of the conditional density and allows for Bayesian inference for the conditional quantile under a model that can adequately describe the behaviour in the tail. In this paper, we adopt a Gamma quantile regression models due to the simplicity that it affords, but remark that further improvements may be achieved by using, for example, a truncated Gamma distribution, so as to eliminate any effect from the body of the distribution of $R \mid \mathbf{W}$.

3.3 Likelihood function

We assume that given a sample $\mathbf{y} = \{(r_i, \mathbf{w}_i) : i = 1, \dots, n\}$ of n observations, there exists an integer $k_0 < n$ such that the limit expression (12) holds exactly $\forall k > k_0$. This type of assumption is the standard practical assumption adopted in extreme value statistics where the distribution of observed extremes is approximated by the limiting theoretical distribution. In what follows, we use this assumption to motivate a likelihood based approach based on the Poisson process convergence (12). Given that \mathbf{X} has standard Laplace margins, this approach leads to a MRS exponential limiting distribution with location parameter \mathcal{Q}_q and scale parameter \mathcal{G} as described in Definition 2. We prefer this approach over the analogous one based on Definition 3 for its parsimony and convenient memoryless stability properties. In this section, the quantities of interest are the limit set \mathcal{G} and the set \mathcal{W} with respective radial functions $r_{\mathcal{G}}$ and $f_{\mathbf{W}}$.

We recall from equation (22) that the set \mathcal{W} can be expressed in terms of a starshaped set \mathcal{L} such that $f_{\mathbf{W}}(\mathbf{w}) = r_{\mathcal{L}}(\mathbf{w})^d / (d|\mathcal{L}|)$. Based on Section 2.4, we motivate three models for \mathcal{W} given by $M_1 : \mathcal{L} = \mathcal{B}$, $M_2 : \mathcal{L} = \mathcal{G}$, and $M_3 : \mathcal{L} = \mathcal{B} \cdot \mathcal{G}$, for $\mathcal{B} \in \star$ independent of $\mathcal{G} \in \star$. We note that the latent starbodies \mathcal{B} in models M_1 and M_3 do not have the same interpretation, but the slight abuse of notation allows to simplify the notation for the parameter space in later sections without loss of interpretation. Figure 6 shows the hierarchical structure of models M_1 , M_2 and M_3 via their directed acyclic conditional independence graphs. It is apparent from Figure 6 that the graph of M_2 forms a sub-graph of M_3 , and that M_3 is the graph sum of M_1 and M_2 . The nested structure of model M_2 within the parameter space of model M_3 translates into a bias-variance trade-off as the latter offers additional flexibility at the cost

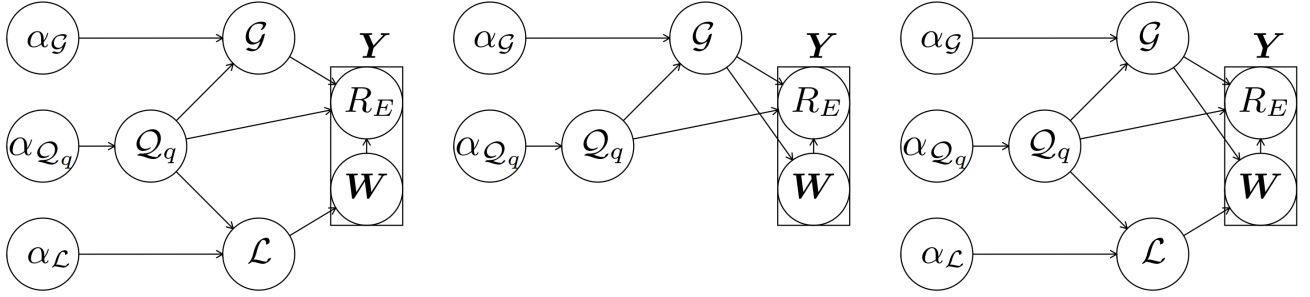


Figure 6: Hierarchical structure of models M_1 (left), M_2 (centre), and M_3 (right). The vectors α_{Q_q} , α_G , and α_L are hyperparameters for the prior distributions of the latent variables Q_q , G and L . The variable R_E denotes the exceedances $R - r_{Q_q}(\mathbf{W}) \mid R > r_{Q_q}(\mathbf{W})$.

of a possibly increased variance for the latent set \mathcal{G} . A similar trade-off occurs for \mathcal{G} between models M_1 and M_3 since the former ignores possible information contained in the observed angles.

Conditionally on the quantile set Q_q and the data \mathbf{y} , the likelihood of $\boldsymbol{\theta} = (G, L)$, is given by $L(\boldsymbol{\theta} \mid Q_q, \mathbf{y}) := \prod_{i=1}^n f_{R, \mathbf{W}}(r_i, \mathbf{w}_i \mid \boldsymbol{\theta}, Q_q)$. Letting $S_q := \{i \in \{1, \dots, n\} : r_i > r_{Q_q}(\mathbf{w}_i)\}$ denote the set of random indices corresponding to exceedances of Q_q , and $S'_q := \{1, \dots, n\} \setminus S_q$, L can be expressed in terms of contributions of the radii $\{r_1, \dots, r_n\}$ above and below r_{Q_q} via

$$L(\boldsymbol{\theta} \mid Q_q, \mathbf{y}) = \left[\prod_{i \in S'_q} f_{R \mid R \leq r_{Q_q}(\mathbf{W}), \mathbf{W}}(r_i) f_{\mathbf{W}}(\mathbf{w}_i) \right] \left[\prod_{i \in S_q} f_{R \mid R > r_{Q_q}(\mathbf{W}), \mathbf{W}}(r_i) f_{\mathbf{W}}(\mathbf{w}_i) \right]. \quad (35)$$

Under the assumption that the data generating mechanism of \mathbf{y} admits a Lebesgue density, Proposition 3 suggests that all angles $\{\mathbf{w}_1, \dots, \mathbf{w}_n\}$ may be used in the likelihood for the inference of $f_{\mathbf{W}} = r_{\mathcal{L}}^d / (d|\mathcal{L}|)$ used to model $\mathbf{W} \mid R > r_{Q_q}(\mathbf{W})$. In particular, when models M_1 or M_3 are used, substantial gains in the inference for G can be attained by also including in inference the angles at which non-exceedances occur. This is well illustrated in the simulation study of Supplemental D. Non-exceedance radii $\{r_i : i \in S'_q\}$, however, are assumed not to carry information about G and L based on Theorem 1 and we hence pose that L is constant with respect to them. Denoting by $S_{\mathbf{w}}$ the set of indices corresponding at least to all exceedances and at most to all observations—or $S_q \subseteq S_{\mathbf{w}} \subseteq \{1, \dots, n\}$ —the likelihood thus reduces to

$$\begin{aligned} L(\boldsymbol{\theta} \mid Q_q, \mathbf{y}) &\propto \prod_{i \in S_q} f_{R \mid R > r_{Q_q}(\mathbf{W}), \mathbf{W}}(r_i \mid \mathbf{w}_i) \prod_{i \in S_{\mathbf{w}}} f_{\mathbf{W}}(\mathbf{w}_i) \\ &= \exp \{-|S_{\mathbf{w}}| \log(d|\mathcal{L}|)\} \prod_{i \in S_q} f_{R_E \mid \mathbf{W}} \left[\frac{r_i - r_{Q_q}(\mathbf{w}_i)}{r_{G_q}(\mathbf{w}_i)} \mid \mathbf{w}_i \right] \prod_{i \in S_{\mathbf{w}}} r_{\mathcal{L}}(\mathbf{w}_i)^d, \end{aligned} \quad (36)$$

where $f_{R_E \mid \mathbf{W}}(z \mid \mathbf{w}) = [1 + \xi(\mathbf{w})z]_+^{-1/\xi(\mathbf{w})-1} / r_G(\mathbf{w})$. The likelihood function (36) is amenable to standard likelihood based inference using either frequentist or Bayesian methods when parametric models are selected for \mathcal{W} and \mathcal{G} .

When interest is in semi-parametric models for, a key complication arises when using the likelihood in expression (36). Evaluating the likelihood function (36) requires computing the constant $d|\mathcal{L}|$ which ensures the density of \mathbf{W} integrates to one. This normalising constant is in most cases impossible to compute exactly, which makes inference difficult. However, using the *Poisson transform* (Baker 1994), we can map the likelihood into an *equivalent* likelihood function $L(\boldsymbol{\theta}, \beta \mid Q_q, \mathbf{y})$ of a Poisson point process

defined in an expanded space given by

$$L(\boldsymbol{\theta}, \beta) = \exp \left[-|\mathcal{S}_{\mathbf{w}}| e^{\beta} (d|\mathcal{L}|) \right] \prod_{i \in \mathcal{S}_q} f_{R_E|\mathbf{W}} \left[\frac{r_i - r_{\mathcal{Q}_q}(\mathbf{w}_i)}{r_{\mathcal{G}_q}(\mathbf{w}_i)} \middle| \mathbf{w}_i \right] \prod_{i \in \mathcal{S}_{\mathbf{w}}} e^{\beta} r_{\mathcal{L}}(\mathbf{w}_i)^d, \quad (37)$$

where the latent variable β estimates the normalising constant $d|\mathcal{L}|$. The normalising constant is inferred as just another parameter at no loss of information (Barthelmé & Chopin 2015), whilst inference can be performed either using frequentist methods or in a fully Bayesian manner by assigning suitable prior distributions on \mathcal{G} , \mathcal{L} , and β (Guillen et al. 2023). We adopt the latter approach due to the optimality of Bayes as an information processing rule (Zellner 1988). The volume $d|\mathcal{L}|$ is computed using the computationally efficient numerical integration scheme of Simpson et al. (2016).

3.4 Inference for latent variables

Given n independent observations $\mathbf{y} := \{r_1 \mathbf{w}_1, \dots, r_n \mathbf{w}_n\}$ from $\mathbf{X} = R\mathbf{W} \in \mathbb{R}^d$, the latent quantities of interest are the set \mathcal{G} , the quantile set \mathcal{Q}_q and the set \mathcal{L} . In what follows, we detail the procedure to obtain realisations from the joint posterior distribution of these quantities.

We model the logarithms of the random radial functions $r_{\mathcal{Q}_q}$, $r_{\mathcal{G}_q}$ and $r_{\mathcal{L}}$ as Matérn (Gaussian) fields on \mathbb{S}^{d-1} using the stochastic partial differential equation (SPDE) approach by Lindgren et al. (2011), using $\alpha = 2$ (see their Equation (2)) which is also the default option in the R-INLA package (www.r-inla.org). We denote the respective random intercepts $\beta_{\mathcal{Q}}, \beta_{\mathcal{G}}, \beta_{\mathcal{L}} \in \mathbb{R}$ as well as their stochastic weights in the finite element representation (Lindgren et al. 2011, Equation (9)) as $\mathbf{z}_{\mathcal{Q}}, \mathbf{z}_{\mathcal{G}}, \mathbf{z}_{\mathcal{L}} \in \mathbb{R}^p$. We denote by $\boldsymbol{\theta} = (\beta_{\mathcal{Q}}, \mathbf{z}_{\mathcal{Q}}, \beta_{\mathcal{G}}, \mathbf{z}_{\mathcal{G}}, \beta_{\mathcal{L}}, \mathbf{z}_{\mathcal{L}}) \in \mathbb{R}^{3p+3}$ the set of all latent variables for our models, and it follows that the joint posterior distribution of $\boldsymbol{\theta}$ fully determines that of \mathcal{Q}_q , \mathcal{G} and \mathcal{L} . Due to the hierarchical structure of all proposed models detailed in Sections 3.2 and 3.3, the joint posterior density of $\boldsymbol{\theta}$ factorises according to $\pi[\boldsymbol{\theta} \mid \mathbf{y}] = \pi[\beta_{\mathcal{G}}, \mathbf{z}_{\mathcal{G}}, \beta_{\mathcal{L}}, \mathbf{z}_{\mathcal{L}} \mid \beta_{\mathcal{Q}}, \mathbf{z}_{\mathcal{Q}}, \mathbf{y}] \pi[\beta_{\mathcal{Q}}, \mathbf{z}_{\mathcal{Q}} \mid \mathbf{y}]$. We first fit the Bayesian Gamma log-linear quantile regression model described in Section 3.2 for a fixed probability q to all observations \mathbf{y} . Samples $\{(\beta_{\mathcal{Q},i}, \mathbf{z}_{\mathcal{Q},i}) : i = 1, \dots, n_{\mathcal{Q}}\}$ from the posterior density $\pi[\beta_{\mathcal{Q}}, \mathbf{z}_{\mathcal{Q}} \mid \mathbf{y}]$ map to a set of radial functions $\{r_{\mathcal{Q}_q,i} : i = 1, \dots, n_{\mathcal{Q}}\}$ which are then interpreted as candidate radial functions of a q -th quantile set. Given a radial function $r_{\mathcal{Q}_q,i}$, we define a set of exceedances through

$$\mathcal{Y}_i = \left\{ (r_j, \mathbf{w}_j) \in (0, \infty) \times \mathbb{S}^{d-1} : r_j > r_{\mathcal{Q}_q,i}(\mathbf{w}_j), r_j \mathbf{w}_j \in \mathbb{R}^d, j = 1, \dots, n \right\}. \quad (38)$$

We then fit model M_1 , M_2 , or M_3 to each collection of exceedances \mathcal{Y}_i , as detailed in Section 3.3, and also possibly include angles from non-exceedance data in the likelihood. This procedure yields a conditional posterior density $\pi[\beta_{\mathcal{G}}, \mathbf{z}_{\mathcal{G}}, \beta_{\mathcal{L}}, \mathbf{z}_{\mathcal{L}} \mid \beta_{\mathcal{Q},i}, \mathbf{z}_{\mathcal{Q},i}, \mathbf{y}]$ for each $i = 1, \dots, n_{\mathcal{Q}}$. Sampling $n_{\mathcal{G}\mathcal{L}}$ realisations jointly from each $\pi[\beta_{\mathcal{G}}, \mathbf{z}_{\mathcal{G}}, \beta_{\mathcal{L}}, \mathbf{z}_{\mathcal{L}} \mid \beta_{\mathcal{Q},i}, \mathbf{z}_{\mathcal{Q},i}, \mathbf{y}]$ provides an assembled sample of $n_{\mathcal{Q}} \cdot n_{\mathcal{G}\mathcal{L}}$ realisations from the joint posterior distribution of $\boldsymbol{\theta}$,

$$\{\boldsymbol{\theta}_{i,j} = (\beta_{\mathcal{Q},i}, \mathbf{z}_{\mathcal{Q},i}, \beta_{\mathcal{G},(i,j)}, \mathbf{z}_{\mathcal{G},(i,j)}, \beta_{\mathcal{L},(i,j)}, \mathbf{z}_{\mathcal{L},(i,j)}) \in \boldsymbol{\Theta} : i = 1, \dots, n_{\mathcal{Q}}, j = 1, \dots, n_{\mathcal{G}\mathcal{L}}\}. \quad (39)$$

For simplicity and without loss, we re-index the sample (39) from the posterior distribution of $\boldsymbol{\theta}$ to $\{\boldsymbol{\theta}_i : i = 1, \dots, n_{\boldsymbol{\theta}}\}$ with $n_{\boldsymbol{\theta}} := n_{\mathcal{Q}} \cdot n_{\mathcal{G}\mathcal{L}}$ and use this notation in the next sections. We shall also refer to the sampled latent functions $r_{\mathcal{Q}_q,i}$, $r_{\mathcal{G}_q,i}$, and $r_{\mathcal{L},i}$ constructed from $\boldsymbol{\theta}_i$.

Interval estimation for the latent fields $r_{\mathcal{Q}_q}$, $r_{\mathcal{G}_q}$, and $r_{\mathcal{L}}$ is accomplished via prediction intervals (see Bolin & Lindgren 2018). A $(1 - \alpha)$ prediction-interval for the value of a random field $Y : \Omega \rightarrow \mathbb{R}^{\mathbb{S}^{d-1}}$ at an angle $\mathbf{w} \in \mathbb{S}^{d-1}$ is the closed line segment $[q_{\alpha}(\mathbf{w})\mathbf{w} : q_{1-\alpha}(\mathbf{w})\mathbf{w}]$ where $q_{\alpha}(\mathbf{w})$ is the α -quantile of the distribution of $Y(\mathbf{w})$. A $(1 - \alpha)$ prediction interval for the process Y defined on \mathbb{S}^{d-1} consists of the strip $R_{1-\alpha} := \cup_{\mathbf{w} \in \mathbb{S}^{d-1}} R_{1-\alpha}(\mathbf{w})$ defined through $R_{1-\alpha}(\mathbf{w}) := [q_{\rho}(\mathbf{w})\mathbf{w} : q_{1-\rho}(\mathbf{w})\mathbf{w}]$ for some ρ such that $q_{\rho}(\mathbf{w})$

and $q_{1-\rho}(\mathbf{w})$ satisfy

$$\mathbb{P}\left[q_{\rho}(\mathbf{w}) \leq Y(\mathbf{w}) \leq q_{1-\rho}(\mathbf{w}), \mathbf{w} \in \mathbb{S}^{d-1}\right] = 1 - \alpha.$$

In the context of our latent fields $r_{\mathcal{Q}_q}$, $r_{\mathcal{G}_1}$, and $r_{\mathcal{L}}$, $(1 - \alpha)$ prediction interval consist of sets withing within which the true functions lie entirely with probability $1 - \alpha$. Prediction intervals can be obtained from a sample from the posterior distribution of a parameter of interest using the `excursions` package in R. (Bolin & Lindgren 2015, 2017).

3.5 Rare event probability estimation

Given n independent observations $\mathbf{y} := \{r_1 \mathbf{w}_1, \dots, r_n \mathbf{w}_n\}$ from $\mathbf{X} = R\mathbf{W} \in \mathbb{R}^d$, interest lies in the estimation of the probability that a new draw from $R\mathbf{W}$ falls within some Borel set $B \in \mathbb{R}^d \setminus \{0\}$ far enough from the origin ($0 \in \mathbb{R}^d$). We provide a framework for inference for $\mathbb{P}_{B|\mathbf{y}} := \mathbb{P}[R\mathbf{W} \in B | \mathbf{y}]$. For practical reasons, we restrict ourselves to sets B that are starshaped at 0 (see Appendix A.2). This is useful in our setting as it allows for an exact probability calculation with respect to our model specification for exceedances (see expression (46) below). In practice, common types of sets of interest are boxes $\{\mathbf{x} \in \mathbb{R}^d : \mathbf{a} \leq \mathbf{x} \leq \mathbf{b}, \mathbf{a}, \mathbf{b} \in \mathbb{R}^d\}$ and sets of the form $\{r\mathbf{w} : r > h(\mathbf{w}) > 0, r \in (0, \infty), \mathbf{w} \in \mathbb{S}^{d-1}\}$ for some positive function h defined on \mathbb{S}^{d-1} , both starshaped at 0, and our choice is hence not too restrictive. Inference for more complex sets is amenable through simple modifications of what follows.

For a set $B \in \mathbb{R}^d \setminus \{0\}$ starshaped at 0, define $S_B := \{\mathbf{w} \in \mathbb{S}^{d-1} : r\mathbf{w} \in B, r \in (0, \infty)\} \subseteq \mathbb{S}^{d-1}$ and consider, for any $\mathbf{w} \in S_B$, the partition $I_{\inf}(\mathbf{w}) \cup I_B(\mathbf{w}) \cup I_{\sup}(\mathbf{w})$ of $(0, \infty)$, where $I_{\inf}(\mathbf{w}) := (0, r_{B_{\inf}}(\mathbf{w}))$, $I_B(\mathbf{w}) := [r_{B_{\inf}}(\mathbf{w}), r_B(\mathbf{w})]$, and $I_{\sup}(\mathbf{w}) := (r_B(\mathbf{w}), \infty)$ for the radial function $r_B(\mathbf{w})$ of B and the function $r_{B_{\inf}}(\mathbf{w}) = \inf\{r > 0 : r\mathbf{w} \in B\}$. Then,

$$\mathbb{P}_{B|\mathbf{y}} = \mathbb{P}[R \in I_B(\mathbf{W}), \mathbf{W} \in S_B | \mathbf{y}], \quad (40)$$

The posterior predictive distribution in expression (40) is given from the posterior density of $\boldsymbol{\theta}$ via

$$\mathbb{P}_{B|\mathbf{y}} = \int_{\mathbb{R}^{3p+3}} \mathbb{P}[R \in I_B(\mathbf{W}), \mathbf{W} \in S_B | \boldsymbol{\theta}] \pi[\boldsymbol{\theta} | \mathbf{y}] d\boldsymbol{\theta}, \quad (41)$$

where $\pi[\boldsymbol{\theta} | \mathbf{y}]$ is obtained following the procedure described in Section 3.4. We now express $\mathbb{P}_{B|\boldsymbol{\theta}} := \mathbb{P}[R \in I_B(\mathbf{W}), \mathbf{W} \in S_B | \boldsymbol{\theta}]$ in terms of our model formulation and assumptions.

Unlike standard approaches that base inference on a fixed threshold and do not take into account the uncertainty in its estimation, all asymptotically motivated models proposed in Section 3.3 are defined in the random tail-region $R > r_{\mathcal{Q}_q}(\mathbf{W})$ where $r_{\mathcal{Q}_q}(\mathbf{w}) = \exp\{\beta_{\mathcal{Q}} + \boldsymbol{\psi}(\mathbf{w})^\top \mathbf{z}_{\mathcal{Q}}\}$ is a latent radial function capturing the uncertainty for the threshold set \mathcal{Q}_q . It follows that $r_{\mathcal{Q}_q}(\mathbf{w})$ intersects with any of the intervals $I_{\inf}(\mathbf{w})$, $I_B(\mathbf{w})$, or $I_{\sup}(\mathbf{w})$ with non-zero probability for $\mathbf{w} \in S_B$. Using total probability, we thus split the calculation of $\mathbb{P}_{B|\boldsymbol{\theta}}$ into the sum

$$\mathbb{P}_{B|\boldsymbol{\theta}} = \mathbb{P}[R\mathbf{W} \in B, R > r_{\mathcal{Q}_q}(\mathbf{W}) | \boldsymbol{\theta}] + \mathbb{P}[R\mathbf{W} \in B, R \leq r_{\mathcal{Q}_q}(\mathbf{W}) | \boldsymbol{\theta}], \quad (42)$$

and our model is best suited for sets B such that the second term in the equation (42) is small. The first term in equation (42) decomposes into

$$\begin{aligned} \mathbb{P}[R\mathbf{W} \in B, R > r_{\mathcal{Q}_q}(\mathbf{W}) | \boldsymbol{\theta}] &= \mathbb{P}[R \in I_B(\mathbf{W}) | \mathbf{W} \in S_B, R > r_{\mathcal{Q}_q}(\mathbf{W}), \boldsymbol{\theta}] \times \\ &\times \mathbb{P}[\mathbf{W} \in S_B | R > r_{\mathcal{Q}_q}(\mathbf{W}), \boldsymbol{\theta}] \mathbb{P}[R > r_{\mathcal{Q}_q}(\mathbf{W}) | \boldsymbol{\theta}]. \end{aligned} \quad (43)$$

By the assumptions detailed in Section 3.2, the last term $\mathbb{P}[R > r_{\mathcal{Q}_q}(\mathbf{W}) | \boldsymbol{\theta}]$ in equation (43) equals $1 - q$ for all $\boldsymbol{\theta} \sim \pi[\boldsymbol{\theta} | \mathbf{y}]$. Following our model formulation for \mathbf{W} , the second term in equation (43) corresponds

to the predictive distribution of the angles given $\boldsymbol{\theta}$ and is given by

$$\mathbb{P}[\mathbf{W} \in S_B \mid R > r_{\mathcal{Q}_q}(\mathbf{W}), \boldsymbol{\theta}] = \int_{S_B} f_{\mathbf{W}|\boldsymbol{\theta}}(\mathbf{w} \mid \boldsymbol{\theta}) d\mathbf{w} = \int_{S_B} \tilde{f}_{\mathbf{W}|\boldsymbol{\theta}}(\mathbf{w} \mid \boldsymbol{\theta}) d\mathbf{w} / \int_{\mathbb{S}^{d-1}} \tilde{f}_{\mathbf{W}|\boldsymbol{\theta}}(\mathbf{w} \mid \boldsymbol{\theta}) d\mathbf{w}, \quad (44)$$

where $\tilde{f}_{\mathbf{W}}$ is chosen from M_1 , M_2 , or M_3 (see Section 2.4), and $r_{\mathcal{G}_q}(\mathbf{w}) = \exp\{\beta_{\mathcal{G}} + \boldsymbol{\psi}(\mathbf{w})^\top \mathbf{z}_{\mathcal{G}}\}$, $r_{\mathcal{L}}(\mathbf{w}) = \beta_{\mathcal{L}} + \boldsymbol{\psi}(\mathbf{w})^\top \mathbf{z}_{\mathcal{L}}$. In practice, the integrals in equation (44) are obtained efficiently via numerical integration for $d = 2$ or 3 . The first term in equation (43) is obtained through

$$\mathbb{P}[R \in I_B(\mathbf{W}) \mid \mathbf{W} \in S_B, R > r_{\mathcal{Q}_q}(\mathbf{W}), \boldsymbol{\theta}] = \mathbb{E}_{\mathbf{W}|\mathbf{W} \in S_B, \boldsymbol{\theta}}(\mathbb{P}[R \in I_B(\mathbf{W}) \mid R > r_{\mathcal{Q}_q}(\mathbf{W}), \boldsymbol{\theta}]), \quad (45)$$

where the term $\mathbb{P}[R \in I_B(\mathbf{w}) \mid \mathbf{W} = \mathbf{w}, R > r_{\mathcal{Q}_q}(\mathbf{w}), \boldsymbol{\theta}]$ needed for the expectation calculation in equation (45) is equal to

$$F_{R_E|\mathbf{W}} \left[\frac{\max\{r_B(\mathbf{w}), r_{\mathcal{Q}_q}(\mathbf{w})\} - r_{\mathcal{Q}_q}(\mathbf{w})}{r_{\mathcal{G}_q}(\mathbf{w})} \middle| \mathbf{w} \right] - F_{R_E|\mathbf{W}} \left[\frac{\max\{r_{B_{\text{inf}}}(\mathbf{w}), r_{\mathcal{Q}_q}(\mathbf{w})\} - r_{\mathcal{Q}_q}(\mathbf{w})}{r_{\mathcal{G}_q}(\mathbf{w})} \middle| \mathbf{w} \right], \quad (46)$$

with $F_{R_E|\mathbf{W}}(z \mid \mathbf{w}) = 1 - [1 + \xi(\mathbf{w})z]_+^{-1/\xi(\mathbf{w})}$. In practice, we approximate expectation (45) through Monte-Carlo integration by sampling angles $\{\tilde{\mathbf{w}}_1, \dots, \tilde{\mathbf{w}}_{n_w}\}$ from $f_{\mathbf{W}}$ restricted to the set S_B via an acceptance-rejection scheme and calculating

$$n_w^{-1} \sum_{i=1}^{n_w} \mathbb{P}[R \in I_B(\tilde{\mathbf{w}}_i) \mid R > r_{\mathcal{Q}_q}(\tilde{\mathbf{w}}_i), \boldsymbol{\theta}] \rightarrow \mathbb{P}[R \in I_B(\mathbf{W}) \mid \mathbf{W} \in S_B, R > r_{\mathcal{Q}_q}(\mathbf{W}), \boldsymbol{\theta}], \quad (47)$$

as $n_w \rightarrow \infty$. The second term in equation (42), $p := \mathbb{P}[R\mathbf{W} \in B, R \leq r_{\mathcal{Q}_q}(\mathbf{W}) \mid \boldsymbol{\theta}]$, corresponds to a probability over a region in which our model is not specified. A simple solution for this issue is to consider the probability in question as the success probability of the binomially distributed random variable that describes the number of observations falling in the set $\mathcal{Q}_q \cap B$. In practice, for each $i \in \{1, \dots, n_{\boldsymbol{\theta}}\}$, we impose a binomial likelihood and beta prior for the parameter p , leading to a closed form beta posterior distribution. When $\mathcal{Q}_q \cap B \neq \emptyset$, we sample a probability from the posterior distribution of p and add it accordingly in equation (42).

In practice, inference for $\mathbb{P}_{B|\mathbf{y}}$ is performed by first collecting a sample $\{\boldsymbol{\theta}_1, \dots, \boldsymbol{\theta}_{n_{\boldsymbol{\theta}}}\}$ from $\pi[\boldsymbol{\theta} \mid \mathbf{y}]$ through the procedure described in Section 3.4, and then calculating $\mathbb{P}_{B|\boldsymbol{\theta}_i}$ for each $i \in \{1, \dots, n_{\boldsymbol{\theta}}\}$. *A posteriori* mean estimates corresponding to the Monte-Carlo integration

$$n_{\boldsymbol{\theta}}^{-1} \sum_{i=1}^{n_{\boldsymbol{\theta}}} \mathbb{P}_{B|\boldsymbol{\theta}_i} \rightarrow \mathbb{P}_{B|\mathbf{y}}, \quad \text{as } n_{\boldsymbol{\theta}} \rightarrow \infty, \quad (48)$$

approximating equation (41). Equal-tailed credible intervals from the sample $\{\mathbb{P}_{B|\boldsymbol{\theta}_i} : i = 1, \dots, n_{\boldsymbol{\theta}}\}$ hence complete the inference procedure for $\mathbb{P}_{B|\mathbf{y}}$.

3.6 Model selection and validation

Our model formulation gives rise to various modelling choices needing to be assessed and validated. For instance, as discussed in Section 3.3, selecting the most appropriate model within the set of candidate models M_1 , M_2 , and M_3 given observed data amounts to analysing the properties of the distribution of $R, \mathbf{W} \mid R > r_{\mathcal{Q}_q}(\mathbf{W})$ with respect to the association between $g_{\mathcal{G}}$ and $f_{\mathbf{W}}$. Another modelling choice requiring assessment is that of the set of angles contributing to likelihood (37) since it translates into a bias-variance trade-off for \mathcal{G} and \mathcal{L} . Further, hyper-parameters values imposed on the prior distributions of \mathcal{Q}_q , \mathcal{G} , and \mathcal{L} imply *a priori* information on the differentiability properties of their boundaries (see Section 3.4), and their impact on the posterior may need assessment. Finally, the usual concern of the

sensitivity of the posterior distribution of the latent variables to the return period for the latent threshold function $r_{\mathcal{Q}_q}$ (Section 3.2) remains. We detail possible methods for model selection and validation below.

The nested structure of model M_2 within the parameter space of model M_3 raises the question of whether model M_2 can serve as a sensible simplification of model M_3 given observed data $\mathbf{y} = \{r_1 \mathbf{w}_1, \dots, r_n \mathbf{w}_n\}$. As discussed in Section 3.3, evidence for a constant $r_{\mathcal{B}}$ in model M_3 points to evidence that M_2 can serve as a sensible simplification of M_3 , or equivalently that the observed data \mathbf{y} may come from a process following a homothetic density with respect to its gauge function $g_{\mathcal{G}}$. Given a sample of random functions $\{\psi(\mathbf{w})^\top \mathbf{z}_{\mathcal{B},i} : i = 1, \dots, n_\theta\}$ from the posterior distribution of the latent random field $\psi(\mathbf{w})^\top \mathbf{z}_{\mathcal{B}}$, we obtain a 0.95 prediction interval, $R_{0.95}$, for $\psi(\mathbf{W})^\top \mathbf{z}_{\mathcal{B}}$ through the procedure described in Section 3.4. We say there is evidence against a homothetic underlying density whenever there is some non-empty subset $S_0 \subset \mathbb{S}^{d-1}$ such that $0 \notin R_{0.95}(\mathbf{w})$ for $\mathbf{w} \in S_0$.

The sensitivity of the posterior distributions of the latent parameters to the remaining modelling choices discussed in the beginning of this section can be assessed through the quality of the calibration of the posterior predictive distribution to the observed data. Given a set of observed exceedances \mathcal{Y}_i of a sampled latent function $r_{\mathcal{Q}_q,i}$ (see expression (38)), we wish to assess the calibration of the predictive distribution for the excess variable $R - r_{\mathcal{Q}_q,i}(\mathbf{W}) \mid R > r_{\mathcal{Q}_q,i}(\mathbf{W})$. We thus compare each observed excess $r_j - r_{\mathcal{Q}_q,i}(\mathbf{w}_j)$ with the quantile of the $\text{Exponential}(r_{\mathcal{G}_q}(\mathbf{w}_j))$, with $\log r_{\mathcal{G}_q}(\mathbf{w}) = \beta_{\mathcal{G}} + \psi(\mathbf{w})^\top \mathbf{z}_{\mathcal{G}}$ and $(\beta_{\mathcal{G}}, \mathbf{z}_{\mathcal{G}}) \sim \pi[\beta_{\mathcal{G}}, \mathbf{z}_{\mathcal{G}} \mid \beta_{\mathcal{Q},i}, \mathbf{z}_{\mathcal{Q},i}, \mathbf{y}]$. We draw exceedance radii $\{\tilde{r}_1, \dots, \tilde{r}_{n_s}\}$ from their predictive distribution $\text{Exp}(r_{\mathcal{G}_q}(\mathbf{w}_j))$, and define the empirical distribution function $F_{\mathbf{w}_j, n_s}(r) := n_s^{-1} \sum_{k=1}^{n_s} \mathbb{1}[\tilde{r}_k \leq r]$, for $r \in (0, \infty)$. A probability-probability (PP) plot for the exceedances \mathcal{Y}_i is then given by

$$\left\{ \left(\frac{j}{|\mathcal{Y}_i| + 1}, p_{(j)} \right) : j = 1, \dots, |\mathcal{Y}_i| \right\}, \quad (49)$$

where $p_{(j)}$ denotes the j -th order statistic of the sample $\{F_{\mathbf{w}_j, n_s}(r_j - r_{\mathcal{Q}_q,i}(\mathbf{w}_j)) : j = 1, \dots, |\mathcal{Y}_i|\}$. A quantile-quantile (QQ) plot in unit exponential margins for the exceedances \mathcal{Y}_i is then easily obtained via probability-probability (PP) plot for the exceedances \mathcal{Y}_i via

$$\left\{ \left(-\log \left(1 - \frac{j}{|\mathcal{Y}_i| + 1} \right), -\log (1 - p_{(j)}) \right) : j = 1, \dots, |\mathcal{Y}_i| \right\}. \quad (50)$$

In a similar fashion, we can obtain PP plots for the predictive distribution of $\mathbf{W} \mid R > r_{\mathcal{Q}_q,i}(\mathbf{W})$. This is achieved by sampling angles $\{\tilde{\mathbf{w}}_1, \dots, \tilde{\mathbf{w}}_{n_s}\}$ from the predictive density $f_{\mathbf{W}|\beta_{\mathcal{G}}, \mathbf{z}_{\mathcal{G}}, \beta_{\mathcal{B}}, \mathbf{z}_{\mathcal{B}}, \mathbf{y}}$ where $(\beta_{\mathcal{G}}, \mathbf{z}_{\mathcal{G}}, \beta_{\mathcal{B}}, \mathbf{z}_{\mathcal{B}}) \sim \pi[\beta_{\mathcal{G}}, \mathbf{z}_{\mathcal{G}}, \beta_{\mathcal{B}}, \mathbf{z}_{\mathcal{B}} \mid \beta_{\mathcal{Q},i}, \mathbf{z}_{\mathcal{Q},i}, \mathbf{y}]$. We transform the sampled angles and the observed angles from \mathcal{Y} to spherical coordinates, respectively denoted $\{\tilde{\boldsymbol{\varphi}}_j = (\tilde{\varphi}_{1,j}, \dots, \tilde{\varphi}_{d-1,j}) \in \Phi : j = 1, \dots, n_s\}$ and $\{\boldsymbol{\varphi}_j = (\varphi_{1,j}, \dots, \varphi_{d-1,j}) \in \Phi : j = 1, \dots, |\mathcal{Y}_i|\}$, and consider the empirical distribution function $F_{n_s}(\boldsymbol{\varphi}) := n_s^{-1} \sum_{k=1}^{n_s} \mathbb{1}[\tilde{\boldsymbol{\varphi}}_k \leq \boldsymbol{\varphi}]$. A PP plot for the calibration of the predictive distribution of angles to the observed angles in \mathcal{Y}_i is then given by expression (49) with $p_{(j)}$ denoting the j -th order statistic of the sample $\{F_{n_s}(\boldsymbol{\varphi}_j) : j = 1, \dots, |\mathcal{Y}_i|\}$.

4 Data analyses

4.1 Thames tributary river flow

We test our model-fitting on a bivariate dataset consisting of river flow measurements for the rivers Pang and Windrush, both tributaries of the River Thames in England, measured in cubic meters per second, $m^3 s^{-1}$. For each site, we are provided with daily measurements from 1968 to 2008. This dataset has been previously analyzed by [Keef et al. \(2013\)](#) who advocated the use of the Laplace distribution in the context of modelling extreme values using the conditional approach to multivariate extremes first introduced in [Heffernan & Tawn \(2004\)](#). Given that there are a total of $n = 14545$ bivariate measurements, we have sufficient data to fit a hierarchical Bayesian quantile regression model for the radial function $r_{\mathcal{Q}_q}$

at the high quantile of $q = 0.95$. In agreement with the previous literature (Keef et al. 2013), we consider data in standard Laplace margins, of which we were already provided. Given the light-tailed nature of the margins, we use the Gamma likelihood family in quantile regression to obtain a radial threshold along angles. Once fitted, we sample 20 radial functions $r_{\mathcal{Q}_q, i}$, $i = 1, \dots, 20$, from the posterior distribution of the threshold $\pi[\beta_{\mathcal{Q}}, z_{\mathcal{Q}} \mid \mathbf{y}]$. Figure 7 shows the fitted posterior radial quantile set \mathcal{Q}_q and it is observed that our posterior mean estimate of the anglewise threshold capture the quantile of radii at given angle values with little uncertainty.

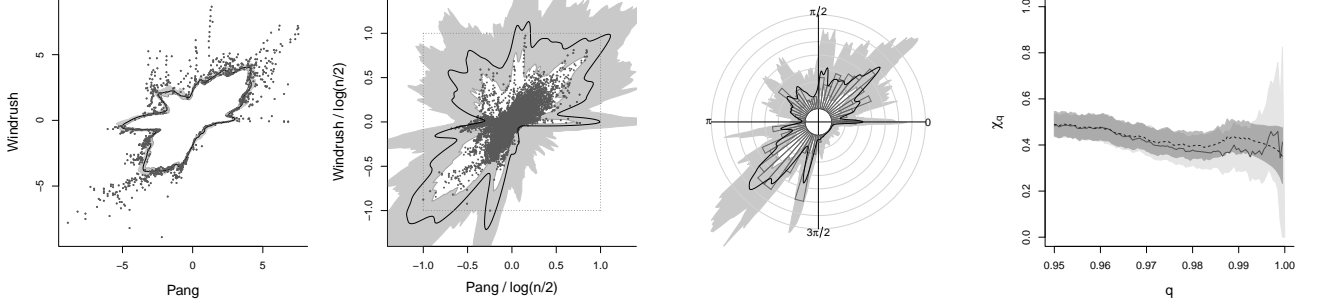


Figure 7: Left to right: Posterior mean of $\partial\mathcal{Q}_q$ with 0.95 predictive intervals. Posterior mean of the boundary of the limit set, $\partial\mathcal{G}$, with 0.95 predictive intervals. Histogram of observed angles with posterior mean density of angles and 0.95 prediction intervals. Empirical (solid line) and posterior mean (dashed line) of χ_q values with 0.95 confidence intervals (light grey) and model predictive intervals (dark grey).

At each of these sampled threshold curves $r_{\mathcal{Q}_q, i}$ we fit the joint model for the gauge function and the angular density via the fitting of the likelihood function (36), and subsequently sample 50 posterior values of the gauge function $g_{\mathcal{G}}$ evaluated at a mesh for the unit sphere \mathbb{S}^1 for $n_{\theta} = 1000$ posterior samples in total. In all, we fit 6 different models for the density of angles, M_1 , M_2 , and M_3 , where each model is fitted using either exceedance angles and the entire dataset’s angles. For simplicity, we assume that normalised exceedances are exponentially-distributed. In other words, we fix the tail index parameter as $\xi = 0$ in the representation given by Assumption 2, and assume we are in the realm of condition (ii) of Proposition 2. A more refined assumption that normalised exceedances follow a GP-type distribution (i.e., assuming $\xi \neq 0$) will be considered in future work. From Figure 26 in Appendix E.1, model M_2 fitted on exceedance angles only produces a posterior estimate of the gauge function whose unit level set best captures the shape of the $\log(n/2)$ -scaled sample cloud of data in Laplace margins with the least amount of uncertainty. Furthermore, Figure 27 shows that this model provides a good approximation of the density of angles, but not the best approximation. Despite this, we say that model M_2 fitted on exceedance angles is best overall. We proceed by only considering this model.

It is of interest to assess how well our joint modeling procedure approximates the distribution of angles in the dataset. As shown in Figure 7, the posterior mean curve overlays nicely with the empirical histogram of angles from the dataset, suggesting our joint modeling of exceedances and angles provide well-fitting posteriors. The PP plot in Figure 29 of Section E.1 shows good agreement between the posterior predictive distribution and the observed data, further justifying the performance of our model.

Figure 7 shows posterior estimates of $\chi_q = \chi_q(1, 2)$ for values of q approaching 1. The agreement with empirical and posterior mean model-based estimates as q varies, as well as the overlapping confidence intervals, show the ability of our posterior model to capture the extremal dependence of this dataset. Furthermore, the return level boundary curves in Figure 2 in Section 1 accurately portray the intricacies of the dataset as angles vary along the unit simplex \mathbb{S}^1 . Above each curve corresponding to a value T , we are given an estimated region in which we expect to observe joint river flow measurements with probability $1/T$. Based on the size of the dataset, we expect to see a small number of points from the initial dataset beyond the return level curve corresponding to $T = 10^3$, which is confirmed by Figure 2. The increased uncertainty in the further return level sets reflect the further extrapolation needed to describe

events occurring in these regions. Lastly, the QQ plots for exponential exceedances in Section E.1 of the supplementary material shows there is good agreement with the empirical and model-based estimates in their abilities to extrapolate extreme values.

4.2 Newlyn wave heights

We now proceed to fit a model on a dataset with dimension $d = 3$. The dataset consists of hourly measurements of wave characteristics: wave height (H , in meters), wave period (P , in seconds), and surge (S , in meters), measured over the period 1971–1977 at the Newlyn port in south-west England. The Newlyn wave height dataset was first analysed in [Coles & Tawn \(1994\)](#) in the case where asymptotic dependence was assumed between all 3 variables. Like in the previous literature, we take componentwise maxima over 15-hour periods, resulting in a dataset of size $n = 2,894$. The margins X_H, X_P, X_S of the data are unknown, and the choice was made to standardise to Laplace using $X_{L,j} = F^{-1}(\hat{F}(X_j))$ for $j = H, S, P$ where F^{-1} is the quantile function of the univariate standard Laplace distribution, and \hat{F} is given by an empirical cdf below a high marginal threshold and by a GP distribution above a high marginal threshold. This marginal operation was previously used in [Coles & Tawn \(1991\)](#) for transforming to unit Fréchet margins, and was implemented in the context of the Newlyn wave dataset in [Wadsworth & Campbell \(2022\)](#) for transforming the margins to standard exponential, with the latter approach allowing for more flexible modelling of the extremal dependence structure. We note that in practice, the GP parameters were estimated using maximum likelihood in a frequentist manner. In future work, a fully Bayesian technique can be used to account for the uncertainty from the estimation of these marginal parameters. For the time being, this additional layer of complexity is neglected.

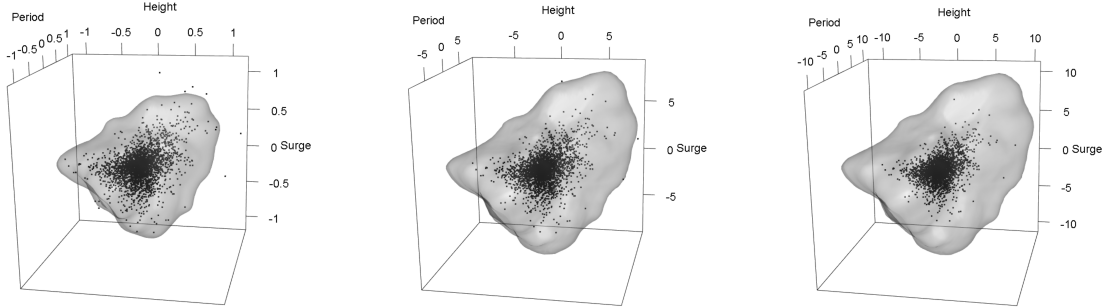


Figure 8: Left: Estimated posterior mean unit level set of the gauge function with $\log(n/2)$ -scaled data in Laplace margins. Centre: Posterior mean return set with $T = 10^3$ and data in Laplace margins. Right: Posterior mean return set with $T = 10^4$ and data in Laplace margins.

As is done in the river flow analysis of Section 4.2, we fit the hierarchical Bayesian gamma quantile regression model described in Section 3 at the $q = 0.9$ quantile to obtain the posterior distribution $\pi[\beta_Q, z_Q \mid \mathbf{y}]$. For the subsequent joint model of exceedances and angles, we once again assume an exponential-type family on normalised exceedances, and it is deemed through our model checks that M_2 fitted on exceedance angles only provides the best overall joint fit (see Section E.2 of the supplementary material), and we are left with the joint posterior model $\pi[\beta_G, z_G \mid \beta_Q, z_Q, \mathbf{y}]$. As in Section 4.1, we sample 20 observations from the posterior threshold model $\pi[\beta_Q, z_Q \mid \mathbf{y}]$, and at each threshold, we sample 50 observations from the joint model of exceedances and angles $\pi[\beta_G, z_G \mid \beta_Q, z_Q, \mathbf{y}]$, resulting in $n_\theta = 1000$. Figure 8 shows the unit level set for the model M_2 with the posterior mean boundaries of the $T = 10^3, 10^4$ return level sets, as described in Section 2.6. We see that we are able to capture the extremal dependence structure of our dataset quite well by the clear correspondence between the posterior mean unit level set of g_G and the scaled sample cloud.

Figure 9 shows posterior mean estimates of $\chi_q(A)$ for $A \in \{HP, HS, PS, HPS\}$ and for $q \in (0.9, 1)$

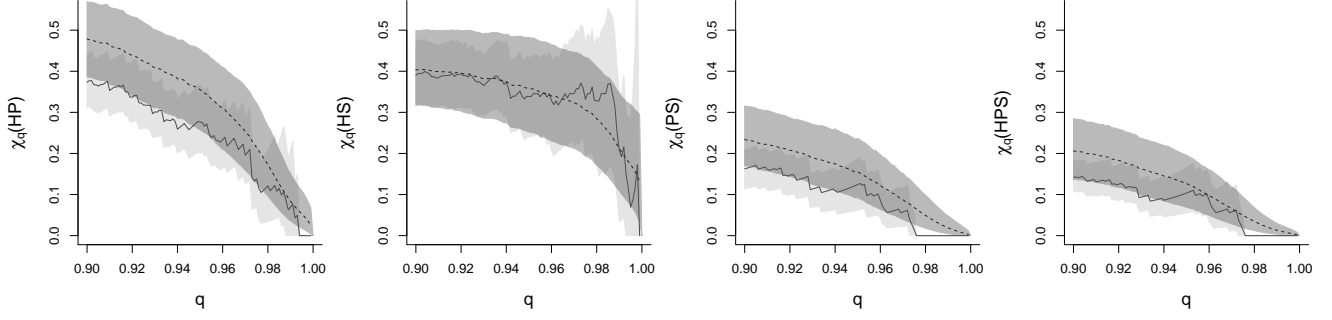


Figure 9: χ_q plots for all pairwise combinations of marginal variables and for all three marginal variables. Solid line is an empirical estimate with 95% bootstrap confidence intervals in light grey, and the dashed line is a model-based estimate with 95% posterior confidence intervals in dark grey.

with posterior 95% confidence intervals. [Wadsworth & Campbell \(2022\)](#) establish that the variable groups *HP*, *PS*, and *HPS* are asymptotically independent, and that *HS* is asymptotically dependent. With this in mind, we conclude that our posterior joint model is able to accurately describe the extremal dependence structure presented in this dataset. Figure 9 correctly shows posterior estimates of $\chi_q(A)$ tending to 0 as q tends to 1 for the asymptotically independent groups, and tending to a nonzero value close to the empirical estimate for the asymptotically dependent pair *HS*. Furthermore, the QQ plots in Figures 31 in Section E.2 of the supplementary material show that there is good agreement with the empirical and model-based estimates in their abilities to extrapolate exceedances to extreme values. Figure 32 in Section E.2 of the supplementary material shows PP plots for angles generated from the posterior density of angles from $\pi[\beta_{\mathcal{L}}, z_{\mathcal{L}} \mid \beta_{\mathcal{Q}}, z_{\mathcal{Q}}, \mathbf{y}]$ have good agreement with the dataset's empirical angular distribution.

Lastly, for random vectors in the dataset's original margins $\mathbf{X} = (X_H, X_S, X_P)^\top$, it is of interest to estimate the return level for the overtopping discharge rate $Q(v; \mathbf{X})$ over a wall of height v . First introduced in [Coles & Tawn \(1994\)](#), Q is interpreted as the volume of water (in cubic meters, m^3) overtopping the sea-wall per unit length (in meters, m) over a fixed duration (in seconds, s) and is thus measured in $m^3 s^{-1} m^{-1}$. For the application at hand, $Q(v; \mathbf{X}) := a_1 X_S X_P \exp\{a_2 (v - X_S - l)/(X_P X_H^{*1/2})\}$. The wave height component X_H^* is a calibration of the wave height marginal variable X_H to approximate the actual off-shore wave height, since measurements are taken on-shore. We estimate the sea-wall height

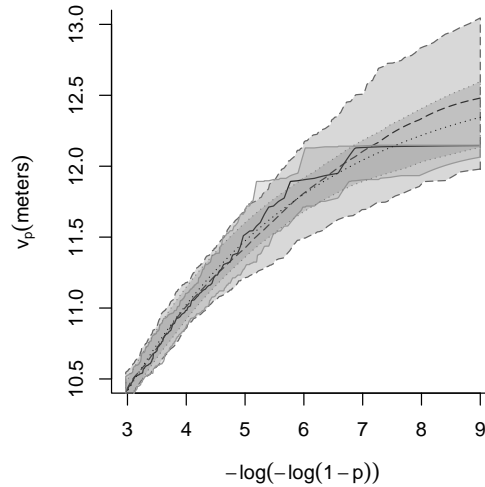


Figure 10: Estimated return levels for sea-wall height. Presented are results from empirical fits (solid black line), GP (dotted black line), and our semi-parametric method (dashed black line). Grey regions are 95% confidence intervals, with the boundary line types agreeing with their corresponding black lines.

structure variable v_p (in meters, m) for which the discharge rate value $Q(v_p; \mathbf{X})$ is expected to exceed the design standard of $0.002m^3s^{-1}m^{-1}$ with probability p . That is, setting $V = Q^{-1}(0.002; \mathbf{X})$, we solve $\Pr(V > v_p) = p$ for v_p using realizations of V generated through simulation and reverse marginal transformation. As in [Bortot et al. \(2000\)](#), we fix the sea-wall design feature constants to $a_1 = 0.25$, $a_2 = 26$, and tidal level relative to the seabed to $l = 4.3$. We obtain three separate estimates for v_p at a range of p values. First, an empirical estimate of v_p is obtained by using the empirical quantile function on values of the structure variable V computed from the dataset. Second, a GP model is fitted using the dataset's computed values of V obtained from the dataset, and quantiles are then obtained for v_p . Lastly, we use our estimated joint posterior distribution for the exceedances and angles $\pi[\beta_G, \mathbf{z}_G \mid \beta_Q, \mathbf{z}_Q, \mathbf{y}]$, to generate exceedance an observed dataset of \mathbf{X}' length $n = 2,894$. We sample a posterior threshold $r_{Q_q,i}(\mathbf{w})$ from the fitted distribution $\pi[\beta_Q, \mathbf{z}_Q \mid \mathbf{y}]$. Based on this threshold, sample angles \mathbf{w} gauge function values $g_G(\mathbf{w})$ from the joint distribution $\pi[\beta_G, \mathbf{z}_G \mid \beta_Q, \mathbf{z}_Q, \mathbf{y}]$ and radial exceedance observations $r - r_{Q_q,i}(\mathbf{w})$ from the $\text{Exponential}(g_G(\mathbf{w}))$ distribution. The values $r\mathbf{w}$ is added to our new dataset, joined with sub-asymptotic values from the initial dataset. With this new dataset \mathbf{X}' , we first convert to original margins via $X_j = \tilde{F}^{-1}(F(X'_{L,j}))$ for $j = H, S, P$, and we compute values of the structure variable, v_p , for p values that correspond to extremal observations of sea-wall height, $p \in (0, 0.10)$. This procedure is repeated 200 times, and we compute p -wise sample means and 95% confidence intervals for v_p . Figure 10 shows the resulting estimates of v_p for a range of p values. In this figure, we follow convention and plot $-\log(-\log(1 - p))$ against v_p , and it can be concluded that, compared to the empirical and GP distribution fit approach, our method accurately estimates the sea-wall height variable v_p across all values of $p \in (0, 0.10)$. The larger confidence intervals corresponding to our semi-parametric method are due to accounting for sampling variation. For each of the 200 repetitions, we generate a new dataset \mathbf{X}' . Each repetition will lead to different structure variable estimates. Note that this variability is not accounted for in the empirical and GPD fits, where bootstrap confidence intervals are computed from the original dataset.

Acknowledgments

We thank Jennifer L. Wadsworth for insightful discussions on the framework of geometric extremes, and Finn Lindgren for guidance with the `inlabru` and `excursions` packages in the **R** computing language. Part of this paper was written during a visit of IP and LDM at King Abdullah University of Science and Technology and during a visit of RC at the University of Edinburgh. RC acknowledges funding by the EPSRC DTP EP/W523811/1 fund at Lancaster University, with additional funding provided by NSERC PGS D (Canada), and the FRQNT doctoral fund (Québec). LDM acknowledges funding by the School of Mathematics, University of Edinburgh.

Disclaimer

The main results of this paper, including Theorem 1 and the concepts presented in Section 2.6 were first presented at the 13th International Conference on Extreme Value Analysis (EVA), June 2023, Milan. After EVA, we became aware through personal communication of parallel independent work related to the notion of return level-sets, as described in Section 2.6, done by Emma S. Simpson at University College London and Jonathan A. Tawn at Lancaster University. As of now, there is no publicly available document to reference their work.

References

- Baker, S. G. (1994), ‘The multinomial-Poisson transformation’, *Journal of the Royal Statistical Society: Series D (The Statistician)* **43**(4), 495–504.

- Balkema, A. A. & de Haan, L. (1974), ‘Residual life time at great age’, *The Annals of probability* **2**(5), 792–804.
- Balkema, G. & Nolde, N. (2010), ‘Asymptotic independence for unimodal densities’, *Advances in Applied Probability* **42**(2), 411–432.
- Barnett, V. (1976), ‘The ordering of multivariate data (with discussion)’, *J. Roy. Statist. Soc., A* **139**, 318–355.
- Barthelmé, S. & Chopin, N. (2015), ‘The Poisson transform for unnormalised statistical models’, *Statistics and Computing* **25**(4), 767–780.
- Bolin, D. & Lindgren, F. (2015), ‘Excursion and contour uncertainty regions for latent Gaussian models’, *Journal of the Royal Statistical Society, Series B (Statistical Methodology)* **77**(1), 85–106.
- Bolin, D. & Lindgren, F. (2017), ‘Quantifying the uncertainty of contour maps’, *Journal of Computational and Graphical Statistics* **26**(3), 513–524.
- Bolin, D. & Lindgren, F. (2018), ‘Calculating probabilistic excursion sets and related quantities using excursions’, *Journal of Statistical Software* **86**(5), 1–20.
- Bortot, P., Coles, S. & Tawn, J. (2000), ‘The multivariate Gaussian tail model: An application to oceanographic data’, *JRSSC* **49**(1), 31–049.
- Coles, S. G. (2001), *An Introduction to Statistical Modeling of Extreme Values*, Springer–Verlag, London.
- Coles, S. G. & Tawn, J. A. (1991), ‘Modelling extreme multivariate events’, *J. Roy. Statist. Soc., B* **53**, 377–392.
- Coles, S. G. & Tawn, J. A. (1994), ‘Statistical methods for multivariate extremes: an application to structural design (with discussion)’, *Appl. Statist.* **43**, 1–48.
- Davison, A. C. & Smith, R. L. (1990), ‘Models for exceedances over high thresholds’, *J. Roy. Statist. Soc., B* **52**, 393–442.
- de Haan, L. (1970), *On Regular Variation and its Application to the Weak Convergence of Sample Extremes*, Vol. 32 of *Mathematical Centre Tracts*, Mathematisch Centrum, Amsterdam.
- de Haan, L. (1984), ‘A spectral representation for max-stable processes’, *Ann. Probab.* **12**, 1194–1204.
- de Haan, L. & Resnick, S. (1987), ‘On regular variation of probability densities’, *Stochastic processes and their applications* **25**, 83–93.
- de Haan, L. & Resnick, S. I. (1977), ‘Limit theory for multivariate sample extremes’, *Z. Wahrsch. Theor.* **40**, 317–337.
- de Haan, L. & Stadtmüller, U. (1996), ‘Generalized regular variation of second order’, *Journal of the Australian Mathematical Society* **61**(3), 381–395.
- Engelke, S. & Hitz, A. S. (2020), ‘Graphical models for extremes (with discussion)’, *J. Roy. Statist. Soc. Ser. B*.
- Fasiolo, M., Wood, S. N., Zaffran, M., Nedellec, R. & Goude, Y. (2021), ‘Fast calibrated additive quantile regression’, *Journal of the American Statistical Association* **116**(535), 1402–1412.
- Gradshteyn, I. S. & Ryzhik, I. M. (2014), *Table of Integrals, Series, and Products*, Academic press.

- Guillen, R. A., Lindgren, F., Muff, S., Glass, T. W., Breed, G. A. & Schlägel, U. E. (2023), ‘Accounting for unobserved spatial variation in step selection analyses of animal movement via spatial random effects’, *bioRxiv* .
- Hansen, G., Herbut, I., Martini, H. & Moszyńska, M. (2020), ‘Starshaped sets’, *Aequationes mathematicae* **94**, 1001–1092.
- Heffernan, J. E. & Tawn, J. A. (2004), ‘A conditional approach for multivariate extreme values (with discussion)’, *J. Roy. Statist. Soc., B* **66**(3), 1–34.
- Keef, C., Papastathopoulos, I. & Tawn, J. A. (2013), ‘Estimation of the conditional distribution of a multivariate variable given that one of its components is large: additional constraints for the Heffernan and Tawn model’, *J. Mult. Anal* **115**, 396–404.
- Kiriliouk, A., Rootzén, H., Segers, J. & Wadsworth, J. L. (2019), ‘Peaks over thresholds modeling with multivariate generalized Pareto distributions’, *Technometrics* **61**(1), 123–135.
- Klain, D. A. (1997), ‘Invariant valuations on star-shaped sets’, *advances in mathematics* **125**(1), 95–113.
- Koenker, R. (2005), *Quantile regression*, Vol. 38, Cambridge university press.
- Kotz, S., Kozubowski, T. J. & Podgorski, K. (2001), ‘The laplace distribution and generalizations’, (*No Title*) .
- Ledford, A. W. & Tawn, J. A. (1996), ‘Statistics for near independence in multivariate extreme values’, *Biometrika* **83**, 169–187.
- Ledford, A. W. & Tawn, J. A. (1997), ‘Modelling dependence within joint tail regions’, *J. Roy. Statist. Soc., B* **59**, 475–499.
- Lindgren, F., Rue, H. & Lindström, J. (2011), ‘An explicit link between Gaussian fields and Gaussian Markov random fields: the stochastic partial differential equation approach (with discussion)’, *J. Roy. Statist. Soc., B* **73**, 423–498.
- Lutwak, E. (1988), ‘Intersection bodies and dual mixed volumes’, *Advances in Mathematics* **71**(2), 232–261.
- Majumder, R., Shaby, B. A., Reich, B. J. & Cooley, D. (2023), ‘Semiparametric estimation of the shape of the limiting multivariate point cloud’.
- Maulik, K. & Resnick, S. (2004), ‘Characterizations and examples of hidden regular variation’, *Extremes* **7**(1), 31–67.
- Nolde, N. (2014), ‘Geometric interpretation of the residual dependence coefficient’, *Journal of Multivariate Analysis* **123**, 85–95.
- Nolde, N. & Wadsworth, J. (2021), ‘Linking representations for multivariate extremes via a limit set’, *Advances in Applied Probability* .
- Papastathopoulos, I. & Paulin, D. (2023), ‘Markov random tail fields and extended multivariate regularly varying functions’. Unpublished research.
- Papastathopoulos, I. & Tawn, J. A. (2013), ‘A generalised Student’s t -distribution’, *Stat. Probabil. Lett.* **83**, 70–77.
- Pickands, J. (1975), ‘Statistical inference using extreme order statistics’, *Ann. Statist.* **3**, 119–131.

- Resnick, S. I. (2007), *Heavy-tail phenomena: probabilistic and statistical modeling*, Springer Science & Business Media.
- Rootzén, H. & Tajvidi (2006), ‘The multivariate generalized Pareto distribution’, *Bernoulli* **12**, 917–930.
- Seneta, E. (2006), *Regularly Varying Functions*, Vol. 508, Springer, New York.
- Simpson, D., Illian, J. B., Lindgren, F., Sørbye, S. H. & Rue, H. (2016), ‘Going off grid: computationally efficient inference for log-Gaussian Cox processes’, *Biometrika* **103**(1), 49–70.
- Simpson, E. S. & Tawn, J. A. (2022), ‘Estimating the limiting shape of bivariate scaled sample clouds for self-consistent inference of extremal dependence properties’, *arXiv preprint* [arXiv:2207.02626](https://arxiv.org/abs/2207.02626).
- Soms, A. P. (1976), ‘An asymptotic expansion for the tail area of the t-distribution’, *Journal of the American Statistical Association* **71**(355), 728–730.
- Wadsworth, J. & Campbell, R. (2022), ‘Statistical inference for multivariate extremes via a geometric approach’, *arXiv preprint* [arXiv:2208.14951](https://arxiv.org/abs/2208.14951).
- Wadsworth, J. & Tawn, J. (2013), ‘A new representation for multivariate tail probabilities’, *Bernoulli* **19**(5B), 2689–2714.
- Waldmann, E., Kneib, T., Yue, Y. R., Lang, S. & Flexeder, C. (2013), ‘Bayesian semiparametric additive quantile regression’, *Statistical Modelling* **13**(3), 223–252.
- Wood, S. N. (2017), *Generalized Additive Models: an Introduction with R*, CRC press.
- Yu, K. & Moyeed, R. A. (2001), ‘Bayesian quantile regression’, *Stat. Probabil. Lett.* **54**(4), 437–447.
- Zellner, A. (1988), ‘Optimal information processing and bayes’s theorem’, *The American Statistician* **42**(4), 278–280.

A Technical background

A.1 Vague convergence

For a detailed exposition of the concept of vague convergence, see [Resnick \(2007\)](#). Let \mathbb{K} be a locally compact metric space with countable base (e.g., \mathbb{R}^d) and let $M_+(\mathbb{K})$ be the class of nonnegative Radon measures on Borel subsets of \mathbb{K} . If $\mu_n \in M_+(\mathbb{K})$ for $n \geq 0$, then we say that μ_n converges vaguely to μ (presented as $\mu_n \xrightarrow{v} \mu$) if

$$\lim_{n \rightarrow \infty} \int_{\mathbb{K}} f d\mu_n = \int_{\mathbb{K}} f d\mu.$$

for all bounded continuous functions f with compact support.

A.2 Background on starshaped sets

An expository review and survey of material about the fundamental mathematical notion of starshaped sets, emphasising their geometric, analytical, combinatorial, and topological properties, is given by [Hansen et al. \(2020\)](#) and references therein.

If a and b are different elements of \mathbb{R}^d , then $[a : b] = \{(1 - t)a + tb : 0 \leq t \leq 1\}$ denotes the segment with endpoints a and b , $[a : b) = \{(1 - t)a + tb : t \geq 0\}$ denotes the half-line with origin a through b , $(a : b) = \{(1 - t)a + tb : 0 \leq t \in \mathbb{R}\}$ denotes the line through a and b , $]a : b] = \{(1 - t)a + tb : 0 < t \leq 1\}$ denotes the segment $[a : b]$ without its endpoint a , $[a : b[= \{(1 - t)a + tb : 0 \leq t < 1\}$ denotes the segment

$[a : b]$ without its endpoint b and $]a : b) = \{(1-t)a + tb : t > 0\}$ denotes the ray $[a, b)$ without its origin a . A set $G \subset \mathbb{R}^d$ is called starshaped if there exists $x \in G$ such that every point $y \in G$ is visible from x in the sense that $[x : y] \subset G$. If G is a set and $x \in G$, the star of x in G is the set of all points in G that are visible from x , that is, $\text{st}(x : G) = \{y \in G : [x : y] \subset G\}$. A set G is starshaped if and only if there exists $x \in G$ such that $\text{st}(x : G) = G$. The kernel of a set G , denoted by $\ker G$, is the convex set of all of its star centres, that is, $\ker G = \{x \in G : \text{st}(x : G) = G\}$. A star set is called a star-body if it is a compact regular domain, that is if G is a compact starshaped set such that G° is connected and $G = \overline{G^\circ}$. Let G be a closed proper subset of \mathbb{R}^d with non-empty interior. Then G is said to be strongly starshaped at a whenever there exists $a \in \mathbb{R}^d$ such that for every $\mathbf{w} \in \mathbb{S}^{d-1}$, the halfline $a + [0 : \mathbf{w})$ does not intersect the boundary ∂G of G more than once. A strongly starshaped set at a is a starshaped set with $a \in \ker G$. A set G is said to be strongly starshaped if it is strongly starshaped at 0. We write $\Delta_{\mathbf{w}}$ for the half-line through the origin $[0 : \mathbf{w})$ passing through $\mathbf{w} \in \mathbb{S}^{d-1}$. If G is starshaped at $m \in \ker G$, we say that $z \in G$ is the last point of a ray $[m : x)$ in G if $z \in [m : x)$ and there is no point $y \in [m : x) \cap G$ such that $y \notin [m : z]$. Let G be a starshaped set such that $(\ker G)^\circ \neq \emptyset$. If $m \in (\ker G)^\circ$ and $x \in \overline{G}$, then $[m : x[\subset G$. If G is a closed starshaped set such that $(\ker G)^\circ \neq \emptyset$, then G° is connected and $G = \overline{(G^\circ)}$, whence a regular domain.

A.3 Radial addition and gauges of starshaped sets

If G is a closed starshaped set, $m \in \ker G$ and $\mathbf{w} \in \mathbb{S}^{d-1}$, then there are two cases. There exists a last point p of $m + \Delta_{\mathbf{w}}$ in G or $m + \Delta_{\mathbf{w}} \subset G$. In the first case, let

$$\rho_{m,G}(\mathbf{w}) = \sup\{\lambda \in \mathbb{R} : m + \lambda\mathbf{w} \in G\}.$$

The *radial function* of G at m is the function $r_{m,G} : \mathbb{S}^{d-1} \rightarrow \mathbb{R}_+$ defined by

$$r_{m,G}(\mathbf{w}) = \begin{cases} \rho_{m,G}(\mathbf{w}) & m + \Delta_{\mathbf{w}} \not\subset G \\ +\infty & m + \Delta_{\mathbf{w}} \subseteq G. \end{cases}$$

We have the equivalence $m \in (\ker G)^\circ \Leftrightarrow r_{m,G} > 0$. Also, if G is compact and $m \in (\ker G)^\circ$, then $r_{m,G}$ is a Lipschitz function.

Let \star denote the space of star-bodies in \mathbb{R}^d and $+, \cdot : \star \times \star \rightarrow \star$ be the operators of *radial addition* and *radial multiplication* respectively, defined by means of radial functions as as

$$\rho_{G_1+G_2}(\mathbf{w}) = \rho_{G_1}(\mathbf{w}) + \rho_{G_2}(\mathbf{w}), \quad G_1, G_2 \in \star, \quad (\text{A.1})$$

$$(\text{A.2})$$

$$\rho_{G_1 \cdot G_2}(\mathbf{w}) = \rho_{G_1}(\mathbf{w}) \rho_{G_2}(\mathbf{w}), \quad G_1, G_2 \in \star. \quad (\text{A.3})$$

Multiplication of a set $G \in \star$ by a nonnegative scalar c is equivalent to radial multiplication of G by $B_c(0)$, that is, $cG := B_c(0) \cdot G$, $c \geq 0$. The set \star equipped with the binary operation $+$ is a commutative monoid. In other words, $(\star, +)$ satisfies the following.

Identity element: There exists an element $0 \in \star$ such that $0 + G = G + 0 = G \ \forall G \in \star$.

Commutative law: For G_1 and G_2 in \star , $G_1 + G_2 = G_2 + G_1$.

Additionally, we have

Scalar Multiplication Closure: The result of \cdot between a compact star set and a non-negative scalar remains within the space of compact star sets.

Distributive Laws: The operations $+$ and \cdot obey distributive laws similar to those in a ring. For example, $(G_1 + G_2) \cdot B_c(0) = G_1 \cdot B_c(0) + G_2 \cdot B_c(0)$.

Associativity: Both $+$ and \cdot are associative operations. For example, $(G_1 + G_2) + G_3 = G_1 + (G_2 + G_3)$.

The monoid $(\star, +)$ is endowed with its algebraic preordering \leq defined by $G_1 \leq G_2$ whenever there exists $H \in \star$ such that $G_1 + H = G_2$. In this case, we define radial subtraction $H = G_2 - G_1$ through ordinary difference of radial functions.

The algebraic structure on the space of compact star sets with the operations $+$ and \cdot provides a mathematical framework to explore relationships, transformations, and compositions of these sets. This algebraic approach facilitates the development of consistent theories and methodologies when dealing with operations involving compact star sets.

Last, let G_1 and G_2 be two star-bodies such that ρ_{S_i} is continuous on \mathbb{S}^{d-1} . Then the dual Brunn-Minkowski inequality (Lutwak 1988) yields

$$|G_1 + G_2|^{1/d} \leq |G_1|^{1/d} + |G_2|^{1/d},$$

and equality holds if $d = 1$ or $d \geq 2$ and $G_2 = rG_1$, for some $r > 0$. If G is compact and strongly starshaped, then the volume of G can be expressed by the formula

$$|G| = \frac{1}{d} \int_{\mathbb{S}^{d-1}} r_G(\mathbf{w})^d d\mathbf{w}, \quad (\text{A.4})$$

see Klain (1997). The reciprocal of the radial function of a set G starshaped at 0 is called the gauge function $g_G : \mathbb{R}^d \setminus \{0\} \rightarrow \mathbb{R}_+$, defined by $g_G(\mathbf{x}) = \inf\{t \geq 0 : \mathbf{x} \in tG\}$ for $\mathbf{x} \in \mathbb{R}^d \setminus \{0\}$.

B Examples

Full details of the derivations for all examples in this section can be found in Supplementary A and Supplementary B.

Example 1 (Multivariate normal distribution with standard normal marginal distributions). *For real-valued entries $\mathbf{x} \in \mathbb{R}^d$ and positive definite precision matrix \mathbf{Q} , the joint density in standard Normal margins is*

$$f(\mathbf{x}) = (2\pi)^{-d/2} |\mathbf{Q}|^{1/2} \exp\left(-\mathbf{x}^\top \mathbf{Q} \mathbf{x} / 2\right) = f_0(g_G(\mathbf{x}))$$

where $f_0(s) = (2\pi)^{-d/2} |\mathbf{Q}|^{1/2} \exp(-s^2/2)$, $g_G(\mathbf{x}) = \sqrt{\mathbf{x}^\top \mathbf{Q} \mathbf{x}}$ and higher-order terms

$$\begin{aligned} u_1(\mathbf{x}) &= \frac{d}{2} \log 2\pi - \frac{1}{2} \log |\mathbf{Q}|, \\ u_2(\mathbf{x}) &= 0. \end{aligned}$$

The density of angles is

$$f_{\mathbf{W}}(\mathbf{w}) = \Gamma(d/2) 2^{-1} \pi^{-d/2} |\mathbf{Q}|^{1/2} (\mathbf{w}^\top \mathbf{Q} \mathbf{w})^{-d/2}, \quad \mathbf{w} \in \mathbb{S}^{d-1}.$$

Example 2 (Multivariate normal distribution with standard Laplace marginal distributions). *For real-valued entries $\mathbf{x} \in \mathbb{R}^d$ and positive definite precision matrix \mathbf{Q} , the joint density in standard Laplace*

margins is

$$f_{[L]}(\mathbf{x}) = |\mathbf{Q}|^{-1/2} 2^{-d} (2\pi)^{-d/2} e^{-\sum |x_i|^{1/2}} \prod_{j=1}^d \frac{f_L(x_j)}{\varphi[\Phi^{-1}\{F_L(x_j)\}]} \\ \times \exp \left\{ -\frac{1}{2} [\Phi^{-1}\{F_L(\mathbf{x})\}]^\top \mathbf{Q} [\Phi^{-1}\{F_L(\mathbf{x})\}] \right\}$$

where ϕ and Φ are the univariate standard normal density and distribution functions, respectively. We obtain the joint density in the form of (A.12) with

$$g_{\mathcal{G}}(\mathbf{x}) = \left\{ \text{sgn}(\mathbf{x}) |\mathbf{x}|^{1/2} \right\}^\top \mathbf{Q} \left\{ \text{sgn}(\mathbf{x}) |\mathbf{x}|^{1/2} \right\} \\ u_1(\mathbf{x}) = \frac{d}{2} - \frac{1}{2} \left\{ \text{sgn}(\mathbf{x}) |\mathbf{x}|^{1/2} \right\}^\top \mathbf{Q} \left\{ \text{sgn}(\mathbf{x}) |\mathbf{x}|^{-1/2} \right\} \\ u_2(\mathbf{x}) = \left\{ \text{sgn}(\mathbf{x}) |\mathbf{x}|^{1/2} \right\}^\top \mathbf{Q} \left\{ \text{sgn}(\mathbf{x}) \log 2 |\mathbf{x}|^{-1/2} \right\} \\ - \frac{1}{2} \left\{ \text{sgn}(\mathbf{x}) |\mathbf{x}|^{1/2} \right\}^\top \mathbf{Q} \left\{ \text{sgn}(\mathbf{x}) |\mathbf{x}|^{-1/2} \log(4\pi |\mathbf{x}|) \right\} \\ + \frac{1}{2} \log |\mathbf{Q}| + \sum_{i=1}^d \frac{1}{2} \log 4\pi |x_i|$$

The angular density is

$$f_{\mathbf{W}}(\mathbf{w}) = (1-q)^{-1} 2^{-d} |\mathbf{Q}|^{-1/2} \left(\prod_{j=1}^d 4\pi |w_j| \right)^{-1/2} \\ \times \exp \left\{ -\sum_{j=1}^d |w_j| - \left(\text{sgn}(\mathbf{w}) |\mathbf{w}|^{1/2} \right)^\top \mathbf{Q} \left((\log 2) \text{sgn}(\mathbf{w}) |\mathbf{w}|^{-1/2} \right) \right. \\ \left. + \frac{1}{2} \left(\text{sgn}(\mathbf{w}) |\mathbf{w}|^{1/2} \right)^\top \mathbf{Q} \left((\log 4\pi |\mathbf{w}|) \text{sgn}(\mathbf{w}) |\mathbf{w}|^{-1/2} \right) \right\} \\ \times \Gamma \left\{ \frac{d}{2} + \left(\text{sgn}(\mathbf{w}) |\mathbf{w}|^{1/2} \right)^\top \mathbf{Q} \left(\text{sgn}(\mathbf{w}) |\mathbf{w}|^{-1/2} \right) \right\} \\ \times \left\{ \left(\text{sgn}(\mathbf{w}) |\mathbf{w}|^{1/2} \right)^\top \mathbf{Q} \left(\text{sgn}(\mathbf{w}) |\mathbf{w}|^{-1/2} \right) \right\}^{-\frac{d}{2} - \left(\text{sgn}(\mathbf{w}) |\mathbf{w}|^{1/2} \right)^\top \mathbf{Q} \left(\text{sgn}(\mathbf{w}) |\mathbf{w}|^{-1/2} \right)} \\ \times \left[1 - F_{\text{Gamma}} \left(r_{\mathcal{Q}_q}(\mathbf{w}); \frac{d}{2} + \left(\text{sgn}(\mathbf{w}) |\mathbf{w}|^{1/2} \right)^\top \mathbf{Q} \left(\text{sgn}(\mathbf{w}) |\mathbf{w}|^{-1/2} \right), \left(\text{sgn}(\mathbf{w}) |\mathbf{w}|^{1/2} \right)^\top \mathbf{Q} \left(\text{sgn}(\mathbf{w}) |\mathbf{w}|^{-1/2} \right) \right) \right] \\ \times \{1 + o(1)\}, \quad \mathbf{w} \in \mathbb{S}^{d-1},$$

where $F_{\text{Gamma}}(\cdot; \alpha, \beta)$ is the cumulative distribution function of the univariate Gamma distribution with shape parameter $\alpha > 0$ and rate parameter $\beta > 0$.

Example 3 (Multivariate Laplace distribution with standard Laplace marginal distributions). For real-valued entries $\mathbf{x} \in \mathbb{R}^d$ and positive definite precision matrix \mathbf{Q} , the joint density of the multivariate Laplace distribution with standard Laplace margins is

$$f_{[L]}(\mathbf{x}) = |\mathbf{Q}|^{1/2} (2\pi)^{-d/2} (\mathbf{x}^\top \mathbf{Q} \mathbf{x})^{v/2} K_v[(\mathbf{x}^\top \mathbf{Q} \mathbf{x})^{1/2}]$$

where $v = (2-d)/2$ and K_v is the modified Bessel function of the second kind (Gradshteyn & Ryzhik

2014). We obtain the joint density in the form of (A.12) with

$$\begin{aligned} g_{\mathcal{G}}(\mathbf{x}) &= (\mathbf{x}^{\top} \mathbf{Q} \mathbf{x})^{1/2} \\ u_1(\mathbf{x}) &= (d-1)/2 \\ u_2(\mathbf{x}) &= -d \log 2 + \frac{d}{2} \log 2\pi - \frac{1}{2} \log |\mathbf{Q}| - \frac{1}{2} \log(\pi/2) + \frac{d}{4} \log (\mathbf{x}^{\top} \mathbf{Q} \mathbf{x}) \end{aligned}$$

The angular density is

$$f_{\mathbf{W}}(\mathbf{w}) = \Gamma(d/2) 2^{-1} \pi^{-d/2} |\mathbf{Q}|^{1/2} (\mathbf{w}^{\top} \mathbf{Q} \mathbf{w})^{-d/2} \quad \mathbf{w} \in \mathbb{S}^{d-1}.$$

Example 4 (Multivariate Student- t_{ν} distribution with Student- t_{ν} marginal distributions (\mathbf{Q} positive definite, $\nu > 0$)). The joint density can be expressed as $f(\mathbf{x}) = f_0(g_{\mathcal{G}}(\mathbf{x}))$, where

$$\begin{aligned} f_0(s) &= k_{\nu, \mathbf{Q}} (1 + \nu^{-1} s^2)^{-\frac{1}{2}(\nu+d)}, \\ g_{\mathcal{G}}(\mathbf{x}) &= (\mathbf{x}^{\top} \mathbf{Q} \mathbf{x})^{1/2}, \end{aligned}$$

and $k_{\nu, \mathbf{Q}} = \Gamma(\frac{\nu+d}{2}) / \left\{ \Gamma(\frac{\nu}{2}) \nu^{d/2} \pi^{d/2} |\mathbf{Q}|^{-1/2} \right\}$. with higher-order terms given by

$$u(\mathbf{x}) = -\frac{1}{2}(\nu + d) \nu g_{\mathcal{G}}(\mathbf{x})^{-2-(\nu+d)} + o(1)$$

The angular density is

$$f_{\mathbf{W}}(\mathbf{w}) = \Gamma\left(\frac{d}{2}\right) 2^{-1/2} \pi^{-d/2} |\mathbf{Q}|^{1/2} (\mathbf{w}^{\top} \mathbf{Q} \mathbf{w})^{-d/2}$$

Example 5 (Multivariate Student- t_{ν} distribution with Student- t_{ν} marginal distributions (\mathbf{Q} positive definite, $\nu < 0$)). The joint density arises from the generalised Student's t_{ν} distribution (Papastathopoulos & Tawn 2013) with $\nu < 2 - d$, and can be expressed in the form $f(\mathbf{x}) = f_0(g_{\mathcal{G}}(\mathbf{x}))$, where

$$\begin{aligned} f_0(s) &= \frac{\pi^{-d/2} |\mathbf{Q}|^{1/2} |\nu|^{1-\frac{d}{2}} \Gamma\left(\frac{|\nu|}{2}\right)}{(|\nu| - d) \Gamma\left(\frac{|\nu|-d}{2}\right)} (1 - s^2)^{-\frac{1}{2}(\nu+d)}; s \in (-1, 1), \\ g_{\mathcal{G}}(\mathbf{x}) &= (-\nu^{-1} \mathbf{x}^{\top} \mathbf{Q} \mathbf{x})^{1/2}, \end{aligned}$$

and the support is given by $\{\mathbf{x} \in \mathbb{R}^d : 1 + \nu^{-1} \mathbf{x}^{\top} \mathbf{Q} \mathbf{x} > 0\}$. Therefore, $r_{\mathcal{G}}(\cdot) = g_{\mathcal{G}}(\cdot)^{-1}$ is a -1 -homogeneous radial function, and $r_{\mathcal{G}}(\mathbf{x}) \mathbf{x}$ lies on the boundary of the support (i.e., $f\{r_{\mathcal{G}}(\mathbf{x}) \mathbf{x}\} = 0$). By the intuition provided by condition (i) in Proposition 2, the rate of convergence can be characterised by

$$\frac{f\{r_{\mathcal{G}}(\mathbf{x}) (\mathbf{x} - t^{-1} \mathbf{1})\}}{k_{\nu, \mathbf{Q}} t^{\frac{1}{2}(\nu+d)}} = -\frac{2}{r_{\mathcal{G}}(\mathbf{x})} \nabla r_{\mathcal{G}}(\mathbf{x}) + o(1)$$

The angular density is

$$f_{\mathbf{W}}(\mathbf{w}) = 2^{-1} \pi^{-d/2} |\mathbf{Q}|^{1/2} \Gamma\left(\frac{d}{2}\right) (\mathbf{w}^{\top} \mathbf{Q} \mathbf{w})^{-d/2}$$

Example 6 (Multivariate Student- t_{ν} distribution with standard Laplace marginal distributions (\mathbf{Q} posi-

tive definite, $\nu > 0$)).

$$f_L(\mathbf{x}) = \frac{c_\nu^{d+2} k_{\nu, \mathbf{Q}} q_{j^* j^*}}{\nu^{d+1}} \exp \left\{ \frac{1}{\nu} \sum_{j=1}^d |x_j| - \left(1 + \frac{d}{\nu} \right) \max_{j=1, \dots, d} |x_j| \right\} (1 + o(1)),$$

where $k_{\nu, \mathbf{Q}} = \Gamma(\frac{\nu+d}{2}) / \left\{ \Gamma(\frac{\nu}{2}) \nu^{d/2} \pi^{d/2} |\mathbf{Q}|^{-1/2} \right\}$, $c_\nu = \left\{ 2\Gamma(\frac{\nu+1}{2}) \nu^{(\frac{1-\nu}{2})} \Gamma(\frac{\nu}{2})^{-1} (\nu\pi)^{-1/2} \right\}^{1/\nu}$, and j^* is such that $|x_{j^*}| = \max_{j=1, \dots, d} |x_j|$. We obtain the joint density in the form of (A.12) with

$$\begin{aligned} g_{\mathcal{G}}(\mathbf{x}) &= -\frac{1}{\nu} \sum_{j=1}^d |x_j| + \left(1 + \frac{d}{\nu} \right) \max_{j=1, \dots, d} |x_j| \\ u_1(\mathbf{x}) &= -\log \left(\frac{c_\nu^{d+2} k_{\nu, \mathbf{Q}} q_{j^* j^*}}{\nu^{d+1}} \right) \\ u_2(\mathbf{x}) &= 0 \end{aligned}$$

The angular density of exceedance angles is

$$\begin{aligned} f_{\mathbf{W}}(\mathbf{w}) &= (1-q)^{-1} \frac{c_\nu^{d+2} q_{j^* j^*} k_{\nu, \mathbf{Q}}}{\nu^{d+2}} \Gamma(d) \left[\left(1 + \frac{d}{\nu} \right) \max_{j=1, \dots, d} |w_j| - \frac{1}{\nu} \sum_{j=1}^d |w_j| \right]^{-d} \\ &\times \left[1 - F_{\text{Gamma}} \left(r_{\mathcal{Q}_q}(\mathbf{w}); d, \left(1 + \frac{d}{\nu} \right) \max_{j=1, \dots, d} |w_j| - \frac{1}{\nu} \sum_{j=1}^d |w_j| \right) \right] \{1 + o(1)\} \end{aligned}$$

Example 7 (Multivariate max-stable Logistic distribution with standard Fréchet marginal distributions). For positive entries $\mathbf{x} \in \mathbb{R}_+^d$, the joint density in standard Fréchet margins is

$$f(\mathbf{x}) = \left(\sum_{\pi \in \Pi} (-1)^{|\pi|} \prod_{s \in \pi} V_s(\mathbf{x}) \right) \exp \{-V(\mathbf{x})\}$$

where $V(\mathbf{x}) = \left(\sum_{j=1}^d x_j^{-1/\theta} \right)^\theta$ is a -1 -homogeneous exponent function with dependence parameter $\theta \in (0, 1)$, and V_s is the $|s|$ -order partial derivative of V with respect to inputs whose indices are in s (see Supplementary A.4). The 1-homogeneous gauge function is

$$g_{\mathcal{G}}(\mathbf{x}) = V(\mathbf{x})^{-1}$$

with higher order term

$$u_1(\mathbf{x}) = -\log \left[\sum_{\pi \in \Pi} (-1)^{|\pi|} \prod_{s \in \pi} \left\{ (-\theta)^{|s|-1} \left(\prod_{k \in s} x_k \right)^{-\frac{1}{\theta}-1} \left(\sum_{j=1}^d x_j^{-1/\theta} \right)^{\theta-|s|} \right\} \right]$$

The density of angles is given by

$$f_{\mathbf{W}}(\mathbf{w}) = \sum_{\pi \in \Pi} (-1)^{|\pi|} \prod_{s \in \pi} \left[(-1)^{|s|} \theta^{|s|-1} \Gamma(|s|) \left(\prod_{k \in s} w_k \right)^{-\frac{1}{\theta}-1} \left(\sum_{j=1}^d w_j^{-1/\theta} \right)^{\theta-|s|-\theta|s|} \right]$$

Example 8 (Multivariate max-stable Logistic distribution with standard Laplace marginal distributions).

For real-valued entries $\mathbf{x} \in \mathbb{R}^d$, the joint density in standard Laplace margins is

$$f_{[L]}(\mathbf{x}) = \left[\prod_{j=1}^d \frac{f(x_j)}{F(x_j) [\log F(x_j)]^2} \right] \left(\sum_{\pi \in \Pi} \prod_{s \in \pi} -V_s \left\{ [-\log F(x_1)]^{-1}, \dots, [-\log F(x_1)]^{-1} \right\} \right) \\ \times \exp \left(-V \left\{ [-\log F(x_1)]^{-1}, \dots, [-\log F(x_1)]^{-1} \right\} \right) \quad (\text{A.5})$$

We obtain the joint density in the form of (A.12) with

$$g_{\mathcal{G}}(\mathbf{x}) = \begin{cases} \frac{1}{\theta} \sum_{j=1}^d x_j + (1 - \frac{d}{\theta}) \min_{k=1, \dots, d} x_k & ; x_j > 0 \forall j \\ \frac{1}{\theta} \sum_{j: x_j > 0} x_j + \left(\sum_{k: x_k < 0} (-x_k)^{1/\theta} \right)^{\theta} & ; \text{o.w.} \end{cases}$$

$$u_1(\mathbf{x}) = \begin{cases} -\log \left(2^{-1} (-1)^{d+1} \left(\prod_{\ell=1}^{d-1} (1 - \frac{\ell}{\theta}) \right) \right) & ; x_j > 0 \forall j \\ d-1 & ; x_j < 0 \forall j \\ -(\frac{1}{\theta} - 1) |B| - 1 + \frac{d}{\theta} & ; \text{o.w.} \end{cases}$$

$$u_2(\mathbf{x}) = \begin{cases} 0 & ; x_j > 0 \forall j \\ -\log \left[(-1)^{d+1} \left(\prod_{\ell=0}^{d-1} (1 - \frac{\ell}{\theta}) \right) \right. \\ \quad \times \left. \left(\prod_{j=1}^d (-x_j) \right)^{\frac{1}{\theta}-1} \left(\sum_{j=1}^d (-x_j)^{1/\theta} \right)^{\theta-d} \right] & ; x_j < 0 \forall j \\ -\log \left[(-1)^{d+1} \left(\prod_{\ell=0}^{d-1} (1 - \frac{\ell}{\theta}) \right) 2^{-\frac{|A|}{\theta}} (\log 2)^{-2|C|} \right. \\ \quad - (\frac{1}{\theta} - 1) \sum_{k \in B} \log(-x_k) \\ \quad \left. - (\theta - d) \log \left(\sum_{k \in B} (-x_k)^{1/\theta} \right) \right] & ; \text{o.w.} \end{cases}$$

where $\theta \in (0, 1)$ is the dependence parameter. The angular density is

$$f_{\mathbf{W}}(\mathbf{w}) = (1-q)^{-1} (-1)^{d+1} \left\{ \prod_{\ell=0}^{d-1} \left(1 - \frac{\ell}{\theta} \right) \right\} 2^{-\frac{1}{\theta} \sum_{j=1}^d \mathbf{1}_{\{w_j > 0\}}} (\log 2)^{-2 \sum_{j=1}^d \mathbf{1}_{\{w_j = 0\}}} \\ \times \left(\prod_{k: x_k < 0} (-w_k)^{\frac{1}{\theta}-1} \right) \left(\sum_{k: w_k < 0} (-x_k)^{1/\theta} \right)^{\theta-d} \\ \times \Gamma \left\{ \left(\frac{1}{\theta} - 1 \right) \left(\sum_{j=1}^d \mathbf{1}_{\{w_j < 0\}} - d \right) + 1 \right\} \left[\frac{1}{\theta} \sum_{j: w_j > 0} x_j + \left(\sum_{k: x_k < 0} (-w_k)^{1/\theta} \right)^{\theta} \right]^{-\left(\frac{1}{\theta}-1\right) \left(\sum_{j=1}^d \mathbf{1}_{\{w_j < 0\}} - d \right) - 1} \\ \times \left[1 - F_{\text{Gamma}} \left(r_{\mathcal{Q}_q}(\mathbf{w}); \left(\frac{1}{\theta} - 1 \right) \left(\sum_{j=1}^d \mathbf{1}_{\{w_j < 0\}} - d \right) + 1, \frac{1}{\theta} \sum_{j: w_j > 0} x_j + \left(\sum_{k: x_k < 0} (-w_k)^{1/\theta} \right)^{\theta} \right) \right] \\ \times \{1 + o(1)\}$$

Example 9 (Wishart distribution). For positive definite entries $\mathbf{x} \in \mathbb{R}^{d \times d}$, positive-definite scale matrix $\mathbf{V} \in \mathbb{R}^{d \times d}$ whose entries are positive, and $\nu > d - 1$ degrees of freedom, the joint density is

$$f_{\mathbf{X}}(\mathbf{x}) = \left\{ 2^{(\nu d)/2} |\mathbf{V}|^{\nu/2} \Gamma_d(\nu/2) \right\}^{-1} |\mathbf{x}|^{(\nu-d-1)/2} \exp\{-\text{tr}(\mathbf{V}^{-1}\mathbf{x})/2\}$$

where Γ_d is the multivariate gamma function. By taking the negative logarithm, we obtain the joint density in the form of (A.12) with

$$\begin{aligned} g_{\mathcal{G}}(\mathbf{x}) &= \frac{1}{2} \text{tr}(\mathbf{V}^{-1}\mathbf{x}) \\ u_1(\mathbf{x}) &= -\frac{d}{2}(\nu - d - 1) \\ u_2(\mathbf{x}) &= \log \left\{ 2^{(\nu d)/2} |\mathbf{V}|^{\nu/2} \Gamma_d(\nu/2) \right\} - \frac{1}{2}(\nu - d - 1) \log \{|\mathbf{x}|\} \end{aligned}$$

The angular density is

$$\begin{aligned} f_{\mathbf{W}}(\mathbf{w}) &= (1-q)^{-1} \left\{ 2^{(\nu d)/2} |\mathbf{V}|^{\nu/2} \Gamma_d(\nu/2) \right\}^{-1} |\mathbf{w}|^{\frac{1}{2}(\nu-d-1)} \Gamma \left\{ \frac{d}{2}(\nu - d + 1) \right\} \left\{ \frac{1}{2} \text{tr}(\mathbf{V}^{-1}\mathbf{w}) \right\}^{-\frac{d}{2}(\nu-d+1)} \\ &\quad \times \left[1 - F_{\text{Gamma}} \left(r_{\mathcal{Q}_d}(\mathbf{w}); \frac{d}{2}(\nu - d + 1), \frac{1}{2} \text{tr}(\mathbf{V}^{-1}\mathbf{w}) \right) \right] \{1 + o(1)\} \end{aligned}$$

where $\mathbf{w} \in \mathbb{R}^{d \times d}$ is a positive definite angular matrix defined by $\mathbf{w} = \mathbf{x}/\|\mathbf{x}\|$ for some matrix-norm $\|\cdot\|$.

C Remainder term and quality of convergence

C.1 Rates of convergence

Let

$$f_{[L]}(t\mathbf{x}) = \exp\{-g_{\mathcal{G}_L}(t\mathbf{x}) + \text{remainder}\}(1 + o(1)), \quad \text{as } t \rightarrow \infty, \quad (\text{A.6})$$

where the remainder is interpreted as the evaluation $u(r\mathbf{w})$ of a function $u : \mathbb{K} \rightarrow \mathbb{R}$ at $r\mathbf{w} \in \mathbb{K}$. The domain of the function u is assumed to be a solid cone \mathbb{K} in $\mathbb{R}^d \setminus \{0\}$. A characterisation of the map u under second-order conditions (de Haan & Stadtmüller 1996) is given in Section C.1. A functional $u : \mathbb{R}^d \setminus \{0\} \rightarrow \mathbb{R}$ is said to determine the rate of convergence to $g_{\mathcal{G}}$ in expression (19) if it satisfies

$$f_{[L]}(t\mathbf{x}) = \exp(-[tg_{\mathcal{G}}(\mathbf{x})\{1 + o(1)\}]) = \exp[-\{g_{\mathcal{G}}(t\mathbf{x}) + u(t\mathbf{x})\}\{1 + o(1)\}], \quad \mathbf{x} \in \mathbb{R}^d \setminus \{0\}, \quad (\text{A.7})$$

as $t \rightarrow \infty$. Two functionals u_1 and u_2 that determine the rate of convergence to $g_{\mathcal{G}}$ are asymptotically equivalent, that is, $\lim_{t \rightarrow \infty} u_1(t\mathbf{x})/u_2(t\mathbf{x}) = 1, \forall \mathbf{x} \in \mathbb{R}^d \setminus \{0\}$. As such, the set of all functionals u satisfying expression (A.7) forms an equivalence class. To better understand the properties of the members of this class, it is helpful to consider the special case where the leading order term of u is equal to the product of a positive scaling function $l_1(t)$ and a function $u_1(\mathbf{x})$, that is, when $u(t\mathbf{x}) = O(l_1(t)u_1(\mathbf{x}))$ as $t \rightarrow \infty$, for $\mathbf{x} \in \mathbb{R}^d \setminus \{0\}$. Assumption 3 delineates a sufficient condition subject to which the rate of convergence has such a behaviour.

Assumption 3. Suppose that condition (ii) of Proposition 2 holds. There exists a non-decreasing function $l_1 : (0, \infty) \rightarrow (0, \infty)$ and a function $u_1 : \mathbb{R}^d \setminus \{0\} \rightarrow \mathbb{R}$ which is not everywhere zero, such that

$$\lim_{t \rightarrow \infty} \frac{\{-\log f_{[L]}(t\mathbf{x})/t\} - g_{\mathcal{G}}(\mathbf{x})}{a_1(t)} = u_1(\mathbf{x}), \quad (\text{A.8})$$

where $a_1(t) = l_1(t)/t$ for $t > 0$.

Due to condition (ii) of Proposition 2 we have that the scale sequence $a_1(t) = o(1)$ as $t \rightarrow \infty$. This implies that $l_1(t) = o(t)$ as $t \rightarrow \infty$. Also Assumption (3) requires that $-\log f_{[L]}$ is a *multivariate extended regularly varying* function in the sense of Definition 1 of Papastathopoulos & Paulin (2023). To be precise, convergence (A.8) is equivalent to assuming that there exists $p_1 : \mathbb{R}^d \setminus \{0\} \rightarrow \mathbb{R}$ which is not everywhere zero, such that

$$\lim_{t \rightarrow \infty} \frac{[-\log f_{[L]}(t\mathbf{x})/g_{\mathcal{G}}(t\mathbf{x})] - [-\log f_{[L]}(t\mathbf{1})/g_{\mathcal{G}}(t\mathbf{1})]}{a_1(t)} = p_1(\mathbf{x}), \quad \mathbf{x} \in \mathbb{R}^d \setminus \{0\}. \quad (\text{A.9})$$

The correspondence between the two limit functions in (A.8) and (A.9) is $p_1(\mathbf{x}) = [u_1(\mathbf{x})/g_{\mathcal{G}}(\mathbf{x})] - [u_1(\mathbf{1})/g_{\mathcal{G}}(\mathbf{1})]$. From this, it immediately follows that $p_1(\mathbf{1}) = 0$. Also, it is known that the only possible non-trivial limit functions that can arise from convergence (A.9) are those that satisfy the functional equation

$$[p_1(t\mathbf{x}) - p_1(t\mathbf{1})]/t^{\gamma-1} = p_1(\mathbf{x}), \quad t > 0, \quad \mathbf{x} \in \mathbb{R}^d \setminus \{0\},$$

for some $\gamma \in \mathbb{R}$, see Theorem 2 of Papastathopoulos & Paulin (2023) for a proof. These observations lead to Proposition 7 which identifies the key properties of the scaling function $a_1(t) = l_1(t)/t$ and of the limit function $u_1(\mathbf{x})$ under Assumption (3).

Proposition 7. *Suppose that Assumption 3 holds. There exists $\gamma < 1$ such that $a_1(t) \in \mathbf{RV}_{\gamma-1}^{\infty}$ and u_1 is γ -homogeneous, that is, $u_1(t\mathbf{x}) = t^{\gamma}u_1(\mathbf{x}) \forall t > 0$ and $\mathbf{x} \in \mathbb{R}^d \setminus \{0\}$.*

From Proposition 7 we obtain $l_1(t) \in \mathbf{RV}_{\gamma}^{\infty}$. Because Assumption 3 requires $l_1(t)$ to be a non-decreasing function, it suffices to consider the following two cases. First, the case when $l_1(t)$ converges to a constant $K \in (0, \infty)$ and second, the case when $l_1(t)$ grows without bound. For the former case we consider without loss of generality the case $l_1(t) = 1 \forall t > 0$. This is because positive real constants can be absorbed in the limit function u_1 . Below, we treat the two cases in turn.

First, when $l_1(t) = 1$, the leading order term of $u(t\mathbf{x})$ is constant in t which implies that the rate of convergence is determined by the function u_1 , that is, $u(t\mathbf{x}) = u_1(t\mathbf{x}) + o(1)$, as $t \rightarrow \infty$. Also, because $l_1 \in \mathbf{RV}_0^{\infty}$, Proposition 7 yields that u_1 is a 0-homogeneous function. Consequently,

$$f_{[L]}(t\mathbf{x}) = \exp[-\{tg_{\mathcal{G}}(\mathbf{x}) + u_1(\mathbf{x})\}]\{1 + o(1)\}, \quad \text{as } t \rightarrow \infty. \quad (\text{A.10})$$

This special case gives a characterisation of the rate of convergence which is independent of the distance from the origin t . This behaviour is specific to the case $l(t) = 1$ and is waived when $l_1(t)$ grows without bound because in the latter case, the rate of convergence may have non-negligible remainder terms.

Using the same working principle as in Assumption 3, below in Assumption 4 we outline a sufficient condition subject to which the rate of convergence exhibits a so-called *second-order* behaviour (de Haan & Stadtmüller 1996, Papastathopoulos & Paulin 2023).

Assumption 4. *Suppose that Assumption 3 holds with $\lim_{t \rightarrow \infty} l_1(t) = \infty$. There exists a non-decreasing function l_2 and a function $u_2 : \mathbb{R}^d \setminus \{0\} \rightarrow \mathbb{R}$ which is not equal to the product of u_1 and a 0-homogeneous function on $\mathbb{R}^d \setminus \{0\}$, such that*

$$\lim_{t \rightarrow \infty} \frac{([\{-\log f_L(t\mathbf{x})/t\} - g_{\mathcal{G}}(\mathbf{x})]/a_1(t)) - u_1(\mathbf{x})}{a_2(t)} = u_2(\mathbf{x}), \quad (\text{A.11})$$

where $a_2(t) = l_2(t)/l_1(t)$.

It is clear that when Assumption 4 holds with $l_2(t) = 1$, then

$$f_{[L]}(t\mathbf{x}) = \exp[-\{tg_{\mathcal{G}}(\mathbf{x}) + l_1(t)u_1(\mathbf{x}) + u_2(\mathbf{x})\}]\{1 + o(1)\}, \quad \text{as } t \rightarrow \infty. \quad (\text{A.12})$$

More generally, we can construct an asymptotic expansion of $-\log f_{[L]}(t\mathbf{x})$ of the form

$$-\log f_{[L]}(t\mathbf{x}) = g_{\mathcal{G}}(t\mathbf{x}) + \sum_{j=1}^{\infty} l_j(t) u_j(\mathbf{x}), \quad \text{as } t \rightarrow \infty. \quad (\text{A.13})$$

for a sequence of positive scale functions $\{l_j\}_{j=1}^M$ with $M \in \mathbb{N} \cup \{\infty\}$, satisfying $l_j(t) = o(l_{j+1}(t))$ as $t \rightarrow \infty$, and a sequence of functions $\{u_j\}_{j=1}^M$ mapping $\mathbb{R}^d \setminus \{0\}$ into \mathbb{R} . The function u_j captures the contribution of $-\log f_{[L]}(t\mathbf{x})$ at a given order of the series and l_j is the scaling factor associated with this term. The j -th term $l_j(t)u_j(\mathbf{x})$ in the sum represents the j -th approximation to $-\log f_{[L]}(t\mathbf{x})$ as $t \rightarrow \infty$, and the scaling factors l_j determine the rate of convergence to u_{j-1} , with $u_0(\mathbf{x}) := g_{\mathcal{G}}(\mathbf{x})$.

Proposition 8. *Suppose that Assumption 4 holds for the random vector \mathbf{X}_L . There exists $\gamma < 1$ and $\rho \leq 0$ such that*

$$u_2(t\mathbf{x}) = t^\gamma u_2(\mathbf{x}) + ct^\gamma \frac{t^\rho - 1}{\rho} u_1(\mathbf{x}).$$

and the solution of this functional equation is

$$u_2(\mathbf{x}) = \|\mathbf{x}\|^{\gamma+\rho} h\left(\frac{\mathbf{x}}{\|\mathbf{x}\|}\right) + c\|\mathbf{x}\|^\gamma \log\|\mathbf{x}\| u_1\left(\frac{\mathbf{x}}{\|\mathbf{x}\|}\right), \quad \mathbf{x} \in \mathbb{R}^d \setminus \{0\}. \quad (\text{A.14})$$

for a measurable function h that maps \mathbb{S}^{d-1} into \mathbb{R} .

Proposition 8 provides key insight into the rate of convergence to the limit function in Proposition 2 (ii). This result is shown to hold in Appendix A for certain known copulas in Examples A.1, A.2, and A.7. We note that a similar approach can be used to study the rate of convergence in Proposition 2 (i) and (iii) for light- and heavy-tailed distributions.

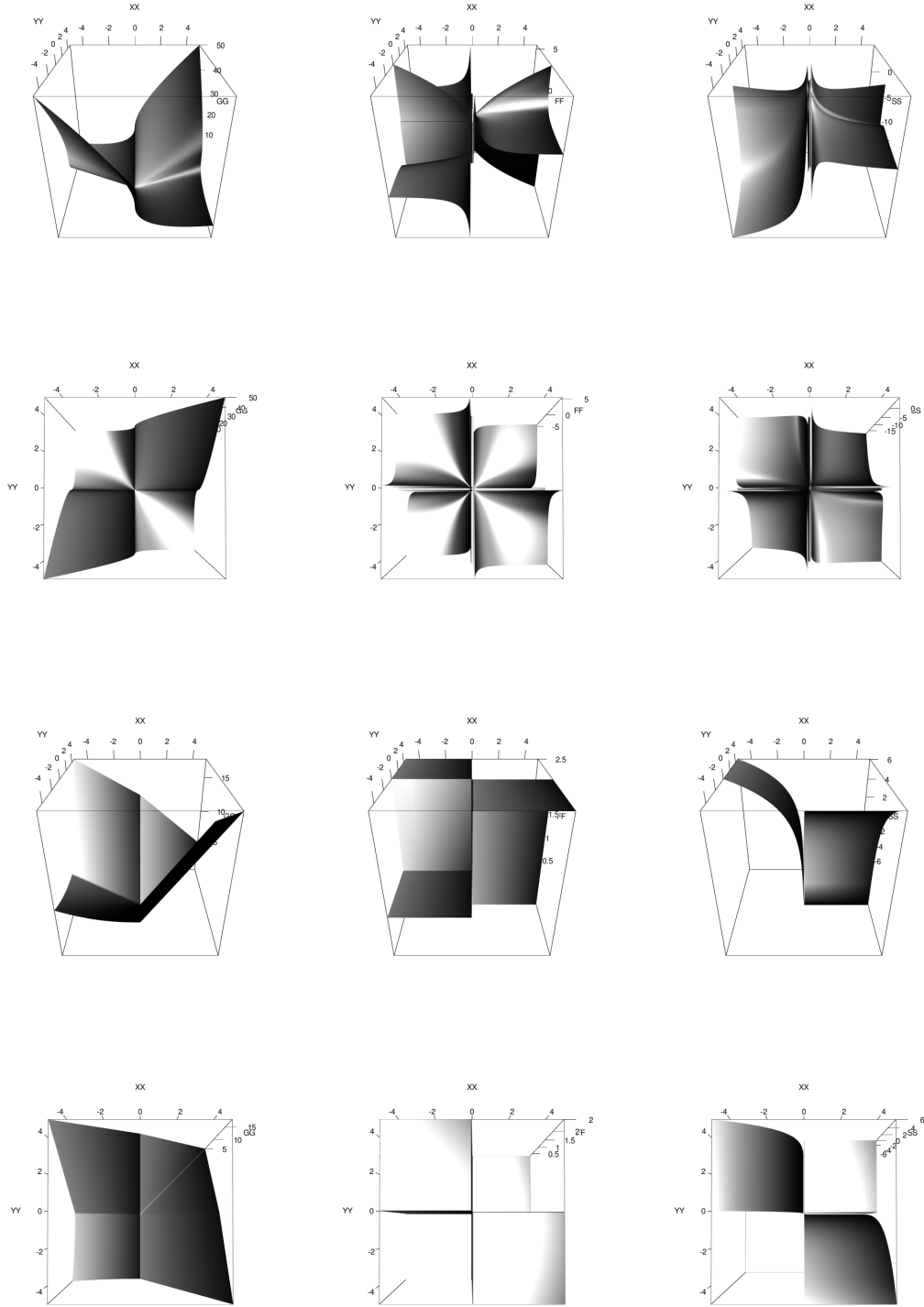


Figure 11: Limit functions in asymptotic expansion of the logarithm of the density of the multivariate normal copula with Laplace marginals. *Left*: gauge function $g_{\mathcal{G}}$ of limit set \mathcal{G} . *Centre*: limit function u_1 . *Right*: Limit function u_2 . *Bottom*: alternative viewing angle obtained by rotating the images shown in top row by 60° about x axis

Proof of Proposition 7. The homogeneity of u_1 follows directly from the correspondence between u_1 and p_1 and the fact that p_1 is $(\gamma - 1)$ -homogeneous. It remains to show that $a_1 \in \text{RV}_{\gamma-1}^\infty$. For any $a > 0$ and $\mathbf{x} \in \mathbb{R}^d \setminus \{0\}$ we have

$$\frac{[-\log f_{[L]} \{t(a\mathbf{x})\}/t] - g_{\mathcal{G}}(a\mathbf{x})}{a_1(t)} = a \frac{[-\log f_{[L]} \{(at)\mathbf{x}\}/(at)] - g_{\mathcal{G}}(\mathbf{x})}{a_1(at)} \frac{a_1(at)}{a_1(t)}.$$

By Assumption 3, the LHS converges to $u_1(a\mathbf{x})$ as $t \rightarrow \infty$ and the second factor of the RHS converges to $u_1(\mathbf{x})$ as $t \rightarrow \infty$. Hence, the third factor of RHS must converge as $t \rightarrow \infty$ which implies that there exists $\gamma \in \mathbb{R}$ such that $a_1 \in \text{RV}_{\gamma-1}^\infty$. The case $\gamma > 1$ is not admissible due to homogeneity of $g_{\mathcal{G}}$ as the latter ensures that the rate of convergence $u(t\mathbf{x})$ is not growing faster than $g_{\mathcal{G}}(t\mathbf{x})$, that is, $\lim_{t \rightarrow \infty} u(t\mathbf{x})/g_{\mathcal{G}}(t\mathbf{x}) = 0$ for all $\mathbf{x} \in \mathbb{R}^d \setminus \{0\}$. When $\gamma = 1$ we have $a_1 \in \text{RV}_{-1}^\infty$, which implies that $l_1(t) \in \text{RV}_0^\infty$. Thus, the case $\gamma = 1$ is not admissible because it requires $l_1(t) \rightarrow 0$ as $t \rightarrow \infty$ for $u(t\mathbf{x})/g_{\mathcal{G}}(t\mathbf{x})$ to converge to zero for all $\mathbf{x} \in \mathbb{R}^d \setminus \{0\}$, which contradicts the assumption that l_1 is a non-decreasing function. \square

Proof of Proposition 8. Since for any $a > 0$ we have

$$\begin{aligned} & \frac{\frac{-t^{-1} \log f_{[L]} \{t(a\mathbf{x})\} - g_{\mathcal{G}}(a\mathbf{x})}{a_1(t)} - u_1(a\mathbf{x})}{a_2(t)} = \frac{a \frac{-(at)^{-1} \log f_{[L]} \{(at)\mathbf{x}\} - g_{\mathcal{G}}(\mathbf{x})}{a_1(at)} \frac{a_1(at)}{a_1(t)} - a^\gamma u_1(\mathbf{x})}{a_2(at)} \frac{a_2(at)}{a_2(t)} \\ &= \frac{a_2(at)}{a_2(t)} a^\gamma \frac{\frac{-(at)^{-1} \log f_{[L]} \{(at)\mathbf{x}\} - g_{\mathcal{G}}(\mathbf{x})}{a_1(at)} - au_1(\mathbf{x})}{a_2(at)} \\ & \quad + a \frac{\left(\frac{a_1(at)}{a_1(t)} - a^{\gamma-1} \right)}{a_2(t)} \frac{-(at)^{-1} \log f_{[L]} \{(at)\mathbf{x}\} - g_{\mathcal{G}}(\mathbf{x})}{a_1(at)}, \end{aligned}$$

it follows that

$$u_2(a\mathbf{x}) = \lim_{t \rightarrow \infty} \frac{a_2(at)}{a_2(t)} a^\gamma u_2(\mathbf{x}) + a \lim_{t \rightarrow \infty} \frac{\left(\frac{a_1(at)}{a_1(t)} - a^{\gamma-1} \right)}{a_2(t)} u_1(\mathbf{x}).$$

Suppose there exist $a > 0$, and sequences t_n, t'_n such that

$$\lim_{t_n \rightarrow \infty} \frac{a_2(at_n)}{a_2(t_n)} = A, \lim_{t'_n \rightarrow \infty} \frac{a_2(at'_n)}{a_2(t'_n)} = A', \lim_{t_n \rightarrow \infty} \frac{\left(\frac{a_1(at_n)}{a_1(t_n)} - a^{\gamma-1} \right)}{a_2(t_n)} = B \quad \text{and} \quad \lim_{t'_n \rightarrow \infty} \frac{\left(\frac{a_1(at'_n)}{a_1(t'_n)} - a^{\gamma-1} \right)}{a_2(t'_n)} = B',$$

with $A \neq A'$ and $B \neq B'$. Then, for all $\mathbf{x} \in \mathbb{R}^d \setminus \{0\}$,

$$0 = (A - A') a^\gamma u_2(\mathbf{x}) + a(B - B') u_1(\mathbf{x})$$

By assumption, u_2 is not equal to the product of u_1 and a 0-homogeneous functional. Hence, $A = A'$ and $B = B'$. This implies that there exists $\rho \leq 0$ and $c \in \mathbb{R}$ such that

$$\lim_{t \rightarrow \infty} \frac{a_2(tx)}{a_2(t)} = x^\rho \quad \text{and} \quad \lim_{t \rightarrow \infty} \frac{\left(\frac{a_1(at)}{a_1(t)} - a^{\gamma-1} \right)}{a_2(t)} = cx^{\gamma-1} \frac{x^\rho - 1}{\rho}, \quad \forall x > 0,$$

for a proof see [de Haan & Stadtmüller \(1996\)](#). Consequently, we arrive at the functional equation

$$u_2 \left(\|\mathbf{x}\| \frac{\mathbf{x}}{\|\mathbf{x}\|} \right) = \|\mathbf{x}\|^{\gamma+\rho} u_2 \left(\frac{\mathbf{x}}{\|\mathbf{x}\|} \right) + c \|\mathbf{x}\|^\gamma \frac{\|\mathbf{x}\|^\rho - 1}{\rho} u_1 \left(\frac{\mathbf{x}}{\|\mathbf{x}\|} \right), \quad \mathbf{x} \in \mathbb{R}^d \setminus \{0\}. \quad (\text{A.15})$$

where u_1 is a γ -homogeneous functional on $\mathbb{R}^d \setminus \{0\}$ and u_2 is an unknown function. Let

$$u_2^*(\mathbf{x}) = \|\mathbf{x}\|^{\gamma+\rho} \tilde{\lambda}_2 \left(\frac{\mathbf{x}}{\|\mathbf{x}\|} \right) + c \|\mathbf{x}\|^\gamma \frac{\|\mathbf{x}\|^\rho - 1}{\rho} u_1 \left(\frac{\mathbf{x}}{\|\mathbf{x}\|} \right), \quad \mathbf{x} \in \mathbb{R}^d \setminus \{0\}, \quad (\text{A.16})$$

where $\tilde{\lambda}_2$ be an arbitrary map from $\mathbb{R}^d \setminus \{0\}$ into \mathbb{R} . A simple calculation shows that the function u_2^* satisfies the functional equation (A.15). This proves that the general solution of the functional equation (A.15) is u_2^* . Last, by Assumption 4 we have $a_2(t) = o(a_1(t))$ as $t \rightarrow \infty$. \square

C.2 Weak convergence to min-max stable distribution

Let $\pi = \mathbb{P}(X/|X| = 1) = \mathbb{P}(X > 0)$. It can be verified that for any $z_L, z_R \in \mathbb{R}$

$$\begin{aligned} \mathbb{P} \left(\frac{-m_n + b_{n,L}}{a_{n,L}} \leq z_L, \frac{M_n - b_{n,R}}{a_{n,R}} \leq z_R \right) &= \mathbb{P} \left(-a_{n,L} z_L + b_{n,L} < X \leq a_{n,R} z_R + b_{n,R} \right)^n = \\ &= \left[1 - \frac{1}{n} \{ 1 - \mathbb{P}(-a_{n,L} z_L + b_{n,L} < X \leq a_{n,R} z_R + b_{n,R}) \} \right]^n \end{aligned} \quad (\text{A.17})$$

It suffices to show that

$$\lim_{n \rightarrow \infty} n \left[1 - \mathbb{P}(-a_{n,L} z_L + b_{n,L} < X \leq a_{n,R} z_R + b_{n,R}) \right] = (1 - \pi)(1 - \xi_L z_L)_+^{-1/\xi_L} + \pi(1 + \xi_R z_R)_+^{-1/\xi_R} \in [0, \infty],$$

since then, expression (A.17) can be written as

$$\left[1 - \{ (1 - \pi)(1 - \xi_L z_L)_+^{-1/\xi_L} + \pi(1 + \xi_R z_R)_+^{-1/\xi_R} \} / n + o(1/n) \right]^n,$$

so that convergence at continuity points of the limit distribution follows at once. Due to Assumption 1, the sequences $-a_{n,L} z_L + b_{n,L}$ and $a_{n,R} z_R + b_{n,R}$ are eventually negative and eventually positive, respectively. Hence, there exists $n_0 = n_0(z_L, z_R) \in \mathbb{N}$, such that for all $n > n_0$,

$$\begin{aligned} n \left[1 - \mathbb{P}(-a_{n,L} z_L + b_{n,L} < X \leq a_{n,R} z_R + b_{n,R}) \right] &= \\ &= n(1 - \pi) - n(1 - \pi) \mathbb{P} \left(\frac{X - b_{n,L}}{a_{n,L}} > -z_L \mid X \leq 0 \right) + n\pi - n\pi \mathbb{P} \left(\frac{X - b_{n,R}}{a_{n,R}} \leq z_R \mid X > 0 \right) \\ &= (1 - \pi)n \mathbb{P} \left(\frac{X - b_{n,L}}{a_{n,L}} \leq -z_L \mid X \leq 0 \right) + \pi n \mathbb{P} \left(\frac{X - b_{n,R}}{a_{n,R}} > z_R \mid X > 0 \right), \end{aligned}$$

where the first equality follows from total probability and by expressing the constant 1 as $\pi + (1 - \pi)$. The result follows from assumption 1.

C.3 Density convergence of rescaled radial excess variable

To prove the proposition, we rely on Lemma 1 below, which is a direct consequence of the Corollary 3.3 of [de Haan & Resnick \(1987\)](#).

Lemma 1 (Potter bounds). *Let $V : \mathbb{R}^d \rightarrow \mathbb{R}$ and suppose there exist $\rho \in \mathbb{R}$, $h : \mathbb{R}_+ \rightarrow \mathbb{R}_+$, and $\mathcal{G} \in \star$ such that $\lim_{t \rightarrow \infty} V(t\mathbf{x})/h(t) = g_{\mathcal{G}}(\mathbf{x})^\rho$ uniformly on \mathbb{S}^{d-1} . Then, for any $\varepsilon > 0$, there exists $t_0 = t_0(\varepsilon) > 0$ such that for all $t > t_0$,*

$$(1 - \varepsilon)\|\mathbf{x}\|^{-\varepsilon} g_{\mathcal{G}}(\mathbf{w})^\rho \leq \frac{V(t\mathbf{x})}{h(t)} \leq (1 + \varepsilon)\|\mathbf{x}\|^\varepsilon g_{\mathcal{G}}(\mathbf{w})^\rho, \quad \forall \mathbf{x} \in \mathbb{R}^d \setminus \{0\}.$$

Proof of Proposition 2. Consider the following relation

$$\frac{\partial}{\partial z} \mathbb{P} \left[\frac{R - r_{\mathcal{Q}_q}(\mathbf{w})}{r_{\mathcal{G}_q}(\mathbf{w})} \leq z \mid R > r_{\mathcal{Q}_q}(\mathbf{W}), \mathbf{W} = \mathbf{w} \right] = \frac{r_{\mathcal{G}_q}(\mathbf{w}) z_q(\mathbf{w})^{d-1} f_{\mathbf{X}}(z_q(\mathbf{w})\mathbf{w})}{\int_{r_{\mathcal{Q}_q}(\mathbf{w})}^{r_{\mathcal{Q}_1}(\mathbf{w})} f_{R, \mathbf{W}}(s, \mathbf{w}) \, ds}, \quad (\text{A.18})$$

where $z_q(\mathbf{w}) = r_{\mathcal{Q}_q}(\mathbf{w}) + r_{\mathcal{G}_q}(\mathbf{w})z$, $z \in [0, \{r_{\mathcal{Q}_1}(\mathbf{w}) - r_{\mathcal{Q}_q}(\mathbf{w})\}/r_{\mathcal{G}_q}(\mathbf{w})]$, and $\mathbf{w} \in \mathbb{S}^{d-1}$.

(i) Write the integral in expression (A.18) using the change of variable $s = \{1 - (t\|\mathbf{w}\|)^{-1}\} r_{\mathcal{Q}_1}(\mathbf{w})$, with $L_q(\mathbf{w}) := r_{\mathcal{Q}_1}(\mathbf{w})/\{r_{\mathcal{Q}_1}(\mathbf{w}) - r_{\mathcal{Q}_q}(\mathbf{w})\}$, as

$$\int_{r_{\mathcal{Q}_q}(\mathbf{w})}^{r_{\mathcal{Q}_1}(\mathbf{w})} f_{R, \mathbf{W}}(s, \mathbf{w}) \, ds = r_{\mathcal{Q}_1}(\mathbf{w})^d \int_{L_q(\mathbf{w})}^{\infty} (1 - 1/t)^{d-1} t^{-2} \{f_{\mathbf{X}}[(1 - 1/t)r_{\mathcal{Q}_1}(\mathbf{w})\mathbf{w}]/\psi_{\mathbf{B}}(t)\} \psi_{\mathbf{B}}(t) \, dt.$$

Due to convergence (i), the map $(0, \infty) \ni s \mapsto f_{\mathbf{X}}[(1 - 1/s)r_{\mathcal{Q}_1}(\mathbf{w})\mathbf{w}]/\psi_{\mathbf{B}}(s) \in \mathbb{R}^+$ is slowly varying at ∞ . Additionally, convergence (i) implies that $\psi_{\mathbf{B}}(s) \in \text{RV}_{1+1/\xi}^\infty$, hence there exists $l_{\mathbf{B}} \in \text{RV}_0^\infty$ such that $\psi_{\mathbf{B}}(s) = l_{\mathbf{B}}(s)s^{1+1/\xi}$. Thus, by Karamata's theorem (Theorem 2.1 [Resnick 2007](#)),

$$\frac{\int_{r_{\mathcal{Q}_q}(\mathbf{w})}^{r_{\mathcal{Q}_1}(\mathbf{w})} f_{R, \mathbf{W}}(s, \mathbf{w}) \, ds}{\{r_{\mathcal{Q}_1}(\mathbf{w}) - r_{\mathcal{Q}_q}(\mathbf{w})\} f_{R, \mathbf{W}}[r_{\mathcal{Q}_q}(\mathbf{w}), \mathbf{w}]} = -\xi\{1 + o(1)\}, \quad \text{as } q \rightarrow 1.$$

Using the assumption that $f_{\mathbf{X}}(r\mathbf{w}) \sim \psi_{\mathbf{B}}[r_{\mathcal{Q}_1}(\mathbf{w})/\{r_{\mathcal{Q}_1}(\mathbf{w}) - r\}]g_{\mathcal{G}}(\mathbf{w})^{1+1/\xi}$ as $r \rightarrow r_{\mathcal{Q}_1}(\mathbf{w})$, and setting $r_{\mathcal{G}_q}(\mathbf{w}) = -\xi\{r_{\mathcal{Q}_1}(\mathbf{w}) - r_{\mathcal{Q}_q}(\mathbf{w})\}$, expression (A.18) converges to

$$\begin{aligned} & \frac{r_{\mathcal{G}_q}(\mathbf{w}) z_q(\mathbf{w})^{d-1} f_{\mathbf{X}}[z_q(\mathbf{w})\mathbf{w}]}{-\xi\{r_{\mathcal{Q}_1}(\mathbf{w}) - r_{\mathcal{Q}_q}(\mathbf{w})\} r_{\mathcal{Q}_q}(\mathbf{w})^{d-1} f_{\mathbf{X}}[r_{\mathcal{Q}_q}(\mathbf{w})\mathbf{w}]} \{1 + o(1)\} = \\ & = \frac{z_q(\mathbf{w})^{d-1}}{r_{\mathcal{Q}_q}(\mathbf{w})^{d-1}} \left[\frac{r_{\mathcal{Q}_1}(\mathbf{w}) - z_q(\mathbf{w})}{r_{\mathcal{Q}_1}(\mathbf{w}) - r_{\mathcal{Q}_q}(\mathbf{w})} \right]^{-1-1/\xi} \{1 + o(1)\} \rightarrow (1 + \xi z)_+^{-1-1/\xi}, \quad \text{as } q \rightarrow 1. \end{aligned}$$

(ii) Consider first the integral term in expression (A.18). The integral is equal to

$$\int_{r_{\mathcal{Q}_q}(\mathbf{w})}^{\infty} s^{d-1} f_{\mathbf{X}}(s\mathbf{w}) \, ds = \int_{r_{\mathcal{Q}_q}(\mathbf{w})}^{\infty} s^{d-1} \exp[-\psi_{\mathbf{L}}(s)\{-\{\log f_{\mathbf{X}}(s\mathbf{w})\}/\psi_{\mathbf{L}}(s)\}] \, ds.$$

Due to Lemma 1 with $V(\mathbf{x}) = -\log f_{\mathbf{X}}(\mathbf{x})$ and $h = \psi$, for all $\varepsilon > 0$ there exists $q_0 > q$ such that

$$\int_{r_{\mathcal{Q}_q}(\mathbf{w})}^{\infty} s^{d-1} \exp[-(1 + \varepsilon)\psi_{\mathbf{L}}(s)g_{\mathcal{G}}(\mathbf{w})^\rho] \, ds \leq \int_{r_{\mathcal{Q}_q}(\mathbf{w})}^{\infty} s^{d-1} f_{\mathbf{X}}(s\mathbf{w}) \, ds \leq \int_{r_{\mathcal{Q}_q}(\mathbf{w})}^{\infty} \exp[-(1 - \varepsilon)\psi_{\mathbf{L}}(s)g_{\mathcal{G}}(\mathbf{w})^\rho] \, ds.$$

Since ε can be made arbitrarily small, we have

$$\int_{r_{\mathcal{Q}_q}(\mathbf{w})}^{\infty} s^{d-1} f_{\mathbf{X}}(s\mathbf{w}) \, ds \sim \int_{r_{\mathcal{Q}_q}(\mathbf{w})}^{\infty} s^{d-1} \exp[-\psi_{\mathbf{L}}(s)g_{\mathcal{G}}(\mathbf{w})^\rho] \, ds.$$

Without loss, $\psi_{\mathbf{L}}$ can be taken smooth (Lemma 1.4, [Seneta \(2006\)](#)) so that $d^k \psi_{\mathbf{L}}(t)/dt^k$ exists for all $t > 0$

and $k \in \mathbb{N}$. Therefore,

$$\begin{aligned} \int_{r_{\mathcal{Q}_q}(\mathbf{w})}^{\infty} s^{d-1} f_{\mathbf{X}}(s\mathbf{w}) \, ds &= \int_{r_{\mathcal{Q}_q}(\mathbf{w})}^{\infty} s^{d-1} \left[\frac{\frac{d}{ds} \exp[-\psi_{\mathbf{L}}(s)g_{\mathcal{G}}(\mathbf{w})^{\rho}]}{-g_{\mathcal{G}}(\mathbf{w})^{\rho}\psi'_{\mathbf{L}}(s)} \right] ds \\ &= r_{\mathcal{Q}_q}(\mathbf{w})^{d-1} \left[\frac{\exp[-\psi_{\mathbf{L}}(r_{\mathcal{Q}_q}(\mathbf{w}))g_{\mathcal{G}}(\mathbf{w})^{\rho}]}{g_{\mathcal{G}}(\mathbf{w})^{\rho}\psi'_{\mathbf{L}}(r_{\mathcal{Q}_q}(\mathbf{w}))} \right] \{1 + o(1)\}, \quad \text{as } q \rightarrow 1. \end{aligned}$$

Using Lemma 1 again, we have that equation (A.18) converges to

$$\begin{aligned} &\frac{r_{\mathcal{G}_q}(\mathbf{w})z_q(\mathbf{w})^{d-1}}{r_{\mathcal{Q}_q}(\mathbf{w})^{d-1}} g_{\mathcal{G}}(\mathbf{w})^{\rho}\psi'_{\mathbf{L}}(r_{\mathcal{Q}_q}(\mathbf{w})) \exp[-g_{\mathcal{G}}(\mathbf{w})^{\rho}\{\psi_{\mathbf{L}}(z_q(\mathbf{w})) - \psi_{\mathbf{L}}(r_{\mathcal{Q}_q}(\mathbf{w}))\}] \{1 + o(1)\} \\ &= r_{\mathcal{G}_q}(\mathbf{w})g_{\mathcal{G}}(\mathbf{w})^{\rho}\psi'_{\mathbf{L}}(r_{\mathcal{Q}_q}(\mathbf{w})) \exp[-g_{\mathcal{G}}(\mathbf{w})^{\rho}\{\psi_{\mathbf{L}}(z_q(\mathbf{w})) - \psi_{\mathbf{L}}(r_{\mathcal{Q}_q}(\mathbf{w}))\}] \{1 + o(1)\}, \quad \text{as } q \rightarrow 1. \end{aligned}$$

A Taylor expansion of $\psi_{\mathbf{L}}(z_q(\mathbf{w}))$ about $r_{\mathcal{Q}_q}$ and local uniform convergence give $\psi_{\mathbf{L}}(z_q(\mathbf{w})) = \psi_{\mathbf{L}}(r_{\mathcal{Q}_q}(\mathbf{w})) + \psi'_{\mathbf{L}}(r_{\mathcal{Q}_q}(\mathbf{w}))r_{\mathcal{G}_q}(\mathbf{w}) + o(1)$. Thus,

$$\begin{aligned} &r_{\mathcal{G}_q}(\mathbf{w})g_{\mathcal{G}}(\mathbf{w})^{\rho}\psi'_{\mathbf{L}}(r_{\mathcal{Q}_q}(\mathbf{w})) \exp[-g_{\mathcal{G}}(\mathbf{w})^{\rho}\{\psi'_{\mathbf{L}}(r_{\mathcal{Q}_q}(\mathbf{w}))r_{\mathcal{G}_q}(\mathbf{w}) + o(1)\}] \{1 + o(1)\} \\ &= r_{\mathcal{G}_q}(\mathbf{w})g_{\mathcal{G}}(\mathbf{w})^{\rho}\psi'_{\mathbf{L}}(r_{\mathcal{Q}_q}(\mathbf{w})) \exp[-g_{\mathcal{G}}(\mathbf{w})^{\rho}\{\psi'_{\mathbf{L}}(r_{\mathcal{Q}_q}(\mathbf{w}))r_{\mathcal{G}_q}(\mathbf{w})\}] \{1 + o(1)\} \rightarrow \exp(-z), \quad \text{as } q \rightarrow 1, \end{aligned}$$

whenever $r_{\mathcal{G}_q}(\mathbf{w}) \sim \{\psi'_{\mathbf{L}}(r_{\mathcal{Q}_q}(\mathbf{w}))g_{\mathcal{G}}(\mathbf{w})^{\rho}\}^{-1}$.

(iii) Consider first the integral term in expression (A.18). The integral is equal to

$$\int_{r_{\mathcal{Q}_q}(\mathbf{w})}^{\infty} f_{R,\mathbf{W}}(s, \mathbf{w}) \, ds = \int_{r_{\mathcal{Q}_q}(\mathbf{w})}^{\infty} s^{d-1} \{f_{\mathbf{X}}(s\mathbf{w})/\psi_{\mathbf{H}}(s)\} \{\psi_{\mathbf{H}}(s)/s^{1-d}\} \, ds.$$

Due to convergence (iii), the map $(0, \infty) \ni s \mapsto \{f_{\mathbf{X}}(s\mathbf{w})/\psi_{\mathbf{H}}(s)\} \in \mathbb{R}^+$ is slowly varying at ∞ for any $\mathbf{w} \in \mathbb{S}^{d-1}$. Additionally, convergence (iii) implies that $\psi_{\mathbf{H}}(s) \in \text{RV}_{-(d+\xi-1)}^{\infty}$, hence there exists $l_{\mathbf{H}} \in \text{RV}_0^{\infty}$ such that $\psi_{\mathbf{H}}(s) = l_{\mathbf{H}}(s)s^{-\{d+(1/\xi)\}}$. Thus, by Karamata's theorem (Theorem 2.1 [Resnick 2007](#)),

$$\frac{\int_{r_{\mathcal{Q}_q}(\mathbf{w})}^{\infty} f_{R,\mathbf{W}}(s, \mathbf{w}) \, ds}{r_{\mathcal{Q}_q}(\mathbf{w})f_{R,\mathbf{W}}(r_{\mathcal{Q}_q}(\mathbf{w}), \mathbf{w})} = \xi \{1 + o(1)\} \quad \text{as } q \rightarrow 1.$$

Thus, when $r_{\mathcal{G}_q}(\mathbf{w}) = \xi r_{\mathcal{Q}_q}(\mathbf{w})$, expression (A.18) converges to

$$\frac{1}{\xi} \frac{r_{\mathcal{G}_q}(\mathbf{w})}{r_{\mathcal{Q}_q}(\mathbf{w})} \left[\frac{z_q(\mathbf{w})}{r_{\mathcal{Q}_q}(\mathbf{w})} \right]^{d-1} \frac{f_{\mathbf{X}}[z_q(\mathbf{w})\mathbf{w}]}{f_{\mathbf{X}}[r_{\mathcal{Q}_q}(\mathbf{w})\mathbf{w}]} \{1 + o(1)\} = \left[1 + \frac{r_{\mathcal{G}_q}(\mathbf{w})z}{r_{\mathcal{Q}_q}(\mathbf{w})} \right]^{-1-1/\xi} \{1 + o(1)\} \rightarrow (1 + \xi z)_+^{-1-1/\xi},$$

as $q \rightarrow 1$. □

C.4 Convergence to Poisson point process

Proof of Theorem 1. It suffices to show that as $n \rightarrow \infty$, the sequence of mean measures

$$\Lambda_n(\cdot) = n \mathbb{P} \left[\left(\frac{R - r_{\mathcal{Q}_{n,k}}(\mathbf{W})}{r_{\mathcal{G}_{n,k}}(\mathbf{W})}, \mathbf{W} \right) \in \cdot \right]$$

converges vaguely in $M_p((-\infty, \infty] \times \mathbb{S}^{d-1})$ (Theorem 5.3, [Resnick 2007](#)). Let $h \in C_K^+((-\infty, \infty] \times \mathbb{S})$. Because $q_{n,k} = 1 - k/n$ and $\mathbb{P}[R > r_{\mathcal{Q}_{q_{n,k}}}(\mathbf{w}) \mid \mathbf{W} = \mathbf{w}] = q_{n,k}$ for all $\mathbf{w} \in \mathbb{S}$, total probability gives that

$$\begin{aligned}\Lambda_n(h) &= n \int_{\mathbb{S}} \int_{-\infty}^{\infty} h(z, \mathbf{w}) \mathbb{P} \left[\frac{R - r_{\mathcal{Q}_{q_{n,k}}}(\mathbf{W})}{r_{\mathcal{G}_{q_{n,k}}}(\mathbf{W})} \in dz, \mathbf{W} \in d\mathbf{w} \right] \\ &= k \int_{\mathbb{S}} \int_{-\infty}^{\infty} h(z, \mathbf{w}) \mathbb{P} \left[\frac{R - r_{\mathcal{Q}_{q_{n,k}}}(\mathbf{W})}{r_{\mathcal{G}_{q_{n,k}}}(\mathbf{W})} \in dz \mid R > r_{\mathcal{Q}_{q_{n,k}}}(\mathbf{w}; q), \mathbf{W} = \mathbf{w} \right] F_{\mathbf{W}}(d\mathbf{w}).\end{aligned}$$

By Assumption 2 and from dominated convergence, we have that as $n \rightarrow \infty$, $\Lambda_n(h) \xrightarrow{v} \Lambda(h)$ in $M_p((-\infty, \infty] \times \mathbb{S})$, where $\Lambda(h) = \int_{\mathbb{S}} \int_{-\infty}^{\infty} h(z, \mathbf{w}) k(1 + \xi z)_+^{-1/\xi-1} dz F_{\mathbf{W}}(d\mathbf{w})$. \square

C.5 Stability of the MRS exponential distribution

Proof of stability equation (29). Let the random vector $\mathbf{Z} \in \mathbb{R}^d$ follow a MRS exponential distribution with location \mathcal{M} , scale Σ , and angular component \mathcal{W} . Then,

$$\begin{aligned}\mathbb{P}[\mathbf{Z} \in [\mathcal{M} + B_{r_1+r_2}(0) \cdot \Sigma]' \mid \mathbf{Z} \in \{\mathcal{M} + B_{r_1}(0) \cdot \Sigma\}'] &= \frac{\mathbb{P}[\mathbf{Z} \in \{\mathcal{M} + B_{r_1+r_2}(0) \cdot \Sigma\}']}{\mathbb{P}[\mathbf{Z} \in \{\mathcal{M} + B_{r_1}(0) \cdot \Sigma\}']} \\ &= \frac{\mathbb{P}[\{\|\mathbf{Z}\| - r_{\mathcal{M}}(\mathbf{Z}/\|\mathbf{Z}\|)\}/r_{\Sigma}(\mathbf{Z}/\|\mathbf{Z}\|) > r_1 + r_2]}{\mathbb{P}[\{\|\mathbf{Z}\| - r_{\mathcal{M}}(\mathbf{Z}/\|\mathbf{Z}\|)\}/r_{\Sigma}(\mathbf{Z}/\|\mathbf{Z}\|) > r_1]} = \exp\{-r_2\} = \mathbb{P}[\mathbf{Z} \in \{\mathcal{M} + B_{r_2}(0)\}' \cdot \Sigma].\end{aligned}$$

\square

C.6 Stability of the MRS generalised Pareto distribution

Proof of stability equation (31). Let the random vector $\mathbf{Z} \in \mathbb{R}^d$ follow a MRS generalised Pareto distribution with location \mathcal{M} , scale Σ , shape $\xi \in \mathbb{R}$, and angular component \mathcal{W} . Then,

$$\begin{aligned}\mathbb{P}[\mathbf{Z} \in [\mathcal{M} + B_{r_1+r_2}(0) \cdot \Sigma]' \mid \mathbf{Z} \in \{\mathcal{M} + B_{r_1}(0) \cdot \Sigma\}'] &= \frac{\mathbb{P}[\mathbf{Z} \in \{\mathcal{M} + B_{r_1+r_2}(0) \cdot \Sigma\}']}{\mathbb{P}[\mathbf{Z} \in \{\mathcal{M} + B_{r_1}(0) \cdot \Sigma\}']} \\ &= \frac{\mathbb{P}[\{\|\mathbf{Z}\| - r_{\mathcal{M}}(\mathbf{Z}/\|\mathbf{Z}\|)\}/r_{\Sigma}(\mathbf{Z}/\|\mathbf{Z}\|) > r_1 + r_2]}{\mathbb{P}[\{\|\mathbf{Z}\| - r_{\mathcal{M}}(\mathbf{Z}/\|\mathbf{Z}\|)\}/r_{\Sigma}(\mathbf{Z}/\|\mathbf{Z}\|) > r_1]} = \frac{[1 + \xi(r_1 + r_2)]_+^{-1/\xi}}{[1 + \xi r_1]_+^{-1/\xi}} = \left[1 + \xi \frac{r_2}{1 + \xi r_1}\right]^{-1/\xi} \\ &= \mathbb{P}\left[\mathbf{Z} \in \left\{\mathcal{M} + \frac{B_{r_2}(0) \cdot \Sigma}{B_1(0) + B_{\xi}(0) \cdot B_{r_1}(0)}\right\}'\right].\end{aligned}$$

\square

C.7 Equality in distribution of the angular variables

Proof of Proposition (3). Suppose that $\mathbf{X} = R\mathbf{W} \in \mathbb{R}^d$ has Lebesgue density $f_{\mathbf{X}}$.

$$\mathbb{P}[\mathbf{W} \in S_B \mid R > r_{\mathcal{Q}_q}(\mathbf{W})] = \frac{\int_{S_B} \left[\int_{r_{\mathcal{Q}_q}(\mathbf{w})}^{\infty} f_{R|\mathbf{W}}(r \mid \mathbf{w}) dr \right] f_{\mathbf{W}}(\mathbf{w}) d\mathbf{w}}{\int_{\mathbb{S}^{d-1}} \left[\int_{r_{\mathcal{Q}_q}(\mathbf{w})}^{\infty} f_{R|\mathbf{W}}(r \mid \mathbf{w}) dr \right] f_{\mathbf{W}}(\mathbf{w}) d\mathbf{w}}. \quad (\text{A.19})$$

By construction of \mathcal{Q}_q , $\int_{r_{\mathcal{Q}_q}(\mathbf{w})}^{\infty} f_{R|\mathbf{W}}(r | \mathbf{w}) dr = 1 - q$ and it thus follows by constant cancellation in equation A.19 that for any measurable $S_B \subseteq \mathbb{S}^{d-1}$,

$$\mathbb{P}[\mathbf{W} \in S_B | R > r_{\mathcal{Q}_q}(\mathbf{W})] = \int_{S_B} f_{\mathbf{W}}(\mathbf{w}) d\mathbf{w} = \mathbb{P}[\mathbf{W} \in S_B], \quad (\text{A.20})$$

directly implying that the distribution of $\mathbf{W} | R > r_{\mathcal{Q}_q}(\mathbf{W})$ is equal to that of \mathbf{W} . \square

C.8 Marginal density of angular variable under homothetic density

Proof of Proposition (4). Suppose that $f_{[L]}(\mathbf{x}) = f_0(g_{\mathcal{G}}(\mathbf{x}))$, $\mathbf{x} \in \mathbb{R}^d$. Then,

$$f_{\mathbf{W}}(\mathbf{w}) = \int_0^{\infty} f_{R,\mathbf{W}}(r, \mathbf{w}) dr = \frac{1}{g_{\mathcal{G}}(\mathbf{w})^d} \int_0^{\infty} s^{d-1} f_0(s) ds = \frac{1}{d |\mathcal{G}| g_{\mathcal{G}}(\mathbf{w})^d}, \quad (\text{A.21})$$

where the last equality follows from [Balkema & Nolde \(2010\)](#), see Section 3.1). \square

A Supplementary material A: Limiting behaviour of known d -dimensional copulas in standard Laplace margins

A.1 Multivariate normal copula

The negative logarithm of the probability density function of the standard d -variate multivariate normal copula with standard Laplace margins and positive-definite precision matrix \mathbf{Q} is

$$\begin{aligned} -\log f(t\mathbf{x}) &= \frac{1}{2} \log |\mathbf{Q}| + d \log 2 + \sum |tx_i|^{1/2} - \sum_{i=1}^d \log f_L(tx_i) + \frac{d}{2} \log 2\pi + \\ &\quad + \sum_{i=1}^d \log \varphi [\Phi^{-1}\{F_L(tx_i)\}] + \frac{1}{2} [\Phi^{-1}\{F_L(t\mathbf{x})\}]^{\top} \mathbf{Q} [\Phi^{-1}\{F_L(t\mathbf{x})\}] \end{aligned} \quad (\text{A.22})$$

where $\Phi^{-1}\{F_L(t\mathbf{x})\} = (\Phi^{-1}\{F_L(tx_i)\} : i = 1, \dots, d)$ and

$$\Phi^{-1}\{F_L(tx_i)\} = \begin{cases} 0 & x_i = 0 \\ \text{sgn}(x_i) [2(\log 2 + |tx_i|) - \log\{4\pi(\log 2 + |tx_i|)\}]^{1/2} + o(t^{-1/2}) & \text{otherwise.} \end{cases}$$

Thus,

$$[\Phi^{-1}\{F_L(tx_i)\}]^2 = \begin{cases} 0 & x_i = 0 \\ 2(\log 2 + |tx_i|) - \log\{4\pi(\log 2 + |tx_i|)\} + o(1) & \text{otherwise.} \end{cases} \quad (\text{A.23})$$

Consider first the case where every $x_i \neq 0$. From the binomial series we have

$$\Phi^{-1}\{F_L(tx_i)\} = \text{sgn}(x_i) \sum_{k=0}^{\infty} \binom{1/2}{k} (-1)^k \{2(\log 2 + |tx_i|)\}^{(1/2)-k} [\log\{4\pi(\log 2 + |tx_i|)\}]^k + o(t^{-1/2}). \quad (\text{A.24})$$

Also, from (A.23) we get

$$\begin{aligned} \sum_{i=1}^d \log \varphi [\Phi^{-1}\{F_L(tx_i)\}] &= -\frac{d}{2} \log 2\pi - \frac{1}{2} \sum_{i=1}^d [\Phi^{-1}\{F_L(tx_i)\}]^2 \\ &= -\frac{d}{2} \log 2\pi - d \log 2 - t \sum_{i=1}^d |x_i|^{1/2} + \frac{d}{2} \log t + \frac{1}{2} \sum_{i=1}^d \log 4\pi |x_i| + o(t^{-1/2}). \end{aligned}$$

Consider next the quadratic form in expression (A.22). Using vector algebra elementwise, we write the quadratic form as

$$\begin{aligned} &[\Phi^{-1}\{F_L(t\mathbf{x})\}]^\top \mathbf{Q} [\Phi^{-1}\{F_L(t\mathbf{x})\}] = \\ &= \sum_{k=0}^{\infty} \left(\frac{\binom{1/2}{k} (-1)^k [\log \{4\pi(\log 2 + t|\mathbf{x}|)\}]^k}{\{2(\log 2 + t|\mathbf{x}|)\}^{k-(1/2)}} \right)^\top \mathbf{Q} \left(\frac{\binom{1/2}{k} (-1)^k [\log \{4\pi(\log 2 + t|\mathbf{x}|)\}]^k}{\{2(\log 2 + t|\mathbf{x}|)\}^{k-(1/2)}} \right) + \\ &+ 2 \sum_{k=0}^{\infty} \sum_{k'=k+1}^{\infty} \left(\frac{\binom{1/2}{k} (-1)^k [\log \{4\pi(\log 2 + t|\mathbf{x}|)\}]^k}{\{2(\log 2 + t|\mathbf{x}|)\}^{k-(1/2)}} \right)^\top \mathbf{Q} \left(\frac{\binom{1/2}{k'} (-1)^{k'} [\log \{4\pi(\log 2 + t|\mathbf{x}|)\}]^{k'}}{\{2(\log 2 + t|\mathbf{x}|)\}^{k'-(1/2)}} \right) + o(1) \end{aligned}$$

We consider each summand from the first two terms separately. The summand associated with $k = 0$ in the first term is

$$\begin{aligned} &[\{2(\log 2 + t|\mathbf{x}|)^{1/2} \text{sgn}(\mathbf{x})\}]^\top \mathbf{Q} [\{2(\log 2 + t|\mathbf{x}|)^{1/2} \text{sgn}(\mathbf{x})\}] = \\ &= (2t) \left[\text{sgn}(\mathbf{x}) |\mathbf{x}|^{1/2} + \text{sgn}(\mathbf{x}) \frac{\log 2}{2t|\mathbf{x}|^{1/2}} \right]^\top \mathbf{Q} \left[\text{sgn}(\mathbf{x}) |\mathbf{x}|^{1/2} + \text{sgn}(\mathbf{x}) \frac{\log 2}{2t|\mathbf{x}|^{1/2}} \right] + O(t^{-1}) \\ &= (2t) \left\{ \text{sgn}(\mathbf{x}) |\mathbf{x}|^{1/2} \right\}^\top \mathbf{Q} \left\{ \text{sgn}(\mathbf{x}) |\mathbf{x}|^{1/2} \right\} + 2 \left\{ \text{sgn}(\mathbf{x}) |\mathbf{x}|^{1/2} \right\}^\top \mathbf{Q} \left\{ \text{sgn}(\mathbf{x}) \frac{\log 2}{|\mathbf{x}|^{1/2}} \right\} + O(t^{-1}). \end{aligned}$$

A similar calculation shows that the summands associated with $k > 1$ in the first term are $O\{(\log t)^{2k}/t^{2k-1}\}$. The summand associated with $(k, k') = (0, 1)$ in the second term is

$$\begin{aligned} &2 \left[\text{sgn}(\mathbf{x}) \{2(\log 2 + t|\mathbf{x}|)\}^{1/2} \right]^\top \mathbf{Q} \left[-\text{sgn}(\mathbf{x}) \frac{\log \{4\pi(\log 2 + t|\mathbf{x}|)\}}{2\{2(\log 2 + t|\mathbf{x}|)\}^{1/2}} \right] = \\ &= -(2 \log t) \left\{ \text{sgn}(\mathbf{x}) |\mathbf{x}|^{1/2} \right\}^\top \mathbf{Q} \left\{ \text{sgn}(\mathbf{x}) (2|\mathbf{x}|^{1/2})^{-1} \right\} - \\ &- \left\{ \text{sgn}(\mathbf{x}) |\mathbf{x}|^{1/2} \right\}^\top \mathbf{Q} \left\{ \text{sgn}(\mathbf{x}) |\mathbf{x}|^{-1/2} \log(4\pi|\mathbf{x}|) \right\} + O(t^{-1}) \end{aligned}$$

Thus, $-\log f(t\mathbf{x}) = tg(\mathbf{x}) + (\log t) u_1(\mathbf{x}) + u_2(\mathbf{x}) + o(1)$ as $t \rightarrow \infty$, where the gauge function is

$$g(\mathbf{x}) = \left\{ \text{sgn}(\mathbf{x}) |\mathbf{x}|^{1/2} \right\}^\top \mathbf{Q} \left\{ \text{sgn}(\mathbf{x}) |\mathbf{x}|^{1/2} \right\}$$

and the higher order terms are given by

$$u_1(\mathbf{x}) = \frac{d}{2} - \frac{1}{2} \left\{ \text{sgn}(\mathbf{x}) |\mathbf{x}|^{1/2} \right\}^\top \mathbf{Q} \left\{ \text{sgn}(\mathbf{x}) |\mathbf{x}|^{-1/2} \right\}$$

and

$$u_2(\mathbf{x}) = \left\{ \text{sgn}(\mathbf{x})|\mathbf{x}|^{1/2} \right\}^\top \mathbf{Q} \left\{ \text{sgn}(\mathbf{x}) \log 2|\mathbf{x}|^{-1/2} \right\} - \frac{1}{2} \left\{ \text{sgn}(\mathbf{x})|\mathbf{x}|^{1/2} \right\}^\top \mathbf{Q} \left\{ \text{sgn}(\mathbf{x})|\mathbf{x}|^{-1/2} \log(4\pi|\mathbf{x}|) \right\} + \frac{1}{2} \log|\mathbf{Q}| + \sum_{i=1}^d \frac{1}{2} \log 4\pi|x_i|$$

A.2 Multivariate Laplace copula

The joint density of the d -variate Laplace distribution in standard Laplace margins with positive definite precision matrix \mathbf{Q} is

$$f_{[L]}(t\mathbf{x}) = \frac{2^{1+\frac{d}{2}}|\mathbf{Q}|^{1/2}}{(2\pi)^{d/2}} t^v \left(\frac{1}{2^2} \mathbf{x}^\top \mathbf{Q} \mathbf{x} \right)^{v/2} K_v \left\{ t \left(\mathbf{x}^\top \mathbf{Q} \mathbf{x} \right)^{1/2} \right\}$$

for $t > 0$, where $v = (2 - d)/2$ and K_v is the modified Bessel function of the second kind (Kotz et al. 2001). Therefore, $-\log f_{[L]}(t\mathbf{x}) =$

$$= - \left(1 + \frac{d}{2} \right) \log 2 + \frac{d}{2} \log(2\pi) - \frac{1}{2} \log|\mathbf{Q}| + v \log(2/t) - \frac{v}{2} \log \left(\mathbf{x}^\top \mathbf{Q} \mathbf{x} \right) - \log \left[K_v \left\{ t \left(\mathbf{x}^\top \mathbf{Q} \mathbf{x} \right)^{1/2} \right\} \right]$$

Asymptotically, we have $K_v(z) \sim (\pi/2z)^{1/2} e^{-z} (1 + O(z^{-1}))$ as $z \rightarrow \infty$ (Gradshteyn & Ryzhik 2014). Applying the negative logarithm, obtain

$$-\log K_v(z) \sim -\frac{1}{2} \log \left(\frac{\pi}{2} \right) + \frac{1}{2} \log z + z + O(z^{-1}).$$

Substituting this in the expression for $-\log f_{[L]}(t\mathbf{x})$, obtain

$$\begin{aligned} -\log f_{[L]}(t\mathbf{x}) &\sim - \left(1 + \frac{d}{2} \right) \log 2 + \frac{d}{2} \log 2\pi - \frac{1}{2} |\mathbf{Q}| - v \log t + v \log 2 - \frac{v}{2} \log \left(\mathbf{x}^\top \mathbf{Q} \mathbf{x} \right) \\ &\quad - \frac{1}{2} \log \left(\frac{\pi}{2} \right) + \frac{1}{2} \log t + \frac{1}{4} \log \left(\mathbf{x}^\top \mathbf{Q} \mathbf{x} \right) + t \left(\mathbf{x}^\top \mathbf{Q} \mathbf{x} \right)^{1/2} + O(t^{-1}) \\ &= t g_{\mathcal{G}}(\mathbf{x}) + (\log t) u_1(\mathbf{x}) + u_2(\mathbf{x}) + O(t^{-1}), \end{aligned}$$

for $t \rightarrow \infty$, where the gauge function is $g_{\mathcal{G}}(\mathbf{x}) = (\mathbf{x}^\top \mathbf{Q} \mathbf{x})^{1/2}$. The higher order terms are given by $u_1(\mathbf{x}) = \frac{1}{2} - v$ and $u_2(\mathbf{x}) = - \left(1 + \frac{d}{2} - v \right) \log 2 + \frac{d}{2} \log 2\pi - \frac{1}{2} \log|\mathbf{Q}| - \frac{1}{2} \log \left(\frac{\pi}{2} \right) + \left(\frac{1}{4} - \frac{v}{2} \right) \log \left(\mathbf{x}^\top \mathbf{Q} \mathbf{x} \right)$.

A.3 Multivariate max-stable Logistic distribution with standard Fréchet marginal distributions

For positive entries $\mathbf{x} \in \mathbb{R}_+^d$, the joint density in standard Fréchet margins is

$$f(\mathbf{x}) = \left(\sum_{\pi \in \Pi} (-1)^{|\pi|} \prod_{s \in \pi} V_s(\mathbf{x}) \right) \exp \{ -V(\mathbf{x}) \}$$

where $V(\mathbf{x}) = \left(\sum_{j=1}^d x_j^{-1/\theta} \right)^\theta$ is a -1 -homogeneous exponent function with dependence parameter $\theta \in (0, 1)$, and V_s is the $|s|$ -order partial derivative of V with respect to inputs whose indices are in s (see

Supplementary A.4). The 1-homogeneous gauge function is

$$\begin{aligned} g_{\mathcal{G}}(\mathbf{x}) &= \lim_{t \rightarrow \infty} \frac{-\log f(t\mathbf{x})}{t^{-1}} \\ &= V(\mathbf{x})^{-1} \end{aligned}$$

with higher order term

$$\begin{aligned} u_1(\mathbf{x}) &= -\log f(t\mathbf{x}) - \frac{1}{t} g_{\mathcal{G}}(\mathbf{x})^{-1} \\ &= -\log \left(\sum_{\pi \in \Pi} (-1)^{|\pi|} \prod_{s \in \pi} V_s(\mathbf{x}) \right) \\ &= -\log \left[\sum_{\pi \in \Pi} (-1)^{|\pi|} \prod_{s \in \pi} \left\{ (-\theta)^{|s|-1} \left(\prod_{k \in s} x_k \right)^{-\frac{1}{\theta}-1} \left(\sum_{j=1}^d x_j^{-1/\theta} \right)^{\theta-|s|} \right\} \right] \end{aligned}$$

A.4 Multivariate max-stable and inverted max-stable copula, logistic dependence

The joint density function in Fréchet margins is

$$f_F(\mathbf{z}) = \left(\sum_{\pi \in \Pi} (-1)^{|\pi|} \prod_{s \in \pi} V_s(\mathbf{z}) \right) \exp \{-V(\mathbf{z})\}$$

where $V(\mathbf{z}) = \left(\sum_{j=1}^d z_j^{-1/\theta} \right)^{\theta}$ is a -1 -homogeneous exponent function with dependence parameter $\theta \in (0, 1)$, and V_s is the $|s|$ -order partial derivative of V with respect to inputs whose indices are in s . Let Π be the set of all partitions of the set of indices $\{1, \dots, d\}$, and let π be the set of all partitions of an arbitrary element in Π . To obtain the joint density in Laplace margins, change of variables is implemented.

Suppose $z_t(x_j) = z(tx_j)$ for $t > 0$ and $j \in \{1, \dots, d\}$. If $x_j < 0$ (or $z_t(x_j) < (\log 2)^{-1}$), then we perform the change of variables from Fréchet to Laplace margins

$$z_t(x_j) = \left(-\log \left(\frac{1}{2} e^{tx_j} \right) \right)^{-1} = (-tx_j)^{-1} \left(1 - \log 2 (-tx_j)^{-1} + O(t^{-2}) \right)$$

with derivative given by

$$\frac{d}{d(tx_j)} z_t(x_j) = (-tx_j)^{-2} \left(1 - 2 \log 2 (-tx_j)^{-1} + O(t^{-2}) \right).$$

If $x_j > 0$ (or $z_t(x_j) > (\log 2)^{-1}$), then

$$z_t(x_j) = \left(-\log \left(1 - \frac{1}{2} e^{-tx_j} \right) \right)^{-1} = 2e^{tx_j} - \frac{1}{2} + O(e^{-tx_j})$$

with derivative given by

$$\frac{d}{d(tx_j)} z_t(x_j) = 2e^{tx_j} + O(e^{-tx_j}).$$

Lastly, if $x_j = 0$, then $z_t(x_j) = (\log 2)^{-1}$. By the inverse function and chain rules,

$$\frac{d}{d(tx_j)} z_t(x_j) = \frac{f_L(tx_j)}{f_F(F_F^{-1}(F_L(tx_j)))} = \begin{cases} \frac{e^{-t|x_j|}}{e^{tx_j}(\log(\frac{1}{2}e^{tx_j}))^2} & ; x_j < 0 \\ \frac{\frac{1}{2}e^{-t|x_j|}}{(1-\frac{1}{2}e^{-tx_j})(\log(1-\frac{1}{2}e^{-tx_j}))^2} & ; x_j > 0 \end{cases} \xrightarrow{x_j \rightarrow 0} (\log 2)^{-2}$$

For a vector $\mathbf{x} = (x_1, \dots, x_d)^\top$, let $A, B, C \subset \{1, \dots, d\}$ be the set of indices such that x_j is positive, negative, and zero for $j \in A, B, C$, respectively such that $|A| + |B| + |C| = d$. By change of variables, the joint density for the max-stable distribution with logistic dependence in Laplace margins is

$$\begin{aligned} f_L(t\mathbf{x}) &= \left| \prod_{j=1}^d \frac{d}{d(tx_j)} z_t(x_j) \right| f_F(z(tx_1), \dots, z(tx_d)) \\ &= (-1)^{d+1} \left\{ \prod_{\ell=0}^{d-1} \left(1 - \frac{\ell}{\theta}\right) \right\} 2^{-\frac{|A|}{\theta} t^{\left(\frac{1}{\theta}-1\right)|B|+1-\frac{d}{\theta}} (\log 2)^{-2|C|} \left(\prod_{k \in B} (-x_k)^{\frac{1}{\theta}-1} \right) \left(\sum_{k \in B} (-x_k)^{1/\theta} \right)^{\theta-d} \\ &\quad \times \exp \left\{ -t \left[\frac{1}{\theta} \sum_{j \in A} x_j + \left(\sum_{k \in B} (-x_k)^{1/\theta} \right)^\theta \left(1 + O\left(e^{-\frac{t}{\theta} \min_{j \in A} x_j}\right) + O(t^{-1}) \right) \right] \right\} (1 + o(1)) \end{aligned}$$

Applying the negative logarithm, obtain the following expression

$$\begin{aligned} -\log f_L(t\mathbf{x}) &= -\log \left[(-1)^{d+1} \left\{ \prod_{\ell=0}^{d-1} \left(1 - \frac{\ell}{\theta}\right) \right\} 2^{-\frac{|A|}{\theta} t^{\left(\frac{1}{\theta}-1\right)|B|+1-\frac{d}{\theta}} (\log 2)^{-2|C|} \right] - \left(\frac{1}{\theta} - 1 \right) \sum_{k \in B} \log(-x_k) \\ &\quad - (\theta - d) \log \left(\sum_{k \in B} (-x_k)^{1/\theta} \right) + \left\{ - \left(\frac{1}{\theta} - 1 \right) |B| - 1 + \frac{d}{\theta} \right\} \log t \\ &\quad + t \left[\frac{1}{\theta} \sum_{j \in A} x_j + \left\{ \sum_{k \in B} (-x_k)^{1/\theta} \right\}^\theta \left\{ 1 + O\left(e^{-\frac{t}{\theta} \min_{j \in A} x_j}\right) + O(t^{-1}) \right\} \right] + o(1) \\ &= tg(\mathbf{x}) + (\log t)u_1(\mathbf{x}) + u_2(\mathbf{x}) \end{aligned}$$

where, when letting $t \rightarrow \infty$, the gauge function is

$$g(\mathbf{x}) = \frac{1}{\theta} \sum_{j \in A} x_j + \left\{ \sum_{k \in B} (-x_k)^{1/\theta} \right\}^\theta$$

the higher order terms are given by

$$u_1(\mathbf{x}) = - \left(\frac{1}{\theta} - 1 \right) |B| - 1 + \frac{d}{\theta}$$

and

$$u_2(\mathbf{x}) = -\log \left[\frac{(-1)^{d+1} 2^{-\frac{|A|}{\theta}}}{(\log 2)^{-2|C|}} \left\{ \prod_{\ell=0}^{d-1} \left(1 - \frac{\ell}{\theta}\right) \right\} \right] - \left(\frac{1}{\theta} - 1 \right) \sum_{k \in B} \log(-x_k) - (\theta - d) \log \left\{ \sum_{k \in B} (-x_k)^{1/\theta} \right\}$$

There are 2 special cases to consider:

- **special case 1:** Suppose $x_j > 0 \forall j \in \{1, \dots, d\}$ and let $x_{(d)} = \min_{j=1, \dots, d} x_j$. Here, the joint

log-density is

$$\begin{aligned} -\log f_L(t\mathbf{x}) &= -\log \left[2^{-1}(-1)^d \left\{ \prod_{\ell=1}^{d-1} \left(1 - \frac{\ell}{\theta} \right) \right\} \right] + t \left\{ \frac{1}{\theta} \sum_{j=1}^d x_j + \left(1 - \frac{d}{\theta} \right) x_{(d)} \right\} + \\ &+ 2^{-1} e^{-tx_{(d)}} (1 + o(1)) + o(1) = tg(\mathbf{x}) + u_1(\mathbf{x}) + o(1) \end{aligned}$$

where the gauge function is

$$g(\mathbf{x}) = \frac{1}{\theta} \sum_{j=1}^d x_j + \left(1 - \frac{d}{\theta} \right) \min_{k=1, \dots, d} x_k$$

and the higher order term is

$$u_1(\mathbf{x}) = -\log \left[2^{-1}(-1)^{d+1} \left\{ \prod_{\ell=1}^{d-1} \left(1 - \frac{\ell}{\theta} \right) \right\} \right], \quad \text{as } t \rightarrow \infty.$$

- **special case 2:** Suppose $x_j < 0 \forall j \in \{1, \dots, d\}$. Here, we have

$$-\log f_L(t\mathbf{x}) = tg(\mathbf{x}) + (\log t)u_1(\mathbf{x}) + u_2(\mathbf{x}) + o(1)$$

where the gauge function is

$$g(\mathbf{x}) = \left\{ \sum_{j=1}^d (-x_j)^{1/\theta} \right\}^\theta$$

the higher order terms are given by

$$u_1(\mathbf{x}) = d - 1$$

and

$$u_2(\mathbf{x}) = -\log \left[(-1)^{d+1} \left\{ \prod_{\ell=0}^{d-1} \left(1 - \frac{\ell}{\theta} \right) \right\} \left\{ \prod_{j=1}^d (-x_j) \right\}^{\frac{1}{\theta}-1} \left\{ \sum_{j=1}^d (-x_j)^{1/\theta} \right\}^{\theta-d} \right], \quad \text{as } t \rightarrow \infty.$$

To study the case of **inverted logistic dependence**, first recall the definition of the joint distribution function in Fréchet margins

$$F_F(\mathbf{z}) = \exp \{-V(\mathbf{z})\}$$

By evaluating at the univariate Frechet quantile function, get the Logistic copula

$$C_{log.}(u_1, \dots, u_d) = F_F \left(-\frac{1}{\log u_1}, \dots, -\frac{1}{\log u_d} \right) = \exp \left\{ -V \left(-\frac{1}{\log u_1}, \dots, -\frac{1}{\log u_d} \right) \right\}$$

where V is specified to be the exponent function commonly associated with logistic dependence. The survival copula associated with the inverted logistic distribution is therefore given by

$$\bar{C}_{inv.log.}(u_1, \dots, u_d) = C_{log.}(1 - u_1, \dots, 1 - u_d) = \exp \left\{ -V \left(-\frac{1}{\log(1 - u_1)}, \dots, -\frac{1}{\log(1 - u_d)} \right) \right\}$$

So $x_j > 0$ (or $u_j > 1/2$) in the logistic case corresponds to $x_j < 0$ (or $u_j < 1/2$) in the inverted logistic case. This leads to the decomposition of the log-joint density in Laplace margins $-\log f_L(t\mathbf{x}) =$

$tg(\mathbf{x}) + (\log t)u_1(\mathbf{x}) + g_0^*(\mathbf{x})$ where the gauge function is

$$g(\mathbf{x}) = \left(\sum_{j \in A} x_j^{1/\theta} \right)^\theta + \frac{1}{\theta} \sum_{k \in B} (-x_k)$$

the higher-order terms are given by

$$u_1(\mathbf{x}) = - \left(\frac{1}{\theta} - 1 \right) |A| - 1 + \frac{d}{\theta}$$

and

$$u_2(\mathbf{x}) = -\log \left[(-1)^{d+1} \left\{ \prod_{\ell=0}^{d-1} \left(1 - \frac{\ell}{\theta} \right) \right\} 2^{-\frac{|B|}{\theta}} (\log 2)^{-2|C|} \right] - \left(\frac{1}{\theta} - 1 \right) \sum_{j \in A} \log(x_j) - (\theta - d) \log \left(\sum_{j \in A} x_j^{1/\theta} \right)$$

In the case where $x_j > 0 \forall j \in \{1, \dots, d\}$ we have $-\log f_L(t\mathbf{x}) = tg(\mathbf{x}) + (\log t)u_1(\mathbf{x}) + u_2(\mathbf{x}) + o(1)$ where the gauge function is

$$g(\mathbf{x}) = \left(\sum_{j=1}^d x_j^{1/\theta} \right)^\theta$$

with higher-order terms given by

$$u_1(\mathbf{x}) = d - 1$$

and

$$u_2(\mathbf{x}) = -\log \left[(-1)^{d+1} \left\{ \prod_{\ell=0}^{d-1} \left(1 - \frac{\ell}{\theta} \right) \right\} \left(\prod_{j=1}^d x_j \right)^{\frac{1}{\theta}-1} \left(\sum_{j=1}^d x_j^{1/\theta} \right)^{\theta-d} \right]$$

as $t \rightarrow \infty$. In the case where $x_j < 0 \forall j \in \{1, \dots, d\}$ we have

$$-\log f_L(t\mathbf{x}) = tg(\mathbf{x}) + u_1(\mathbf{x}) + o(1)$$

where the gauge function is

$$g(\mathbf{x}) = \frac{1}{\theta} \sum_{j=1}^d (-x_j) + \left(1 - \frac{d}{\theta} \right) \min_{k=1, \dots, d} |x_k|$$

and the higher order term is

$$u_1(\mathbf{x}) = -\log \left[2^{-1} (-1)^d \left\{ \prod_{\ell=1}^{d-1} \left(1 - \frac{\ell}{\theta} \right) \right\} \right], \quad \text{as } t \rightarrow \infty.$$

The joint density function in Fréchet margins is

$$f_F(\mathbf{z}) = \left(\sum_{\pi \in \Pi} (-1)^{|\pi|} \prod_{s \in \pi} V_s(\mathbf{z}) \right) \exp \{-V(\mathbf{z})\}$$

where $V(\mathbf{z}) = \left(\sum_{j=1}^d z_j^{-1/\theta} \right)^\theta$ is a -1 -homogeneous exponent function with dependence parameter $\theta \in (0, 1)$, and V_s is the $|s|$ -order partial derivative of V with respect to inputs whose indices are in s . Let Π be the set of all partitions of the set of indices $\{1, \dots, d\}$, and let π be the set of all partitions of an arbitraty

element in Π . To obtain the joint density in Laplace margins, change of variables is implemented.

Suppose $z_t(x_j) = z(tx_j)$ for $t > 0$ and $j \in \{1, \dots, d\}$. If $x_j < 0$ (or $z_t(x_j) < (\log 2)^{-1}$), then we perform the change of variables from Fréchet to Laplace margins

$$z_t(x_j) = \left(-\log \left(\frac{1}{2} e^{tx_j} \right) \right)^{-1} = (-tx_j)^{-1} \left(1 - \log 2 (-tx_j)^{-1} + O(t^{-2}) \right)$$

with derivative given by

$$\frac{d}{d(tx_j)} z_t(x_j) = (-tx_j)^{-2} \left(1 - 2 \log 2 (-tx_j)^{-1} + O(t^{-2}) \right).$$

If $x_j > 0$ (or $z_t(x_j) > (\log 2)^{-1}$), then

$$z_t(x_j) = \left(-\log \left(1 - \frac{1}{2} e^{-tx_j} \right) \right)^{-1} = 2e^{tx_j} - \frac{1}{2} + O(e^{-tx_j})$$

with derivative given by

$$\frac{d}{d(tx_j)} z_t(x_j) = 2e^{tx_j} + O(e^{-tx_j}).$$

Lastly, if $x_j = 0$, then $z_t(x_j) = (\log 2)^{-1}$. By the inverse function and chain rules,

$$\frac{d}{d(tx_j)} z_t(x_j) = \frac{f_L(tx_j)}{f_F(F_F^{-1}(F_L(tx_j)))} = \begin{cases} \frac{e^{-t|x_j|}}{e^{tx_j} (\log(\frac{1}{2} e^{tx_j}))^2} & ; x_j < 0 \\ \frac{\frac{1}{2} e^{-t|x_j|}}{(1 - \frac{1}{2} e^{-tx_j}) (\log(1 - \frac{1}{2} e^{-tx_j}))^2} & ; x_j > 0 \end{cases} \xrightarrow{x_j \rightarrow 0} (\log 2)^{-2}$$

For a vector $\mathbf{x} = (x_1, \dots, x_d)^\top$, let $A, B, C \subset \{1, \dots, d\}$ be the set of indices such that x_j is positive, negative, and zero for $j \in A, B, C$, respectively such that $|A| + |B| + |C| = d$. By change of variables, the joint density for the max-stable distribution with logistic dependence in Laplace margins is

$$\begin{aligned} f_L(t\mathbf{x}) &= \left| \prod_{j=1}^d \frac{d}{d(tx_j)} z_t(x_j) \right| f_F(z(tx_1), \dots, z(tx_d)) \\ &= (-1)^{d+1} \left\{ \prod_{\ell=0}^{d-1} \left(1 - \frac{\ell}{\theta} \right) \right\} 2^{-\frac{|A|}{\theta}} t^{\left(\frac{1}{\theta}-1\right)|B|+1-\frac{d}{\theta}} (\log 2)^{-2|C|} \left(\prod_{k \in B} (-x_k)^{\frac{1}{\theta}-1} \right) \left(\sum_{k \in B} (-x_k)^{1/\theta} \right)^{\theta-d} \\ &\quad \times \exp \left\{ -t \left[\frac{1}{\theta} \sum_{j \in A} x_j + \left(\sum_{k \in B} (-x_k)^{1/\theta} \right)^\theta \left(1 + O \left(e^{-\frac{t}{\theta} \min_{j \in A} x_j} \right) + O(t^{-1}) \right) \right] \right\} (1 + o(1)) \end{aligned}$$

Applying the negative logarithm, obtain the following expression

$$\begin{aligned}
-\log f_L(t\mathbf{x}) &= -\log \left[(-1)^{d+1} \left\{ \prod_{\ell=0}^{d-1} \left(1 - \frac{\ell}{\theta} \right) \right\} 2^{-\frac{|A|}{\theta}} (\log 2)^{-2|C|} \right] - \left(\frac{1}{\theta} - 1 \right) \sum_{k \in B} \log(-x_k) \\
&\quad - (\theta - d) \log \left(\sum_{k \in B} (-x_k)^{1/\theta} \right) + \left\{ - \left(\frac{1}{\theta} - 1 \right) |B| - 1 + \frac{d}{\theta} \right\} \log t \\
&\quad + t \left[\frac{1}{\theta} \sum_{j \in A} x_j + \left\{ \sum_{k \in B} (-x_k)^{1/\theta} \right\}^\theta \left\{ 1 + O \left(e^{-\frac{t}{\theta} \min_{j \in A} x_j} \right) + O(t^{-1}) \right\} \right] + o(1) \\
&= tg(\mathbf{x}) + (\log t)u_1(\mathbf{x}) + u_2(\mathbf{x})
\end{aligned}$$

where, when letting $t \rightarrow \infty$, the gauge function is

$$g(\mathbf{x}) = \frac{1}{\theta} \sum_{j \in A} x_j + \left\{ \sum_{k \in B} (-x_k)^{1/\theta} \right\}^\theta$$

the higher order terms are given by

$$u_1(\mathbf{x}) = - \left(\frac{1}{\theta} - 1 \right) |B| - 1 + \frac{d}{\theta}$$

and

$$u_2(\mathbf{x}) = -\log \left[\frac{(-1)^{d+1} 2^{-\frac{|A|}{\theta}}}{(\log 2)^{-2|C|}} \left\{ \prod_{\ell=0}^{d-1} \left(1 - \frac{\ell}{\theta} \right) \right\} \right] - \left(\frac{1}{\theta} - 1 \right) \sum_{k \in B} \log(-x_k) - (\theta - d) \log \left\{ \sum_{k \in B} (-x_k)^{1/\theta} \right\}$$

There are 2 special cases to consider:

- **special case 1:** Suppose $x_j > 0 \forall j \in \{1, \dots, d\}$ and let $x_{(d)} = \min_{j=1, \dots, d} x_j$. Here, the joint log-density is

$$\begin{aligned}
-\log f_L(t\mathbf{x}) &= -\log \left[2^{-1} (-1)^d \left\{ \prod_{\ell=1}^{d-1} \left(1 - \frac{\ell}{\theta} \right) \right\} \right] + t \left\{ \frac{1}{\theta} \sum_{j=1}^d x_j + \left(1 - \frac{d}{\theta} \right) x_{(d)} \right\} + \\
&\quad + 2^{-1} e^{-tx_{(d)}} (1 + o(1)) + o(1) = tg(\mathbf{x}) + u_1(\mathbf{x}) + o(1)
\end{aligned}$$

where the gauge function is

$$g(\mathbf{x}) = \frac{1}{\theta} \sum_{j=1}^d x_j + \left(1 - \frac{d}{\theta} \right) \min_{k=1, \dots, d} x_k$$

and the higher order term is

$$u_1(\mathbf{x}) = -\log \left[2^{-1} (-1)^{d+1} \left\{ \prod_{\ell=1}^{d-1} \left(1 - \frac{\ell}{\theta} \right) \right\} \right], \quad \text{as } t \rightarrow \infty.$$

- **special case 2:** Suppose $x_j < 0 \forall j \in \{1, \dots, d\}$. Here, we have

$$-\log f_L(t\mathbf{x}) = tg(\mathbf{x}) + (\log t)u_1(\mathbf{x}) + u_2(\mathbf{x}) + o(1)$$

where the gauge function is

$$g(\mathbf{x}) = \left\{ \sum_{j=1}^d (-x_j)^{1/\theta} \right\}^\theta$$

the higher order terms are given by

$$u_1(\mathbf{x}) = d - 1$$

and

$$u_2(\mathbf{x}) = -\log \left[(-1)^{d+1} \left\{ \prod_{\ell=0}^{d-1} \left(1 - \frac{\ell}{\theta} \right) \right\} \left\{ \prod_{j=1}^d (-x_j) \right\}^{\frac{1}{\theta}-1} \left\{ \sum_{j=1}^d (-x_j)^{1/\theta} \right\}^{\theta-d} \right], \quad \text{as } t \rightarrow \infty.$$

To study the case of **inverted logistic dependence**, first recall the definition of the joint distribution function in Fréchet margins

$$F_F(\mathbf{z}) = \exp \{-V(\mathbf{z})\}$$

By evaluating at the univariate Frechet quantile function, get the Logistic copula

$$C_{log.}(u_1, \dots, u_d) = F_F \left(-\frac{1}{\log u_1}, \dots, -\frac{1}{\log u_d} \right) = \exp \left\{ -V \left(-\frac{1}{\log u_1}, \dots, -\frac{1}{\log u_d} \right) \right\}$$

where V is specified to be the exponent function commonly associated with logistic dependence. The survival copula associated with the inverted logistic distribution is therefore given by

$$\bar{C}_{inv.log.}(u_1, \dots, u_d) = C_{log.}(1 - u_1, \dots, 1 - u_d) = \exp \left\{ -V \left(-\frac{1}{\log(1 - u_1)}, \dots, -\frac{1}{\log(1 - u_d)} \right) \right\}$$

So $x_j > 0$ (or $u_j > 1/2$) in the logistic case corresponds to $x_j < 0$ (or $u_j < 1/2$) in the inverted logistic case. This leads to the decomposition of the log-joint density in Laplace margins $-\log f_L(t\mathbf{x}) = tg(\mathbf{x}) + (\log t)u_1(\mathbf{x}) + g_0^*(\mathbf{x})$ where the gauge function is

$$g(\mathbf{x}) = \left(\sum_{j \in A} x_j^{1/\theta} \right)^\theta + \frac{1}{\theta} \sum_{k \in B} (-x_k)$$

the higher-order terms are given by

$$u_1(\mathbf{x}) = - \left(\frac{1}{\theta} - 1 \right) |A| - 1 + \frac{d}{\theta}$$

and

$$u_2(\mathbf{x}) = -\log \left[(-1)^{d+1} \left\{ \prod_{\ell=0}^{d-1} \left(1 - \frac{\ell}{\theta} \right) \right\} 2^{-\frac{|B|}{\theta}} (\log 2)^{-2|C|} \right] - \left(\frac{1}{\theta} - 1 \right) \sum_{j \in A} \log(x_j) - (\theta - d) \log \left(\sum_{j \in A} x_j^{1/\theta} \right)$$

In the case where $x_j > 0 \forall j \in \{1, \dots, d\}$ we have $-\log f_L(t\mathbf{x}) = tg(\mathbf{x}) + (\log t)u_1(\mathbf{x}) + u_2(\mathbf{x}) + o(1)$ where the gauge function is

$$g(\mathbf{x}) = \left(\sum_{j=1}^d x_j^{1/\theta} \right)^\theta$$

with higher-order terms given by

$$u_1(\mathbf{x}) = d - 1$$

and

$$u_2(\mathbf{x}) = -\log \left[(-1)^{d+1} \left\{ \prod_{\ell=0}^{d-1} \left(1 - \frac{\ell}{\theta} \right) \right\} \left(\prod_{j=1}^d x_j \right)^{\frac{1}{\theta}-1} \left(\sum_{j=1}^d x_j^{1/\theta} \right)^{\theta-d} \right]$$

as $t \rightarrow \infty$. In the case where $x_j < 0 \ \forall j \in \{1, \dots, d\}$ we have

$$-\log f_L(t\mathbf{x}) = tg(\mathbf{x}) + u_1(\mathbf{x}) + o(1)$$

where the gauge function is

$$g(\mathbf{x}) = \frac{1}{\theta} \sum_{j=1}^d (-x_j) + \left(1 - \frac{d}{\theta} \right) \min_{k=1, \dots, d} |x_k|$$

and the higher order term is

$$u_1(\mathbf{x}) = -\log \left[2^{-1} (-1)^d \left\{ \prod_{\ell=1}^{d-1} \left(1 - \frac{\ell}{\theta} \right) \right\} \right], \quad \text{as } t \rightarrow \infty.$$

A.5 Multivariate Student- t_ν copula, Student- t_ν margins, $\nu > 0$

Suppose \mathbf{Q} positive definite and $\nu > 0$. The joint density can be expressed as $f(\mathbf{x}) = f_0(g_{\mathcal{G}}(\mathbf{x}))$, where the homothetic function f_0 and gauge function is given by

$$\begin{aligned} f_0(s) &= k_{\nu, \mathbf{Q}} (1 + \nu^{-1} s^2)^{-\frac{1}{2}(\nu+d)}, \\ g_{\mathcal{G}}(\mathbf{x}) &= \left(\mathbf{x}^\top \mathbf{Q} \mathbf{x} \right)^{1/2}, \end{aligned}$$

where $k_{\nu, \mathbf{Q}} = \Gamma\left(\frac{\nu+d}{2}\right) / \left\{ \Gamma\left(\frac{\nu}{2}\right) \nu^{d/2} \pi^{d/2} |\mathbf{Q}|^{-1/2} \right\}$. By the third condition of Proposition 2, setting $\psi(t) = k_{\nu, \mathbf{Q}} \nu^{\frac{1}{2}(\nu+d)} t^{-(\nu+d)}$, and for $t > 0$ large, the higher-order term is

$$\begin{aligned} u(\mathbf{x}) &= \frac{\frac{f(t\mathbf{x})}{\psi(t)} - g(\mathbf{x})^{-(\nu+d)}}{t^{-2}} \\ &= t^2 \left[\psi(t)^{-1} k_{\nu, \mathbf{Q}} \nu^{\frac{1}{2}(\nu+d)} t^{-(\nu+d)} g_{\mathcal{G}}(\mathbf{x})^{-(\nu+d)} \left\{ 1 + \nu t^{-2} g_{\mathcal{G}}(\mathbf{x})^{-2} \right\}^{-\frac{1}{2}(\nu+d)} - g_{\mathcal{G}}(\mathbf{x})^{-(\nu+d)} \right] \\ &= t^2 \left[g_{\mathcal{G}}(\mathbf{x})^{-(\nu+d)} \left\{ 1 - \frac{1}{2}(\nu+d) \nu t^{-2} g_{\mathcal{G}}(\mathbf{x})^{-2} + O(t^{-4}) \right\} - g_{\mathcal{G}}(\mathbf{x})^{-(\nu+d)} \right] \\ &= -\frac{1}{2}(\nu+d) \nu g_{\mathcal{G}}(\mathbf{x})^{-2-(\nu+d)} + O(t^{-2}) \\ &= -\frac{1}{2}(\nu+d) \nu g_{\mathcal{G}}(\mathbf{x})^{-2-(\nu+d)} + o(1) \end{aligned}$$

A.6 Multivariate Student- t_ν copula, Student- t_ν margins, $\nu < 0$

Suppose \mathbf{Q} positive definite and $\nu < 0$ and $\nu < 2 - d$ (Papastathopoulos & Tawn 2013). For support $\{\mathbf{x} \in \mathbb{R}^d : 1 + \nu^{-1} \mathbf{x}^\top \mathbf{Q} \mathbf{x} > 0\}$, the joint density is given by

$$f(\mathbf{x}) = k_{\nu, \mathbf{Q}} \left(1 + \nu^{-1} \mathbf{x}^\top \mathbf{Q} \mathbf{x} \right)^{-\frac{1}{2}(\nu+d)}$$

where $k_{\nu, \mathbf{Q}} = \pi^{-d/2} |\mathbf{Q}|^{1/2} |\nu|^{1-\frac{d}{2}} (|\nu| - d)^{-1} \Gamma\left(\frac{|\nu|}{2}\right) \Gamma\left(\frac{|\nu|-d}{2}\right)^{-1}$. Note the homothetic form $f(\mathbf{x}) = f_0(g_{\mathcal{G}}(\mathbf{x}))$, where $f_0(s) = k_{\nu, \mathbf{Q}}(1 - s^2)^{-\frac{1}{2}(\nu+d)}$ for $s \in (-1, 1)$. Therefore, we extract the gauge function

$$g_{\mathcal{G}}(\mathbf{x}) = \left(-\nu^{-1} \mathbf{x}^\top \mathbf{Q} \mathbf{x} \right)^{1/2}$$

Therefore, $r_{\mathcal{G}}(\cdot) = g_{\mathcal{G}}(\cdot)^{-1}$ is a -1 -homogeneous radial function, and $r_{\mathcal{G}}(\mathbf{x})\mathbf{x}$ lies on the boundary of the support (i.e., $f\{r_{\mathcal{G}}(\mathbf{x})\mathbf{x}\} = 0$). By the intuition provided by condition (i) in Proposition 2, the rate of convergence can be characterised by

$$\begin{aligned} f\{r_{\mathcal{G}}(\mathbf{x})(\mathbf{x} - t^{-1}\mathbf{1})\} &= k_{\nu, \mathbf{Q}} \left[1 - r_{\mathcal{G}}\{r_{\mathcal{G}}(\mathbf{x})(\mathbf{x} - t^{-1}\mathbf{1})\}^2 \right]_+^{-\frac{1}{2}(\nu+d)} \\ &= k_{\nu, \mathbf{Q}} \left[1 - r_{\mathcal{G}}(\mathbf{x})^2 r_{\mathcal{G}}(\mathbf{x} - t^{-1}\mathbf{1})^2 \right]_+^{-\frac{1}{2}(\nu+d)} \\ &= k_{\nu, \mathbf{Q}} \left[1 - r_{\mathcal{G}}(\mathbf{x})^2 \{r_{\mathcal{G}}(\mathbf{x}) - \nabla r_{\mathcal{G}}(\mathbf{x})t^{-1} + O(t^{-2})\}^2 \right]_+^{-\frac{1}{2}(\nu+d)} \\ &= k_{\nu, \mathbf{Q}} t^{\frac{1}{2}(\nu+d)} \left\{ -\frac{2}{r_{\mathcal{G}}(\mathbf{x})} \nabla r_{\mathcal{G}}(\mathbf{x}) + O(t^{-1}) \right\} \end{aligned}$$

Therefore,

$$\frac{f\{r_{\mathcal{G}}(\mathbf{x})(\mathbf{x} - t^{-1}\mathbf{1})\}}{k_{\nu, \mathbf{Q}} t^{\frac{1}{2}(\nu+d)}} = -\frac{2}{r_{\mathcal{G}}(\mathbf{x})} \nabla r_{\mathcal{G}}(\mathbf{x}) + o(1)$$

A.7 Multivariate Student- t_ν copula, $\nu > 0$, Laplace margins

The multivariate t-distribution with positive definite precision matrix $\mathbf{Q} = (q_{ij})_{i,j=1}^d$ and with univariate t-distribution margins with ν degrees of freedom is given has joint density

$$f(\mathbf{z}) = k_{\nu, \mathbf{Q}} \left(1 + \frac{1}{\nu} \sum_{j=1}^d q_{jj} z_j^2 + \frac{2}{\nu} \sum_{1 \leq j < k \leq d} q_{jk} z_j z_k \right)^{-\frac{1}{2}(\nu+d)}$$

where $k_{\nu, \mathbf{Q}} = \Gamma\left(\frac{\nu+d}{2}\right) / \left\{ \Gamma\left(\frac{\nu}{2}\right) \nu^{d/2} \pi^{d/2} |\mathbf{Q}|^{-1/2} \right\}$. Perform the change of variables to the standard Laplace distribution, where we take advantage of a univariate t-distribution analogue of Mill's ratio (Soms 1976). Let f_{t_ν} and F_{t_ν} be the density and distribution functions of the univariate t-distribution with ν degrees of freedom, respectively.

Suppose $z = z(tx) > 0$ (or $x > 0$), then for $t > 0$ large, the change of variables from the t-distribution to

the standard Laplace distribution

$$tx = -\log [2 \{1 - F_{t\nu}(z(tx))\}] = -\log \left[\frac{2\Gamma\left(\frac{\nu+1}{2}\right) \nu^{\left(\frac{1-\nu}{2}\right)}}{\Gamma\left(\frac{\nu}{2}\right) \sqrt{\nu\pi}} \right] + \nu \log z(tx) + O(z(tx)^{-2}).$$

Inverting this transformation, obtain

$$z(tx) = c_\nu e^{\frac{t}{\nu}x} \left(1 + O\left(e^{\frac{-2t}{\nu}}\right)\right),$$

with partial derivative with respect to tx given by

$$\frac{d}{dtx} z(tx) = \frac{c_\nu}{\nu} e^{\frac{t}{\nu}x} \left(1 + O\left(e^{\frac{-2t}{\nu}}\right)\right),$$

where $c_\nu = \left\{2\Gamma\left(\frac{\nu+1}{2}\right) \nu^{\left(\frac{1-\nu}{2}\right)} \Gamma\left(\frac{\nu}{2}\right)^{-1} (\nu\pi)^{-1/2}\right\}^{1/\nu}$. When $z(tx) < 0$ (or $x < 0$), the transformation to Laplace margins is

$$tx = \log [2F_{t\nu}(z(tx))] = \log 2 + \log [1 - F_{t\nu}(-z(tx))].$$

Negating,

$$-tx = -\log 2 - \log (1 - F_{t\nu}(-z(tx))) = -\log \left[\frac{2\Gamma\left(\frac{\nu+1}{2}\right) \nu^{\left(\frac{1-\nu}{2}\right)}}{\Gamma\left(\frac{\nu}{2}\right) \sqrt{\nu\pi}} \right] + \nu \log(-z(tx)) + O(z(tx)^{-2}).$$

Inverting this transformation,

$$z(tx) = -c_\nu e^{\frac{t}{\nu}|x|} \left(1 + O\left(e^{\frac{-2t}{\nu}}\right)\right),$$

with partial derivative

$$\frac{d}{dtx} z(tx) = \frac{c_\nu}{\nu} e^{\frac{t}{\nu}|x|} \left(1 + O\left(e^{\frac{-2t}{\nu}}\right)\right).$$

Therefore, by change of variables, obtain the joint density in Laplace margins

$$\begin{aligned} f_L(t\mathbf{x}) &= \left| \prod_{j=1}^d \frac{d}{d(tx_j)} z(tx_j) \right| f(z(tx_1), \dots, z(tx_d)) \\ &= \frac{c_\nu^d k_{\nu, \mathbf{Q}}}{\nu^d} \exp \left\{ \frac{t}{\nu} \sum_{j=1}^d |x_j| \right\} \frac{q_{j^* j^*} c_\nu^2}{\nu} \exp \left\{ -t \left(1 + \frac{d}{\nu}\right) \max_{j=1, \dots, d} |x_j| \right\} (1 + o(1)), \end{aligned}$$

where j^* is the index such that $|x_{j^*}| = \max_{j=1, \dots, d} |x_j|$. Taking the negative logarithm, we obtain

$$-\log f_L(t\mathbf{x}) = tg(\mathbf{x}) + u_1(\mathbf{x}) + o(1),$$

where the gauge function is

$$g(\mathbf{x}) = -\frac{1}{\nu} \sum_{j=1}^d |x_j| + \left(1 + \frac{d}{\nu}\right) \max_{j=1, \dots, d} |x_j|,$$

and the higher order term is

$$u_1(\mathbf{x}) = -\log \left(\frac{c_\nu^{d+2} k_{\nu, \mathbf{Q}} q_{j^* j^*}}{\nu^{d+1}} \right).$$

B Supplementary material B: Angular densities

B.1 Multivariate normal distribution, standard normal margins

The joint density can be written in the form $f(\mathbf{x}) = f_0(g_{\mathcal{G}}(\mathbf{x}))$, where $f(s) = (2\pi)^{-d/2} |\mathbf{Q}|^{1/2} \exp \{-s^2/2\}$. By (A.21),

$$\begin{aligned} f_{\mathbf{W}}(\mathbf{w}) &= g_{\mathcal{G}}(\mathbf{x})^{-d} \int_0^\infty s^{d-1} f_0(s) ds \\ &= (2\pi)^{-d/2} |\mathbf{Q}|^{1/2} \left(\mathbf{w}^\top \mathbf{Q} \mathbf{w} \right)^{-d/2} \int_0^\infty s^{d-1} e^{-\frac{1}{2}s^2} ds \\ &= \Gamma(d/2) 2^{\frac{d}{2}-1} (2\pi)^{-d/2} |\mathbf{Q}|^{1/2} \left(\mathbf{w}^\top \mathbf{Q} \mathbf{w} \right)^{-d/2} \\ &= \Gamma(d/2) 2^{-1} \pi^{-d/2} |\mathbf{Q}|^{1/2} \left(\mathbf{w}^\top \mathbf{Q} \mathbf{w} \right)^{-d/2} \end{aligned}$$

B.2 Multivariate normal distribution, standard Laplace margins

The density of exceedance angles is

$$\begin{aligned}
f_{\mathbf{W}|R>r_{\mathcal{Q}_q}(\mathbf{W})}(\mathbf{w}) &= \frac{f_{\mathbf{W},R>r_{\mathcal{Q}_q}(\mathbf{W})}(\mathbf{w})}{\Pr(R > r_{\mathcal{Q}_q}(\mathbf{W}))} \\
&= (1-q)^{-1} \int_{r_{\mathcal{Q}_q}(\mathbf{w})}^{\infty} f_{R,\mathbf{W}}(r, \mathbf{w}) dr \\
&= (1-q)^{-1} \int_{r_{\mathcal{Q}_q}(\mathbf{w})}^{\infty} r^{d-1} f_{[L]}(r\mathbf{w}) dr \\
&= (1-q)^{-1} 2^{-d} |\mathbf{Q}|^{-1/2} \left(\prod_{j=1}^d 4\pi |w_j| \right)^{-1/2} \\
&\quad \times \exp \left\{ - \sum_{j=1}^d |w_j| - \left(\text{sgn}(\mathbf{w}) |\mathbf{w}|^{1/2} \right)^{\top} \mathbf{Q} \left((\log 2) \text{sgn}(\mathbf{w}) |\mathbf{w}|^{-1/2} \right) \mathbf{w} \right. \\
&\quad \left. + \frac{1}{2} \left(\text{sgn}(\mathbf{w}) |\mathbf{w}|^{1/2} \right)^{\top} \mathbf{Q} \left((\log 4\pi) \text{sgn}(\mathbf{w}) |\mathbf{w}|^{-1/2} \right) \right\} \\
&\quad \times \int_{r_{\mathcal{Q}_q}(\mathbf{w})}^{\infty} r^{\frac{d}{2} + \left(\text{sgn}(\mathbf{w}) |\mathbf{w}|^{1/2} \right)^{\top} \mathbf{Q} \left(\text{sgn}(\mathbf{w}) |\mathbf{w}|^{-1/2} \right) - 1} e^{-r \left(\text{sgn}(\mathbf{w}) |\mathbf{w}|^{1/2} \right)^{\top} \mathbf{Q} \left(\text{sgn}(\mathbf{w}) |\mathbf{w}|^{-1/2} \right)} dr \\
&\quad \times \{1 + o(1)\} \\
&= (1-q)^{-1} 2^{-d} |\mathbf{Q}|^{-1/2} \left(\prod_{j=1}^d 4\pi |w_j| \right)^{-1/2} \\
&\quad \times \exp \left\{ - \sum_{j=1}^d |w_j| - \left(\text{sgn}(\mathbf{w}) |\mathbf{w}|^{1/2} \right)^{\top} \mathbf{Q} \left((\log 2) \text{sgn}(\mathbf{w}) |\mathbf{w}|^{-1/2} \right) \right. \\
&\quad \left. + \frac{1}{2} \left(\text{sgn}(\mathbf{w}) |\mathbf{w}|^{1/2} \right)^{\top} \mathbf{Q} \left((\log 4\pi) \text{sgn}(\mathbf{w}) |\mathbf{w}|^{-1/2} \right) \right\} \\
&\quad \times \Gamma \left\{ \frac{d}{2} + \left(\text{sgn}(\mathbf{w}) |\mathbf{w}|^{1/2} \right)^{\top} \mathbf{Q} \left(\text{sgn}(\mathbf{w}) |\mathbf{w}|^{-1/2} \right) \right\} \\
&\quad \times \left\{ \left(\text{sgn}(\mathbf{w}) |\mathbf{w}|^{1/2} \right)^{\top} \mathbf{Q} \left(\text{sgn}(\mathbf{w}) |\mathbf{w}|^{-1/2} \right) \right\}^{-\frac{d}{2} - \left(\text{sgn}(\mathbf{w}) |\mathbf{w}|^{1/2} \right)^{\top} \mathbf{Q} \left(\text{sgn}(\mathbf{w}) |\mathbf{w}|^{-1/2} \right)} \\
&\quad \times \left[1 - F_{\text{Gamma}} \left(r_{\mathcal{Q}_q}(\mathbf{w}); \frac{d}{2} + \left(\text{sgn}(\mathbf{w}) |\mathbf{w}|^{1/2} \right)^{\top} \mathbf{Q} \left(\text{sgn}(\mathbf{w}) |\mathbf{w}|^{-1/2} \right), \left(\text{sgn}(\mathbf{w}) |\mathbf{w}|^{1/2} \right)^{\top} \mathbf{Q} \left(\text{sgn}(\mathbf{w}) |\mathbf{w}|^{-1/2} \right) \right) \right] \\
&\quad \times \{1 + o(1)\}
\end{aligned}$$

where $F_{Gamma}(x; \alpha, \beta)$ is the univariate Gamma cumulative distribution function evaluated at $x > 0$ with shape parameter $\alpha > 0$ and rate parameter $\beta > 0$. By Proposition 3, obtain the density of angles

$$\begin{aligned}
f_{\mathbf{W}}(\mathbf{w}) = & (1-q)^{-1} 2^{-d} |\mathbf{Q}|^{-1/2} \left(\prod_{j=1}^d 4\pi |w_j| \right)^{-1/2} \\
& \times \exp \left\{ - \sum_{j=1}^d |w_j| - \left(\text{sgn}(\mathbf{w}) |\mathbf{w}|^{1/2} \right)^\top \mathbf{Q} \left((\log 2) \text{sgn}(\mathbf{w}) |\mathbf{w}|^{-1/2} \right) \mathbf{w} \right. \\
& \quad \left. + \frac{1}{2} \left(\text{sgn}(\mathbf{w}) |\mathbf{w}|^{1/2} \right)^\top \mathbf{Q} \left((\log 4\pi |\mathbf{w}|) \text{sgn}(\mathbf{w}) |\mathbf{w}|^{-1/2} \right) \right\} \\
& \times \Gamma \left\{ \frac{d}{2} + \left(\text{sgn}(\mathbf{w}) |\mathbf{w}|^{1/2} \right)^\top \mathbf{Q} \left(\text{sgn}(\mathbf{w}) |\mathbf{w}|^{-1/2} \right) \right\} \\
& \times \left\{ \left(\text{sgn}(\mathbf{w}) |\mathbf{w}|^{1/2} \right)^\top \mathbf{Q} \left(\text{sgn}(\mathbf{w}) |\mathbf{w}|^{-1/2} \right) \right\}^{-\frac{d}{2} - \left(\text{sgn}(\mathbf{w}) |\mathbf{w}|^{1/2} \right)^\top \mathbf{Q} \left(\text{sgn}(\mathbf{w}) |\mathbf{w}|^{-1/2} \right)} \\
& \times \left[1 - F_{Gamma} \left(r_{\mathcal{Q}_q}(\mathbf{w}); \frac{d}{2} + \left(\text{sgn}(\mathbf{w}) |\mathbf{w}|^{1/2} \right)^\top \mathbf{Q} \left(\text{sgn}(\mathbf{w}) |\mathbf{w}|^{-1/2} \right), \left(\text{sgn}(\mathbf{w}) |\mathbf{w}|^{1/2} \right)^\top \mathbf{Q} \left(\text{sgn}(\mathbf{w}) |\mathbf{w}|^{-1/2} \right) \right) \right] \\
& \times \{1 + o(1)\}
\end{aligned}$$

B.3 Multivariate Laplace distribution, standard Laplace margins

We have $f_{[L]}(\mathbf{x}) = f_0(g_{\mathcal{G}}(\mathbf{x}))$, where $f_0(s) = |\mathbf{Q}|^{1/2} (2\pi)^{-d/2} s^v K_v(s)$. By (A.21), the density of angles is

$$\begin{aligned}
f_{\mathbf{W}}(\mathbf{w}) &= \int_0^\infty r^{d-1} f_0(r g_{\mathcal{G}}(\mathbf{w})) dr \\
&= g_{\mathcal{G}}(\mathbf{w})^{-d} \int_0^\infty s^{d-1} f_0(s) ds \\
&= |\mathbf{Q}|^{1/2} (2\pi)^{-d/2} \left(\mathbf{w}^\top \mathbf{Q} \mathbf{w} \right)^{-d/2} \int_0^\infty s^{d+v-1} K_v(s) ds \\
&= \Gamma(d/2) 2^{\frac{d}{2}-1} (2\pi)^{-d/2} |\mathbf{Q}|^{1/2} \left(\mathbf{w}^\top \mathbf{Q} \mathbf{w} \right)^{-d/2} \\
&= \Gamma(d/2) 2^{-1} \pi^{-d/2} |\mathbf{Q}|^{1/2} \left(\mathbf{w}^\top \mathbf{Q} \mathbf{w} \right)^{-d/2}
\end{aligned}$$

where the integral solution can be found in [Gradshteyn & Ryzhik \(2014\)](#).

B.4 Multivariate Student t_ν distribution, Student t_ν margins, $\nu > 0$

We have $f(\mathbf{x}) = f_0(g_{\mathcal{G}}(\mathbf{x}))$, where $f_0(s) = k_{\nu, \mathbf{Q}} (1 + \nu^{-1} s^2)^{-\frac{1}{2}(\nu+d)}$. By (A.21), the density of angles is

$$\begin{aligned}
f_{\mathbf{W}}(\mathbf{w}) &= \int_0^\infty r^{d-1} f_0(r g_{\mathcal{G}}(\mathbf{w})) dr \\
&= g_{\mathcal{G}}(\mathbf{w})^{-d} \int_0^\infty s^{d-1} f_0(s) ds \\
&= k_{\nu, \mathbf{Q}} (\mathbf{w}^\top \mathbf{Q} \mathbf{w})^{-d/2} \int_0^\infty s^{d-1} (1 + \nu^{-1} s^2)^{-\frac{1}{2}(\nu+d)} ds \\
&= \Gamma\left(\frac{\nu+d}{2}\right) \Gamma\left(\frac{\nu}{2}\right)^{-1} \nu^{-d/2} \pi^{-d/2} |\mathbf{Q}|^{1/2} (\mathbf{w}^\top \mathbf{Q} \mathbf{w})^{-d/2} \nu^{-1+d/2} \Gamma\left(\frac{\nu+d}{2}\right)^{-1} \Gamma\left(\frac{\nu}{2}\right) \Gamma\left(1 + \frac{\nu}{2}\right) \\
&= \Gamma\left(\frac{d}{2}\right) 2^{-1/2} \pi^{-d/2} |\mathbf{Q}|^{1/2} (\mathbf{w}^\top \mathbf{Q} \mathbf{w})^{-d/2}
\end{aligned}$$

B.5 Multivariate Student t_ν distribution, Student t_ν margins, $\nu < 0$

We have the joint d -dimensional density $f(\mathbf{x}) = f_0(g_{\mathcal{G}}(\mathbf{x}))$, where $f_0(s) = k_{\nu, \mathbf{Q}} (1 - s^2)^{-\frac{1}{2}(\nu+d)}$ for $s \in (-1, 1)$, where $k_{\nu, \mathbf{Q}} = \pi^{-d/2} |\mathbf{Q}|^{1/2} |\nu|^{1-\frac{d}{2}} (|\nu| - d)^{-1} \Gamma\left(\frac{|\nu|}{2}\right) \Gamma\left(\frac{|\nu|-d}{2}\right)^{-1}$, and $g_{\mathcal{G}}(\mathbf{x}) = (-\nu^{-1} \mathbf{w}^\top \mathbf{Q} \mathbf{w})^{1/2}$.

Given an angle \mathbf{w} and knowing that the upper bound on radii is given by $r_{\mathcal{Q}_1}(\mathbf{w}) = (-\nu^{-1} \mathbf{w}^\top \mathbf{Q} \mathbf{w})^{-1/2}$ we can derive an explicit form of the density of angles

$$\begin{aligned}
f_{\mathbf{W}}(\mathbf{w}) &= \int_0^{r_{\mathcal{Q}_1}(\mathbf{w})} f_{R, \mathbf{W}}(r, \mathbf{w}) dr \\
&= \int_0^{r_{\mathcal{Q}_1}(\mathbf{w})} r^{d-1} f_0(r g_{\mathcal{G}}(\mathbf{w})) dr \\
&= k_{\nu, \mathbf{Q}} \int_0^{g_{\mathcal{G}}(\mathbf{w})^{-1}} r^{d-1} (1 - g_{\mathcal{G}}(\mathbf{w})^2 r^2)^{-\frac{1}{2}(\nu+d)} dr \\
&= \pi^{-d/2} |\mathbf{Q}|^{1/2} |\nu|^{1-\frac{d}{2}} (|\nu| - d)^{-1} \Gamma\left(\frac{|\nu|}{2}\right) \Gamma\left(\frac{|\nu|-d}{2}\right)^{-1} \\
&\quad \times 2^{-1} g_{\mathcal{G}}(\mathbf{w})^{-d} \Gamma\left(\frac{d}{2}\right) \Gamma\left(\frac{|\nu|-d}{2} + 1\right) \Gamma\left(1 + \frac{|\nu|}{2}\right)^{-1} \\
&= 2^{-1} \pi^{-d/2} |\mathbf{Q}|^{1/2} \Gamma\left(\frac{d}{2}\right) (\mathbf{w}^\top \mathbf{Q} \mathbf{w})^{-d/2}
\end{aligned}$$

B.6 Multivariate Student t_ν distribution, standard Laplace margins, $\nu > 0$

$$\begin{aligned}
f_{\mathbf{W}|R>r_{\mathcal{Q}_q}(\mathbf{W})}(\mathbf{w}) &= (1-q)^{-1} \int_{r_{\mathcal{Q}_q}(\mathbf{w})}^{\infty} r^{d-1} f_{[L]}(r\mathbf{w}) dr \\
&= (1-q)^{-1} \frac{c_\nu^{d+2} q_{j^*j^*} k_{\nu,\mathbf{Q}}}{\nu^{d+2}} \int_{r_{\mathcal{Q}_q}(\mathbf{w})}^{\infty} r^{d-1} \exp \left\{ -r \left[\left(1 + \frac{d}{\nu}\right) \max_{j=1,\dots,d} |w_j| - \frac{1}{\nu} \sum_{j=1}^d |w_j| \right] \right\} dr \{1 + o(1)\} \\
&= (1-q)^{-1} \frac{c_\nu^{d+2} q_{j^*j^*} k_{\nu,\mathbf{Q}}}{\nu^{d+2}} \Gamma(d) \left[\left(1 + \frac{d}{\nu}\right) \max_{j=1,\dots,d} |w_j| - \frac{1}{\nu} \sum_{j=1}^d |w_j| \right]^{-d} \\
&\quad \times \left[1 - F_{Gamma} \left(r_{\mathcal{Q}_q}(\mathbf{w}); d, \left(1 + \frac{d}{\nu}\right) \max_{j=1,\dots,d} |w_j| - \frac{1}{\nu} \sum_{j=1}^d |w_j| \right) \right] \{1 + o(1)\}
\end{aligned}$$

Proposition 3, obtain the density of angles

$$\begin{aligned}
f_{\mathbf{W}}(\mathbf{w}) &= (1-q)^{-1} \frac{c_\nu^{d+2} q_{j^*j^*} k_{\nu,\mathbf{Q}}}{\nu^{d+2}} \Gamma(d) \left[\left(1 + \frac{d}{\nu}\right) \max_{j=1,\dots,d} |w_j| - \frac{1}{\nu} \sum_{j=1}^d |w_j| \right]^{-d} \\
&\quad \times \left[1 - F_{Gamma} \left(r_{\mathcal{Q}_q}(\mathbf{w}); d, \left(1 + \frac{d}{\nu}\right) \max_{j=1,\dots,d} |w_j| - \frac{1}{\nu} \sum_{j=1}^d |w_j| \right) \right] \{1 + o(1)\}
\end{aligned}$$

B.7 Multivariate max-stable distribution, logistic dependence, standard Fréchet margins

$$\begin{aligned}
f_{\mathbf{W}}(\mathbf{w}) &= \int_0^\infty r^{d-1} f(r\mathbf{w}) dr \\
&= \int_0^\infty \left[\sum_{\pi \in \Pi} (-1)^{|\pi|} \prod_{s \in \pi} r^{-|s|-1} \left\{ (-\theta)^{|s|-1} \left(\prod_{k \in s} w_k \right)^{-\frac{1}{\theta}-1} \left(\sum_{j=1}^d w_j^{-1/\theta} \right)^{\theta-|s|} \right\} \right] \\
&\quad \times \exp \left\{ -r^{-1} \left(\sum_{j=1}^d w_j^{-1/\theta} \right)^\theta \right\} dr \\
&= \sum_{\pi \in \Pi} (-1)^{|\pi|} \prod_{s \in \pi} \left[(-\theta)^{|s|-1} \left(\prod_{k \in s} w_k \right)^{-\frac{1}{\theta}-1} \left(\sum_{j=1}^d w_j^{-1/\theta} \right)^{\theta-|s|} \int_0^\infty r^{-|s|-1} \exp \left\{ -r^{-1} \left(\sum_{j=1}^d w_j^{-1/\theta} \right)^\theta \right\} dr \right] \\
&= \sum_{\pi \in \Pi} (-1)^{|\pi|} \prod_{s \in \pi} \left[(-1)^{|s|} \theta^{|s|-1} \left(\prod_{k \in s} w_k \right)^{-\frac{1}{\theta}-1} \left(\sum_{j=1}^d w_j^{-1/\theta} \right)^{\theta-|s|} \int_0^\infty u^{|s|-1} \exp \left\{ -u \left(\sum_{j=1}^d w_j^{-1/\theta} \right)^\theta \right\} du \right] \\
&= \sum_{\pi \in \Pi} (-1)^{|\pi|} \prod_{s \in \pi} \left[(-1)^{|s|} \theta^{|s|-1} \Gamma(|s|) \left(\prod_{k \in s} w_k \right)^{-\frac{1}{\theta}-1} \left(\sum_{j=1}^d w_j^{-1/\theta} \right)^{\theta-|s|-\theta|s|} \right]
\end{aligned}$$

B.8 Multivariate max-stable distribution, logistic dependence, standard Laplace margins

$$\begin{aligned}
f_{\mathbf{W}|R>r_{\mathcal{Q}_q}(\mathbf{w})} &= (1-q)^{-1} \int_{r_{\mathcal{Q}_q}(\mathbf{w})}^{\infty} r^{d-1} f_{[L]}(r\mathbf{w}) \\
&= (1-q)^{-1} (-1)^{d+1} \left\{ \prod_{\ell=0}^{d-1} \left(1 - \frac{\ell}{\theta}\right) \right\} 2^{-\frac{1}{\theta} \sum_{j=1}^d \mathbf{1}_{\{w_j > 0\}}} (\log 2)^{-2 \sum_{j=1}^d \mathbf{1}_{\{w_j = 0\}}} \\
&\quad \times \left(\prod_{k:x_k < 0} (-w_k)^{\frac{1}{\theta}-1} \right) \left(\sum_{k:w_k < 0} (-x_k)^{1/\theta} \right)^{\theta-d} \\
&\quad \times \int_{r_{\mathcal{Q}_q}(\mathbf{w})}^{\infty} r^{(\frac{1}{\theta}-1) \sum_{j=1}^d \mathbf{1}_{\{w_j < 0\}} + 1 - \frac{d}{\theta} + d-1} \exp \left\{ -r \left[\frac{1}{\theta} \sum_{j:w_j > 0} x_j + \left(\sum_{k:x_k < 0} (-w_k)^{1/\theta} \right)^{\theta} \right] \right\} dr \\
&\quad \times \{1 + o(1)\} \\
&= (1-q)^{-1} (-1)^{d+1} \left\{ \prod_{\ell=0}^{d-1} \left(1 - \frac{\ell}{\theta}\right) \right\} 2^{-\frac{1}{\theta} \sum_{j=1}^d \mathbf{1}_{\{w_j > 0\}}} (\log 2)^{-2 \sum_{j=1}^d \mathbf{1}_{\{w_j = 0\}}} \\
&\quad \times \left(\prod_{k:x_k < 0} (-w_k)^{\frac{1}{\theta}-1} \right) \left(\sum_{k:w_k < 0} (-x_k)^{1/\theta} \right)^{\theta-d} \\
&\quad \times \Gamma \left\{ \left(\frac{1}{\theta} - 1 \right) \left(\sum_{j=1}^d \mathbf{1}_{\{w_j < 0\}} - d \right) + 1 \right\} \left[\frac{1}{\theta} \sum_{j:w_j > 0} x_j + \left(\sum_{k:x_k < 0} (-w_k)^{1/\theta} \right)^{\theta} \right]^{-\left(\frac{1}{\theta}-1\right) \left(\sum_{j=1}^d \mathbf{1}_{\{w_j < 0\}} - d \right) - 1} \\
&\quad \times \left[1 - F_{Gamma} \left(r_{\mathcal{Q}_q}(\mathbf{w}); \left(\frac{1}{\theta} - 1 \right) \left(\sum_{j=1}^d \mathbf{1}_{\{w_j < 0\}} - d \right) + 1, \frac{1}{\theta} \sum_{j:w_j > 0} x_j + \left(\sum_{k:x_k < 0} (-w_k)^{1/\theta} \right)^{\theta} \right) \right] \\
&\quad \times \{1 + o(1)\}
\end{aligned}$$

Proposition 3, obtain the density of angles

$$\begin{aligned}
f_{\mathbf{W}}(\mathbf{w}) = & (1-q)^{-1}(-1)^{d+1} \left\{ \prod_{\ell=0}^{d-1} \left(1 - \frac{\ell}{\theta}\right) \right\} 2^{-\frac{1}{\theta} \sum_{j=1}^d \mathbf{1}_{\{w_j > 0\}}} (\log 2)^{-2 \sum_{j=1}^d \mathbf{1}_{\{w_j = 0\}}} \\
& \times \left(\prod_{k: x_k < 0} (-w_k)^{\frac{1}{\theta}-1} \right) \left(\sum_{k: w_k < 0} (-x_k)^{1/\theta} \right)^{\theta-d} \\
& \times \Gamma \left\{ \left(\frac{1}{\theta} - 1 \right) \left(\sum_{j=1}^d \mathbf{1}_{\{w_j < 0\}} - d \right) + 1 \right\} \left[\frac{1}{\theta} \sum_{j: w_j > 0} x_j + \left(\sum_{k: x_k < 0} (-w_k)^{1/\theta} \right)^{\theta} \right]^{-\left(\frac{1}{\theta}-1\right) \left(\sum_{j=1}^d \mathbf{1}_{\{w_j < 0\}} - d \right) - 1} \\
& \times \left[1 - F_{Gamma} \left(r_{\mathcal{Q}_q}(\mathbf{w}); \left(\frac{1}{\theta} - 1 \right) \left(\sum_{j=1}^d \mathbf{1}_{\{w_j < 0\}} - d \right) + 1, \frac{1}{\theta} \sum_{j: w_j > 0} x_j + \left(\sum_{k: x_k < 0} (-w_k)^{1/\theta} \right)^{\theta} \right) \right] \\
& \times \{1 + o(1)\}
\end{aligned}$$

B.9 Wishart distribution

The density of exceedance angles is

$$\begin{aligned}
& f_{\mathbf{W}|R>r_{\mathcal{Q}_q}(\mathbf{W})}(\mathbf{w}) \\
& = (1-q)^{-1} \int_{r_{\mathcal{Q}_q}(\mathbf{w})}^{\infty} r^{d-1} f(r\mathbf{w}) dr \\
& = (1-q)^{-1} \left\{ 2^{(\nu d)/2} |\mathbf{V}|^{\nu/2} \Gamma_d(\nu/2) \right\}^{-1} |\mathbf{w}|^{\frac{1}{2}(\nu-d-1)} \\
& \quad \times \int_{r_{\mathcal{Q}_q}(\mathbf{w})}^{\infty} r^{\frac{d}{2}(\nu-d+1)-1} \exp \left\{ -\frac{r}{2} \text{tr}(\mathbf{V}^{-1}\mathbf{w}) \right\} dr \\
& = (1-q)^{-1} \left\{ 2^{(\nu d)/2} |\mathbf{V}|^{\nu/2} \Gamma_d(\nu/2) \right\}^{-1} |\mathbf{w}|^{\frac{1}{2}(\nu-d-1)} \Gamma \left\{ \frac{d}{2}(\nu-d+1) \right\} \left\{ \frac{1}{2} \text{tr}(\mathbf{V}^{-1}\mathbf{w}) \right\}^{-\frac{d}{2}(\nu-d+1)} \\
& \quad \times \left[1 - F_{Gamma} \left(r_{\mathcal{Q}_q}(\mathbf{w}); \frac{d}{2}(\nu-d+1), \frac{1}{2} \text{tr}(\mathbf{V}^{-1}\mathbf{w}) \right) \right] \{1 + o(1)\}
\end{aligned}$$

Proposition 3, obtain the density of angles

$$\begin{aligned}
f_{\mathbf{W}}(\mathbf{w}) = & (1-q)^{-1} \left\{ 2^{(\nu d)/2} |\mathbf{V}|^{\nu/2} \Gamma_d(\nu/2) \right\}^{-1} |\mathbf{w}|^{\frac{1}{2}(\nu-d-1)} \Gamma \left\{ \frac{d}{2}(\nu-d+1) \right\} \left\{ \frac{1}{2} \text{tr}(\mathbf{V}^{-1}\mathbf{w}) \right\}^{-\frac{d}{2}(\nu-d+1)} \\
& \times \left[1 - F_{Gamma} \left(r_{\mathcal{Q}_q}(\mathbf{w}); \frac{d}{2}(\nu-d+1), \frac{1}{2} \text{tr}(\mathbf{V}^{-1}\mathbf{w}) \right) \right] \{1 + o(1)\}
\end{aligned}$$

C Supplementary material C

C.1 Extremal coefficients

Given a random vector $R\mathbf{W} \in \mathbb{R}^d$, we let the sets of indices \mathcal{I} and \mathcal{J} denote subsets of $\{1, \dots, d\}$ such that $\mathcal{I} \cap \mathcal{J} = \emptyset$. The sub-asymptotic coefficient of tail dependence, $\chi_{\mathcal{J}|\mathcal{I}}(t)$, provides information on the

probability of joint excesses of high an increasingly high threshold $t \in \mathbb{R}_+$ for random vectors $R\mathbf{W}_{\mathcal{I}}$ and $R\mathbf{W}_{\mathcal{J}}$. It is defined as

$$\chi_{\mathcal{J}|\mathcal{I}}(t) = \mathbb{P}[R\mathbf{W}_{\mathcal{J}} > t\mathbf{1}_{|\mathcal{J}|} \mid R\mathbf{W}_{\mathcal{I}} > t\mathbf{1}_{|\mathcal{I}|}], \quad (\text{A.25})$$

and gives rise to the coefficient of tail dependence $\chi_{\mathcal{J}|\mathcal{I}} = \lim_{t \rightarrow \infty} \chi_{\mathcal{J}|\mathcal{I}}(t)$, when the limit exists. The latter is of natural importance as it defines the frontier between asymptotic dependence and independence respectively for $\chi_{\mathcal{J}|\mathcal{I}} > 0$ and $\chi_{\mathcal{J}|\mathcal{I}} = 0$. A closely related quantity, the coefficient of residual tail dependence η (Ledford & Tawn 1996), measures the rate of decay of the joint survival probability of all components of $R\mathbf{W}$. It is defined through

$$\mathbb{P}[R\mathbf{W} > t\mathbf{1}_d] \sim \ell(e^t)e^{-t/\eta}, \quad t \rightarrow \infty, \eta \in (0, 1],$$

where $\ell \in \text{RV}_0^\infty$ is a slowly varying function. The case $\lim_{t \rightarrow \infty} \ell(e^t)e^{-t/\eta} = 0$ corresponds to asymptotic independence between some components of $R\mathbf{W}$ and is attained either if $\eta < 1$ or if $\eta = 1$ and $\lim_{t \rightarrow \infty} \ell(e^t) = 0$. The coefficient of residual tail dependence hence measures the strength of dependence between asymptotically independent random variables. Nolde (2014) shows that η can be obtained from $\partial\mathcal{G}$ via

$$\eta = \inf\{s \in [0, 1] : (s, \infty)^d \cap \partial\mathcal{G} = \emptyset\}.$$

We also consider the conditional extremes model, which is based on the assumption that there exist functions $\mathbf{a}_{|i} : \mathbb{R}_+ \rightarrow \mathbb{R}^{d-1}$ and $\mathbf{b}_{|i} : \mathbb{R}_+ \rightarrow \mathbb{R}_+^{d-1}$ such that

$$\mathbb{P}\left[RW_i - t > x, \frac{(R\mathbf{W})_{-i} - \mathbf{a}_{|i}(R_i W_i)}{\mathbf{b}_{|i}(R_i W_i)} \leq \mathbf{z} \mid R_i W_i > t\right] \xrightarrow{w} \exp(-x)K_{|i}(\mathbf{z}), \quad \text{as } t \rightarrow \infty,$$

at continuity points of the limit, where $K_{|i}$ is a probability measure on \mathbb{R}^{d-1} with marginal distributions denoted by $K_{j|i}$, satisfying $\lim_{x \rightarrow \infty} K_{j|i}(x) = 1$, for all $j \in \{1, \dots, d\} \setminus \{i\}$. As in Nolde & Wadsworth (2021), we also assume that density convergence, that is,

$$\frac{\partial}{\partial \mathbf{z}} \mathbb{P}\left[\frac{(R\mathbf{W})_{-i} - \mathbf{a}_{|i}(R_i W_i)}{\mathbf{b}_{|i}(R_i W_i)} \leq \mathbf{z} \mid R_i W_i = t\right] \rightarrow \frac{\partial}{\partial \mathbf{z}} K_{|i}(\mathbf{z}) =: k_{|i}(\mathbf{z}), \quad \text{as } t \rightarrow \infty. \quad (\text{A.26})$$

Under mild assumptions, Nolde & Wadsworth (2021) show that if convergence (A.26) holds and $\lim_{x \rightarrow \infty} a_{j|i}(x)/x$ exists, then

$$\alpha_{j|i} = \max\{\alpha \in [0, 1] : g_{ij}(1, \alpha) = 1\}, \quad (\text{A.27})$$

where g_{ij} denotes the gauge function of the limit set of $(X_{L,i}, X_{L,j})$ which can be obtained from the full gauge $g_{\mathcal{G}}$ by $g_{ij}(x_i, x_j) = \min_{\mathbf{x}_{-ij}} g_{\mathcal{G}}(\mathbf{x})$. Owing to the marginal standardisation to Laplace margins, it follows that $\mathcal{G} \subseteq [-1, 1]^d$ and $\mathcal{G} \cap \square^d \neq \emptyset$, where $\square^d := [-1, 1]^d \setminus (-1, 1)^d$. In practice, however, realisations from the posterior distribution of \mathcal{G} do not satisfy these constraints. In the following Section, we discuss some implications for the estimation of the above coefficients.

C.2 Bayesian inference

Again in the bivariate setting, we motivate a first estimator from the geometric definition of $\alpha_{|i}$ (and argue by symmetry for $\alpha_{|j}$, $i \neq j \in \{1, 2\}$) from the fact that if $\partial\mathcal{G}$ satisfies the two constraints of a limit set stated in Section C.1, then a reformulation of expression (A.27) yields

$$\alpha_{|i} = \max\{r^* w_j^* \in [0, 1] : r^* w_i^* = 1, r^* \mathbf{w}^* \in \partial\mathcal{G}\}, \quad (\text{A.28})$$

and more generally, the component-wise maximum of $\partial\mathcal{G}$ is 1, *i.e.*, $1 = \max\{r w_i : r \mathbf{w} \in \partial\mathcal{G}\}$. As mentioned above, this condition is not met in practice and we therefore replace $r^* w_i^* = 1$ by $r^* w_i^* = \max\{r w_i : r \mathbf{w} \in$

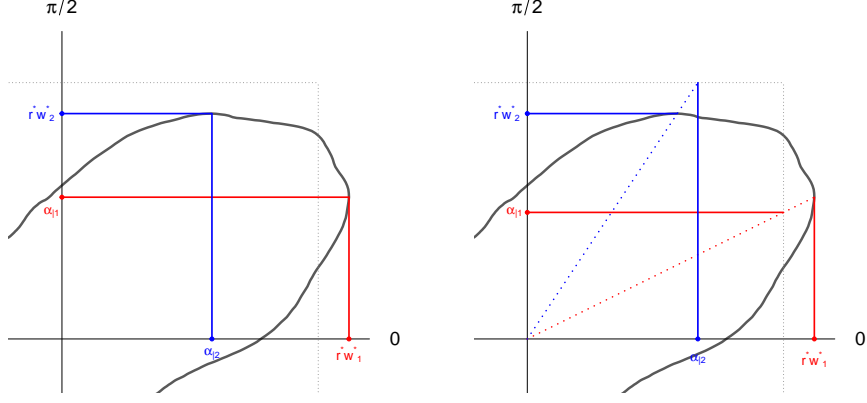


Figure 12: Fictitious realisation from the posterior distribution of $\partial\mathcal{G}$ (black). Left: $\alpha_{|1}$ and $\alpha_{|2}$ obtained from method 1. Right: $\alpha_{|1}$ and $\alpha_{|2}$ obtained from method 2.

$\partial\mathcal{G}$ in equation (A.28) for the estimation procedure. Due to the model construction, $r^*w_i^*$ is unique with probability one, and the max operation in equation (A.28) is superfluous in practice. We motivate a second estimator by arguing that if $r^*w_i^* \neq 1$, w_i^* still preserves the angle corresponding to $\alpha_{|i}$ so that

$$\alpha_{|i} = \{rw_i^* \in \mathbb{R} : rw_i^* = 1, r^*w_i^* = \max\{rw_i : r\mathbf{w} \in \partial\mathcal{G}\}, r^*\mathbf{w}^* \in \partial\mathcal{G}\},$$

for suitably chosen $r \in \mathbb{R}_+$. A visual explanation of the two methods is given in Figure 12. We note that neither of the two proposed methods are guaranteed to yield $\alpha_{|i} \in [-1, 1]$, but we consider the values outside of this interval as Bayesian evidence for $\alpha_{|i} = -1$ or $\alpha_{|i} = 1$.

We suggest two methods to obtain samples from the posterior distribution of η by relying on its geometric definition adapted to the context of the posterior boundary $\partial\mathcal{G}$. The first approach consists of collecting, for each posterior realisation of $\partial\mathcal{G}$, the value

$$\eta = \{rw_1 = rw_2 \in \mathbb{R}_+ : \mathbf{w} = (1/\sqrt{2}, 1/\sqrt{2}), r\mathbf{w} \in \partial\mathcal{G}\}. \quad (\text{A.29})$$

In the second method, we apply a linear transformation to the realisations from the posterior distribution of $\partial\mathcal{G}$ through a transformation matrix M_T and obtain the transformed posterior $\partial\mathcal{G}_T$ via

$$\partial\mathcal{G}_T = \{M_T r\mathbf{w} : r\mathbf{w} \in \partial\mathcal{G}\},$$

where M_T has eigenvectors and eigenvalues suitably chosen such that the coordinate-wise maxima of $\partial\mathcal{G}$ are mapped to the boundary of the unit hypercube $[-1, 1]^d$ while conserving their angle. Details on the construction of M_T are given in Supplementals C.3. The coefficient η is then calculated as in expression (A.29), but for $r\mathbf{w} \in \partial\mathcal{G}_T$. Samples from the posterior distribution of $\alpha_{|i}$ and η are obtained by using the above described estimators for every realisation from the posterior distribution of $\partial\mathcal{G}$ or $\partial\mathcal{G}_T$.

C.3 Linear transformation of the limit set

We apply a linear transformation to the realisations from the posterior distribution of $\partial\mathcal{G}$ through the transformation matrix M_T and obtain the transformed posterior $\partial\mathcal{G}_T$ via

$$\partial\mathcal{G}_T = \{M_T r\mathbf{w} : r\mathbf{w} \in \partial\mathcal{G}\},$$

where the transformation matrix M_T has eigenvectors and eigenvalues suitably chosen such that the coordinate-wise maxima of $\partial\mathcal{G}$ are mapped to the boundary of the unit box while conserving their angle.

Suppose the points $r^{(1)}\mathbf{w}^{(1)}$ and $r^{(2)}\mathbf{w}^{(2)}$ correspond to the coordinate-wise maxima of $\partial\mathcal{G}$, then M_T is constructed as

$$M_T = SMS^{-1}$$

where S is a matrix with column vectors $r^{(1)}\mathbf{w}^{(1)}$ and $r^{(2)}\mathbf{w}^{(2)}$, and $M = \text{diag}(r_1/r^{(1)}, r_2/r^{(2)})$ is a diagonal matrix—with non-zero entries corresponding to the eigenvalues of M_T —with r_i chosen such that $r_i\mathbf{w}^{(i)}/r^{(i)}$ is on the boundary of the unit box. If $r^{(1)}\mathbf{w}^{(1)} = r^{(2)}\mathbf{w}^{(2)}$, S is singular and M_T is undefined. In this case, we find any vector $\mathbf{u} \in \mathbb{R}^2$ orthogonal to $r^{(1)}\mathbf{w}^{(1)}$. The matrix S then has column vectors given by $r^{(1)}\mathbf{w}^{(1)}$ and \mathbf{u} , and M is assigned its second diagonal entry to 1. This guarantees that stretching of the posterior realisations of $\partial\mathcal{G}$ is only performed along the direction of $\mathbf{w}^{(1)} = \mathbf{w}^{(2)}$.

D Simulation study

D.1 Setting

We here describe the setting of a simulation study performed using samples from classical parametric bivariate copulas. We provide a brief summary of the properties of these distributions and detail how they are linked with the extremal coefficients and quantities described in Section C.1.

A random variable \mathbf{X}_L is said to follow a bivariate Laplace distribution with precision matrix $\mathbf{Q} = \Sigma^{-1}$ for a positive definite covariance Σ —with unit diagonal terms and a correlation value $\rho \in [-1, 1]$ on the remaining off-diagonal terms—if satisfies the properties of Example 3 of Appendix B. The parameter ρ hence fully determines a member of the family of the bivariate normal distribution as well as its extremal properties and in the subsequent sections, we use $\rho = 0.5$.

A random vector $\mathbf{X} \in \mathbb{R}^2$ has a bivariate normal distribution with Laplace marginal distributions and precision matrix $\mathbf{Q} = \Sigma^{-1}$ for a positive definite covariance Σ —with unit diagonal terms and a correlation value $\rho \in [-1, 1]$ on the remaining off-diagonal terms—if satisfies the properties of Example 2 of Appendix B. In what follows, we use the bivariate normal distribution as an instance of asymptotically independent distribution and draw samples using the value $\rho = 0.8$.

A random vector $\mathbf{X} \in \mathbb{R}^2$ has a bivariate max-stable logistic distribution with Laplace margins if satisfies the properties of Example 8 of Appendix B with exponent measure given by $V(x_1, \dots, x_d) = \left(\sum_{j=1}^d x_j^{-1/\theta}\right)^\theta$ and the dependence parameter $\theta \in (0, 1)$ fully determines a member of the family. The max-stable logistic family of distributions belongs the class of asymptotic dependence. For any $\theta \in (0, 1)$, $\alpha_{|i} = 1$ and $\eta = 1$. We carry the simulation study using $\theta = 0.3$. Table 1 presents, for each family of distributions, the values of extremal coefficients associated with fixed parameters.

Extremal coefficient	Laplace	Normal	Max-stable logistic
$\alpha_{ i}$	$\rho = 0.5$	$\rho^2 = 0.64$	1
η	$\sqrt{(1 - \rho^2)/(2 - 2\rho)} \approx 0.866$	$(1 + \rho)/2 = 0.9$	1

Table 1: Values of the extremal coefficients $\alpha_{|i}$ and η for the bivariate Laplace, normal, and max-stable logistic distributions with specified parameters.

D.2 Posterior distribution of latent variables

We perform a simulation study to obtain realisations from the posterior distribution of the latent sets \mathcal{Q}_q , \mathcal{L} , and \mathcal{G} , as well as from the posterior predictive distribution of R and \mathbf{W} . We centre the simulation study on the bivariate Laplace, normal, and max-stable logistic families of distributions. The bivariate Laplace distribution is chosen for the homothetic structure of its density with respect to its gauge function gg , implying that its marginal density of the angles is exactly that assumed by model M_2 . The bivariate

max-stable logistic and normal distributions are chosen respectively for their asymptotic dependence and independence properties. From each of these distributions, we generate 100 samples of size $n_1 = 1000$ and 100 samples of size $n_2 = 10000$, resulting in six cases (600 samples) with which we carry our analyses.

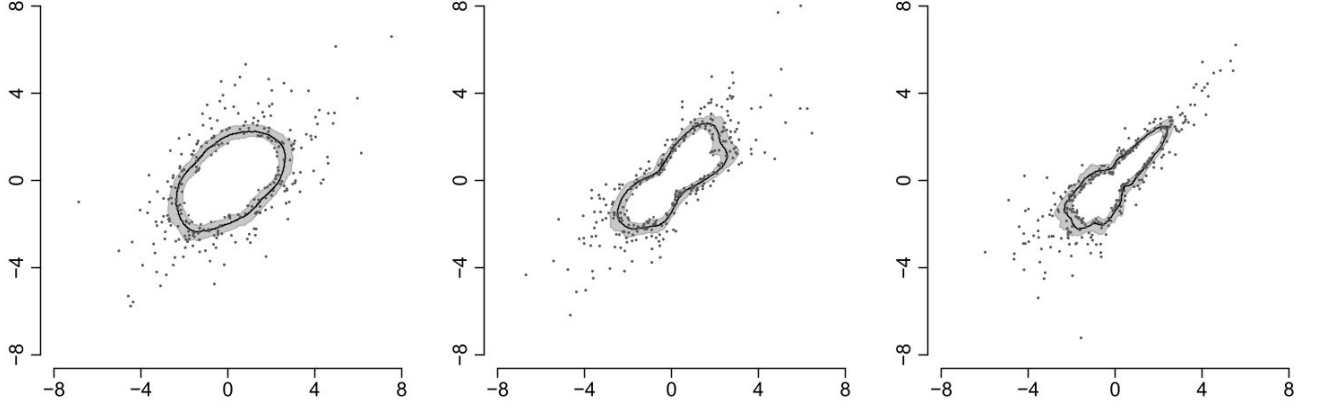


Figure 13: Angle-wise posterior mean and 0.95 prediction intervals for 100 samples from the posterior distribution of $r_{Q_{0.8}}$ obtained from n_1 draws from a bivariate Laplace (left), normal (centre), max-stable logistic (right) distributions in Laplace margins. Points correspond to exceedances of at least one sampled posterior $r_{Q_{0.8}}$.

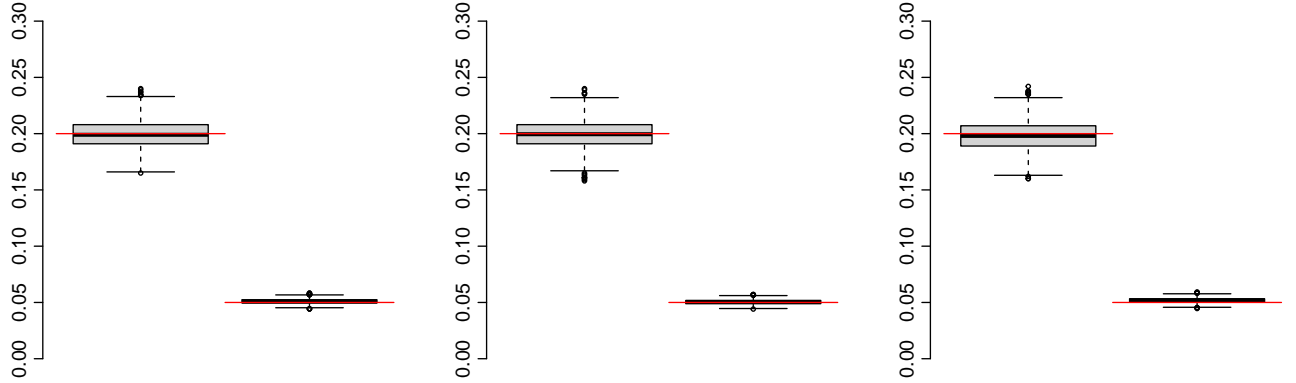


Figure 14: Boxplots of the proportion of data assigned as exceedances by each realisation from the posterior distribution of r_{Q_q} for n draws from the bivariate Laplace (left), normal (centre), max-stable logistic (right) distributions in Laplace margins. Within panels: n_1 , $1 - q_1 = 0.2$ (left), n_2 , $1 - q_2 = 0.05$ (right). Red segments: values of $1 - q_k$ used in the fitting procedure.

Following the posterior sampling procedure described in Section 3.4, we first fit a bayesian Gamma quantile regression to each of the 600 samples described above using $q_1 = 0.8$ for each sample of size n_1 and $q_2 = 0.98$ for each samples of size n_2 . Here, q_1 and q_2 are chosen such that the expected number of exceedances of \mathcal{Q}_{q_k} , $n_k \cdot \mathbb{P}[RW \in \mathcal{Q}'_{q_k} \mid \mathbf{y}]$, equals 200 for $k = \{1, 2\}$. Again for each sample, we obtain 20 realisations $\{r_{Q_{q_k,i}} : i = 1, \dots, 20\}$ from the posterior distribution of $r_{Q_{q_k}}$ and define 20 sets of exceedances accordingly. Figure 13 displays the angle-wise posterior mean and 0.95 prediction intervals for $r_{Q_{0.8}}$ resulting from fitting quantile regressions to one sample of n_1 draws from each of the three distributions of interest. Figure 13 also displays the data points defined as exceedances for at least one realisation from the posterior distribution of $r_{Q_{0.8}}$. A brief assessment of the performance of the quantile regression is made through Figure 14, which consists of boxplots of the number of exceedances of each realisation from the posterior distribution of $r_{Q_{q_k}}$ for each of the 600 samples described above grouped by family of distributions and sample size.

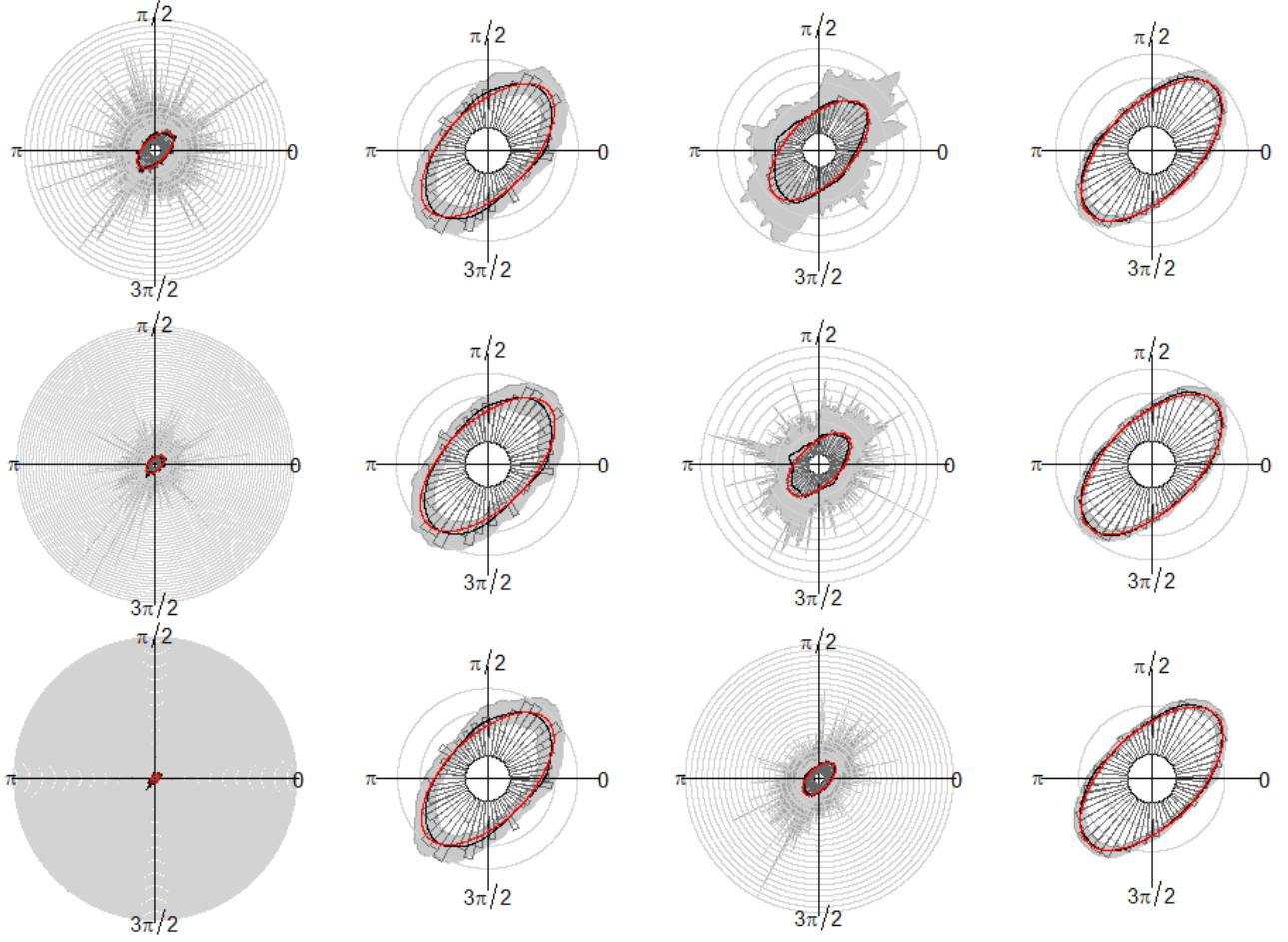


Figure 15: Histogram of the angles $\{\varphi_j \in [0, 2\pi] : \mathbf{w}_j = (\cos \varphi_j, \sin \varphi_j), j = 1, \dots, n_k\}$ from a sample of n observations from a bivariate Laplace distribution with angle-wise posterior mean of $\pi[\mathbf{W} \mid \mathcal{G}, \mathcal{L}, \mathbf{y}]$ (black line), 0.95 prediction interval for $\pi[\mathbf{W} \mid \mathcal{G}, \mathcal{L}, \mathbf{y}]$ (grey band) output from model \mathcal{M}_i , and the true density $f_{\mathbf{W}}$ for the bivariate Laplace (red line). Rows from top to bottom: \mathcal{M}_1 , \mathcal{M}_2 , and \mathcal{M}_3 . First column: $\pi[\mathbf{W} \mid \mathcal{G}, \mathcal{L}, \mathbf{y}]$ fitted using exceedances of $\mathcal{Q}_{0.8}$ only (sample size n_1). Second column: $\pi[\mathbf{W} \mid \mathcal{G}, \mathcal{L}, \mathbf{y}]$ fitted using all sampled angles (sample size n_1). Third column: $\pi[\mathbf{W} \mid \mathcal{G}, \mathcal{L}, \mathbf{y}]$ fitted using exceedances of $\mathcal{Q}_{0.98}$ only (sample size n_2). Fourth column: $\pi[\mathbf{W} \mid \mathcal{G}, \mathcal{L}, \mathbf{y}]$ fitted using all sampled angles (sample size n_2).

Given the satisfying properties of the posterior distribution of $r_{\mathcal{Q}_{q_k}}$, we proceed with the investigation of the joint model for R and \mathbf{W} . Following the procedure described in Section 3.4, we obtain realisations from the posterior distributions of $r_{\mathcal{G}}$ and $r_{\mathcal{L}}$ —say $\{r_{\mathcal{G}_i} : i = 1, \dots, n_{\theta}\}$ and $\{r_{\mathcal{L}_i} : i = 1, \dots, n_{\theta}\}$ for $n_{\theta} = n_{\mathcal{Q}}n_{\mathcal{G}\mathcal{L}} = 20 \cdot 50$ —using each model M_1 , M_2 , and M_3 on each sample described above. By virtue of Proposition 3, we consider the two cases of including only the angles of exceedances of the sampled quantile sets $\mathcal{Q}_{q_k, i}$ and including all observed angles $(\mathbf{w}_1, \dots, \mathbf{w}_n)$ in the model likelihood. Figure 15 provides a comparison of the posterior predictive density of angles $\pi[\mathbf{W} \mid \mathcal{G}, \mathcal{L}, \mathbf{y}]$ output by models M_1 , M_2 , and M_3 fitted on samples of sizes n_1 and n_2 from a multivariate Laplace distribution in Laplace margins. As discussed in Section 2.4, the marginal density of angles for the multivariate Laplace distribution is known exactly given the homothetic structure of its density with respect to its gauge function $g_{\mathcal{G}}$. This allows for validation of the performance of M_1 , M_2 , and M_3 . It is clear from Figure 15 that all three models recover the true or the empirical marginal density of angles of the multivariate Laplace distribution well. As expected, including all angles in the fitting procedure and increasing the sample size both lead to reduction in the uncertainty of the posterior predictive density $\pi[\mathbf{W} \mid \mathcal{G}, \mathcal{L}, \mathbf{y}]$.

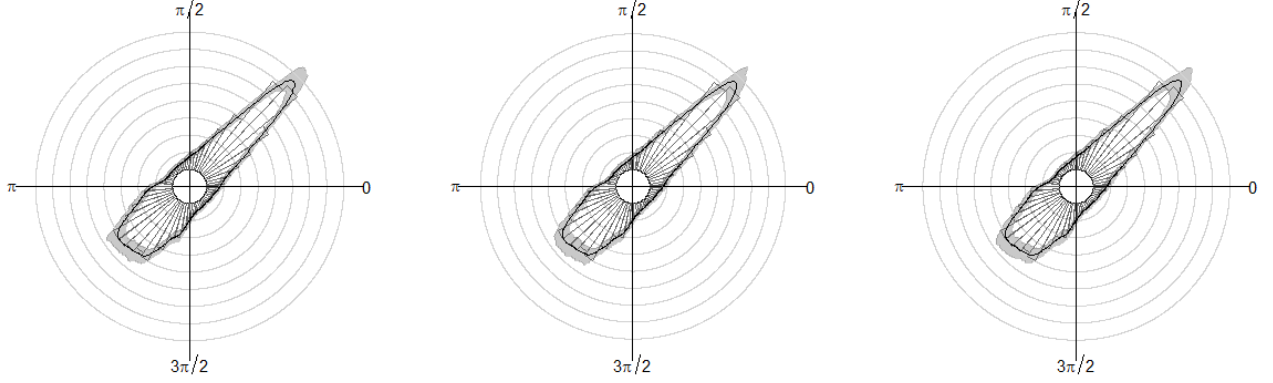


Figure 16: Histogram of the angles $\{\varphi_j \in [0, 2\pi] : \mathbf{w}_j = (\cos \varphi_j, \sin \varphi_j), j = 1, \dots, n_2\}$ of n_2 draws from a bivariate max-stable logistic distribution, with angle-wise posterior mean (black line) and 0.95 prediction intervals (grey) for the marginal distribution of angles $\pi[\mathbf{W} \mid \mathcal{G}, \mathcal{L}, \mathbf{y}]$. From left to right: outputs of M_1 , M_2 , and M_3 .

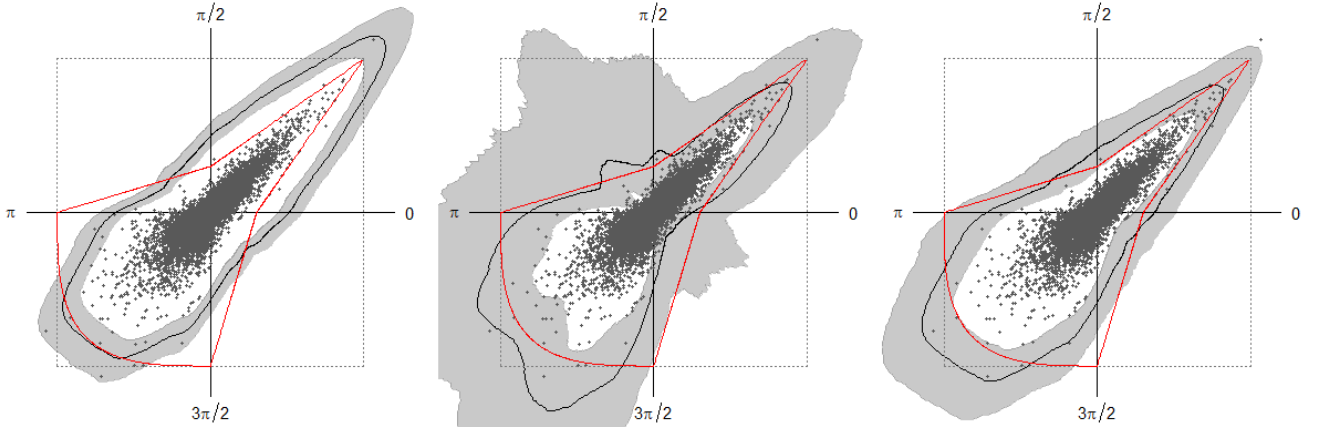


Figure 17: Estimated limit sets from n_2 draws from a scaled bivariate max-stable logistic distribution, with posterior mean (black line), 0.95 prediction interval (grey), and true limit set (red line). From left to right: outputs of M_1 , M_2 , and M_3 .

The max-stable logistic distribution is an instance of family of distributions for which M_2 is known to be a wrong model for the marginal density of the angles. However, it is observed from Figure 16—

which displays the mean of the posterior predictive density $\pi[\mathbf{W} \mid \mathcal{G}, \mathcal{L}, \mathbf{y}]$ as well as its 0.95 prediction interval—that all three models possess the ability to capture the empirical distribution of angles when incorporating all sampled angles in the model likelihood. Figure 17 depicts some consequences of this. When the number of data used to fit $\pi[\mathbf{W} \mid \mathcal{G}, \mathcal{L}, \mathbf{y}]$ is greater than the number of exceedances of \mathcal{Q}_{q_k} , the posterior distribution of the gauge function $g_{\mathcal{G}}$ obtained from M_2 is allowed to over-fit to the angular component of the model. This generates bias and over-confidence in the posterior distribution of the gauge function $g_{\mathcal{G}}$ and of its associated limit boundary $\partial\mathcal{G}$. Under M_1 , the decoupling of the dependence of the density of angles $\pi[\mathbf{W} \mid \mathcal{G}, \mathcal{L}, \mathbf{y}]$ on the gauge function $g_{\mathcal{G}}$ (so that $\pi[\mathbf{W} \mid \mathcal{G}, \mathcal{L}, \mathbf{y}] = \pi[\mathbf{W} \mid \mathbf{y}]$) is expected to remove potential bias in $g_{\mathcal{G}}$ coming from the observed angles. A clear consequence, however, is the increase in the variance of the posterior distribution of $g_{\mathcal{G}}$.

Figure 18 provides, for each of the modelling choices detailed in the beginning of this Section, a boxplot of the mean of the mean integrated square distance (MISD) from each realisation of the posterior of $\partial\mathcal{G}$. Model M_3 , in all cases, seems to be the best—or approximately as valid as the best—model in terms of MISD. Figure 19 presents the angle-wise mean of the posterior distribution of the limit boundaries $\partial\mathcal{G}$

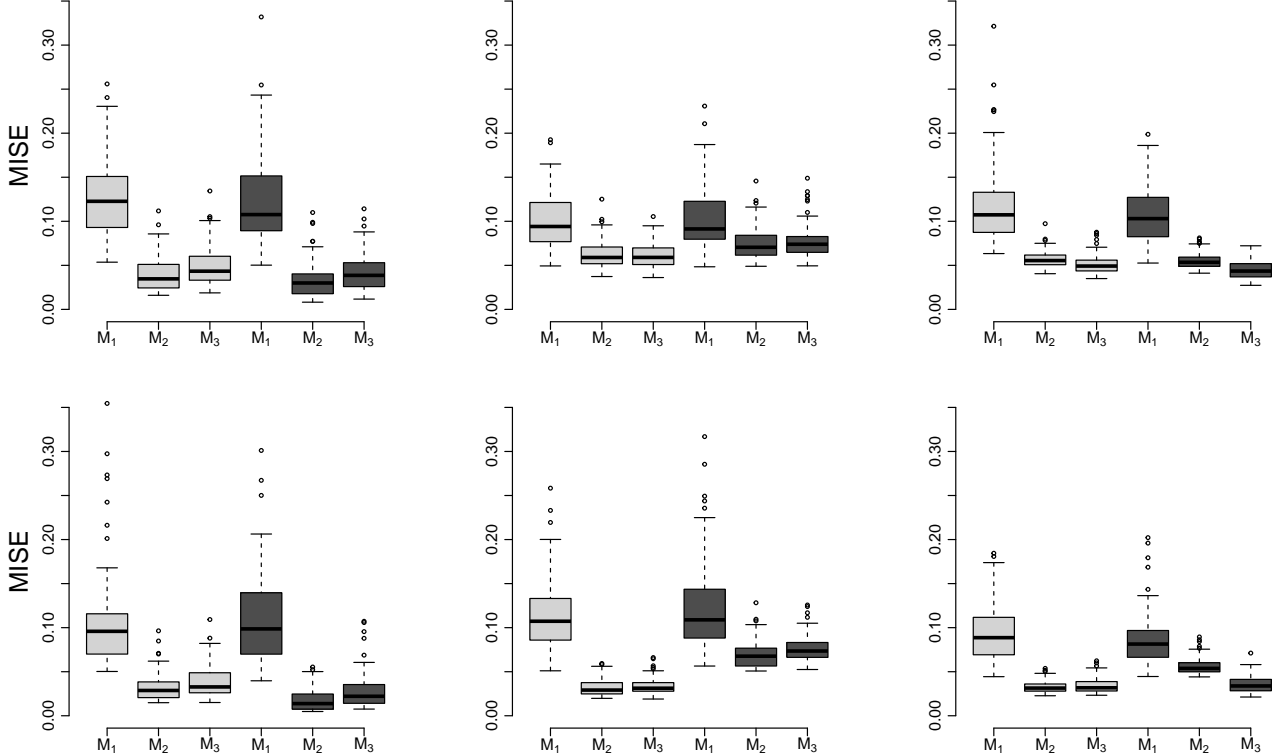


Figure 18: Boxplots of the means of the mean integrated squared error (MISE) from each posterior realisations of $\partial\mathcal{G}$ from each of the 600 samples to the true limit sets. From top to bottom rows: n_1 , n_2 . From left to right columns: Bivariate Laplace, normal, and max-stable logistic distributions. Within panels: Results for models M_1 , M_2 , and M_3 using only angles of exceedances (light grey) and using all angles (dark grey).

estimated from M_3 with the associated 0.95 prediction interval. As expected, increasing the sample size decreases uncertainty in the estimated limit boundaries. One may also infer that when it is reasonable to assume that observed extremes come from the same data generating mechanism as all other observations, including all sampled angles into the likelihood provides smoother estimates of $\partial\mathcal{G}$ than a procedure using only the exceedances of \mathcal{Q}_{q_k} . We argue that while there may be valid reasons to select M_1 or M_2 —respectively for evidence of a homothetic data generating mechanism or of a poor matching between

the density of angles $\pi[\mathbf{W} \mid \mathcal{G}, \mathcal{L}, \mathbf{y}]$ and the homothetic density $\mathcal{G}^d/|\mathcal{G}^d|$ —, M_3 generally provides a better-behaved and more balanced choice.

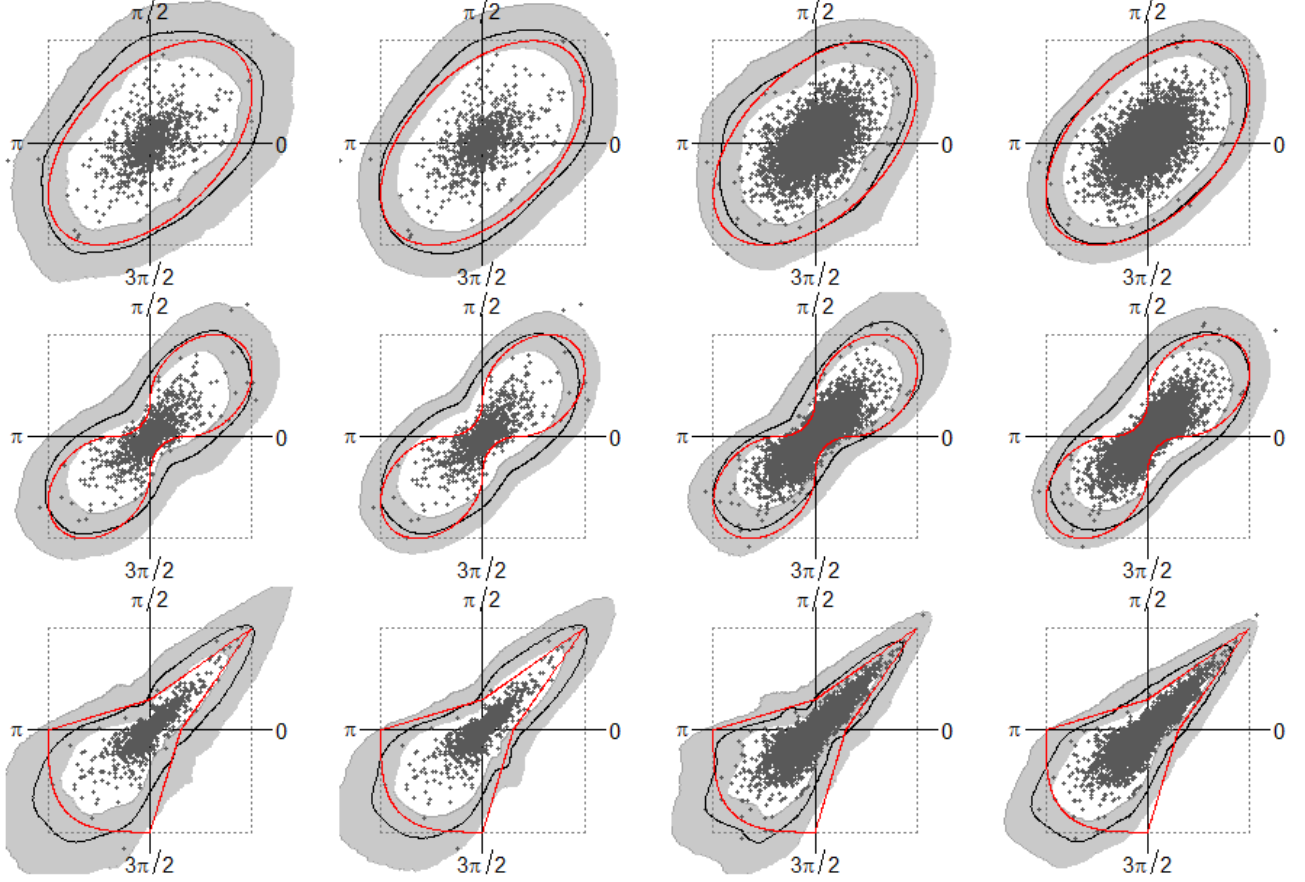


Figure 19: Limit set estimated from samples of size n by M_3 via the posterior mean of $\partial\mathcal{G}$ (black line) and 0.95 prediction interval (grey bands) with true limit set (red line) and unit square (dotted grey). Rows from top to bottom rows: Draws from the bivariate normal, max stable logistic, and multivariate Laplace distributions. Columns from left to right: M_3 fitted only exceedances of $r_{Q_{0.8}}$ (sample size n_1), M_3 fitted using all angles (sample size n_1), M_3 fitted only exceedances of $r_{Q_{0.98}}$ (sample size n_2), M_3 fitted using all angles (sample size n_2).

D.3 Estimating rare event probabilities

Based on the results of Figures 18 and 19, we carry the remainder of this simulation study under the framework of model M_3 and use all observed angles for the cases of the bivariate Laplace and max-stable logistic distributions and only those of exceedances of Q_{q_k} for the bivariate normal distribution. For each of the 600 samples defined in Section D.2, we obtain realisations from the posterior distribution of $\mathbb{P}_{B_i|\mathbf{y}}$ according to the procedure described in Section 3.4 to estimate the probability that a new observation $R\mathbf{W}$ falls within extreme sets B_1 , B_2 , and B_3 as defined in Figure 20. Figure 21 displays boxplots of the log-mean of the realisations from the posterior predictive distribution of each set B_i and each sample. It is clear that the mean of predictive posterior distribution is well-behaved for the sets B_i corresponding to angular subsets of \mathbb{S} where the posterior distribution of the limit sets presented in Section D.2 is itself well-behaved. Table 2 details the coverage obtained from 100 samples for the probability that a new observation $R\mathbf{W}$ falls within the sets B_1 , B_2 , and B_3 based on 0.95 prediction intervals based on the quantile method for the posterior predictive distributions. The coverage properties of the prediction intervals seem to be satisfying, except for the set B_2 where the true probability is on the order of 10^{-16} .

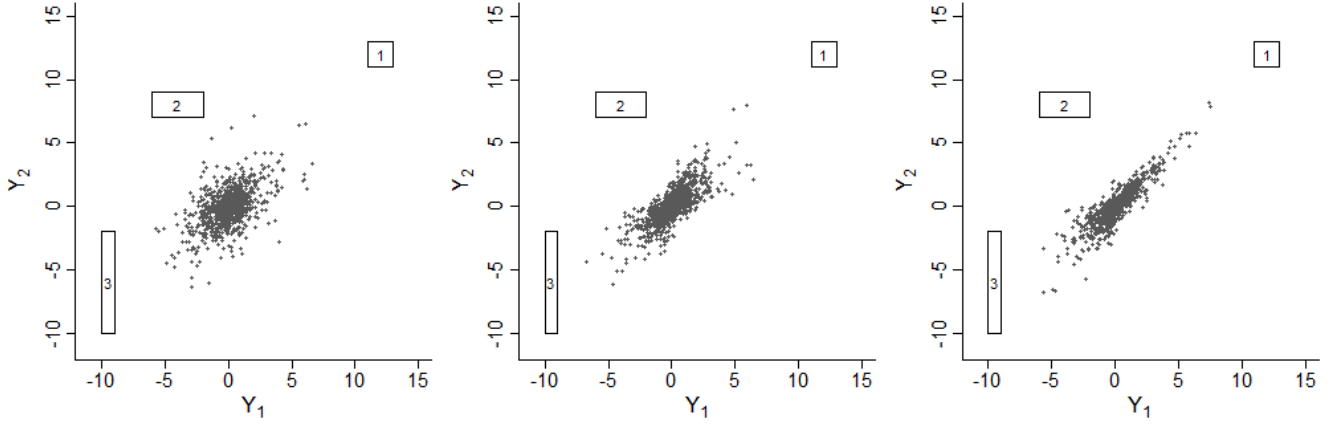


Figure 20: Regions $B_1 = [11, 13] \times [11, 13]$, $B_2 = [-6, -2] \times [7, 9]$, and $B_3 = [-10, -9] \times [-2, -10]$ for probability estimation superposed with samples of size n_1 for the Gaussian (left), logistic (centre), and multivariate Laplace (right) distributions in Laplace margins.

and 10^{-14} for the bivariate normal and max-stable logistic distributions respectively. We again note that these correspond to regions in which the posterior distributions of r_G are biased in the case of the bivariate normal distribution. We argue that reasonable coverage properties are obtained in other cases.

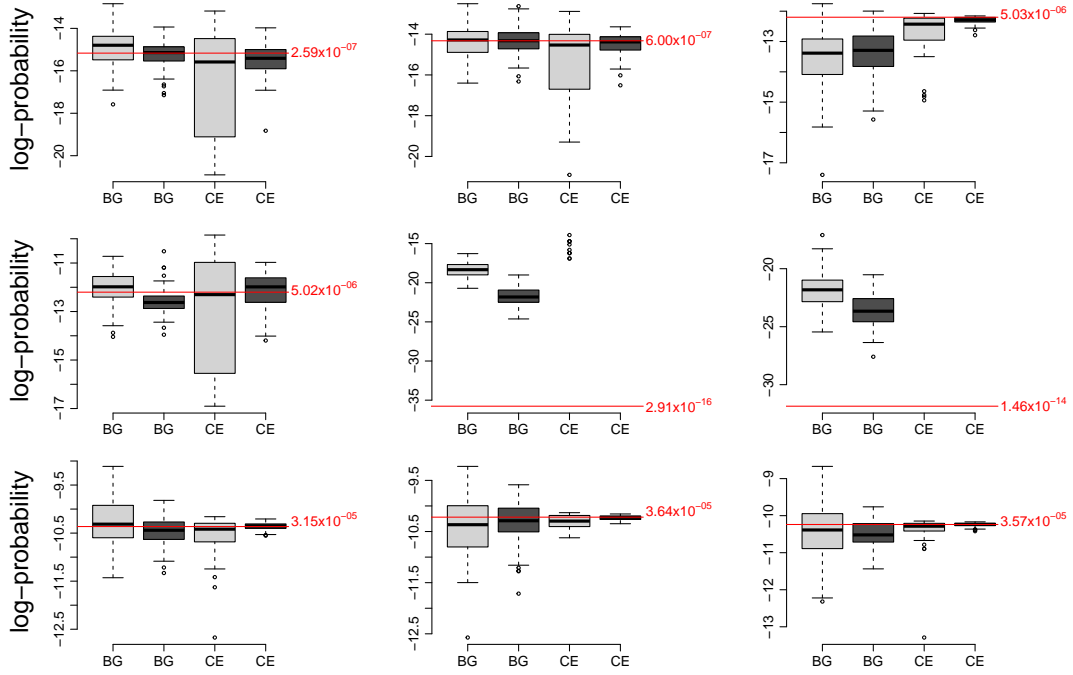


Figure 21: Boxplots of 100 log-means of posterior predictive samples for regions B_i . Panels from left to right: Output of M_3 fitted on draws from the bivariate Laplace, Gaussian, and max-stable logistic distributions in Laplace margins. Panels from top to bottom: $\log \mathbb{P}_{B_1|\mathbf{y}}$, $\log \mathbb{P}_{B_2|\mathbf{y}}$, and $\log \mathbb{P}_{B_3|\mathbf{y}}$. Within panels, light grey: sample size n_1 , dark grey: sample size n_2 .

Bivariate distribution	Laplace		Normal		Max-stable logistic	
n	1000	10000	1000	10000	1000	10000
Coverage for $\mathbb{P}_{B_1 \mathbf{y}}$	0.97	0.94	0.99	0.97	0.56	0.57
Coverage for $\mathbb{P}_{B_2 \mathbf{y}}$	0.96	0.88	0.13	0.70	0.89	0.85
Coverage for $\mathbb{P}_{B_2 \mathbf{y}}$	0.98	0.97	0.97	0.94	0.92	0.92

Table 2: Coverage study of the 0.95 prediction intervals from the posterior predictive distribution $\mathbb{P}_{B_i|\mathbf{y}}$ for the bivariate Laplace, normal, and max-stable logistic distributions.

D.4 Return sets

We obtain realisations from the posterior distribution of the radial function of the return set $\mathcal{Q}_{1-1/T}$ using equation (33) on each realisation from the posterior distribution of the radial functions of \mathcal{Q}_q and \mathcal{G} . The angle-wise posterior mean of $r_{\mathcal{Q}_{1-1/T}}$ hence defines a the boundary of a return set with period T as well as its associated 0.95 simultaneous prediction interval. Figure 22 displays canonical return boundaries and return sets of period $T \in \{100, 1000, 10000\}$ estimated from one sample of n_2 draws from the bivariate Laplace, normal, and max-stable logistic distributions.

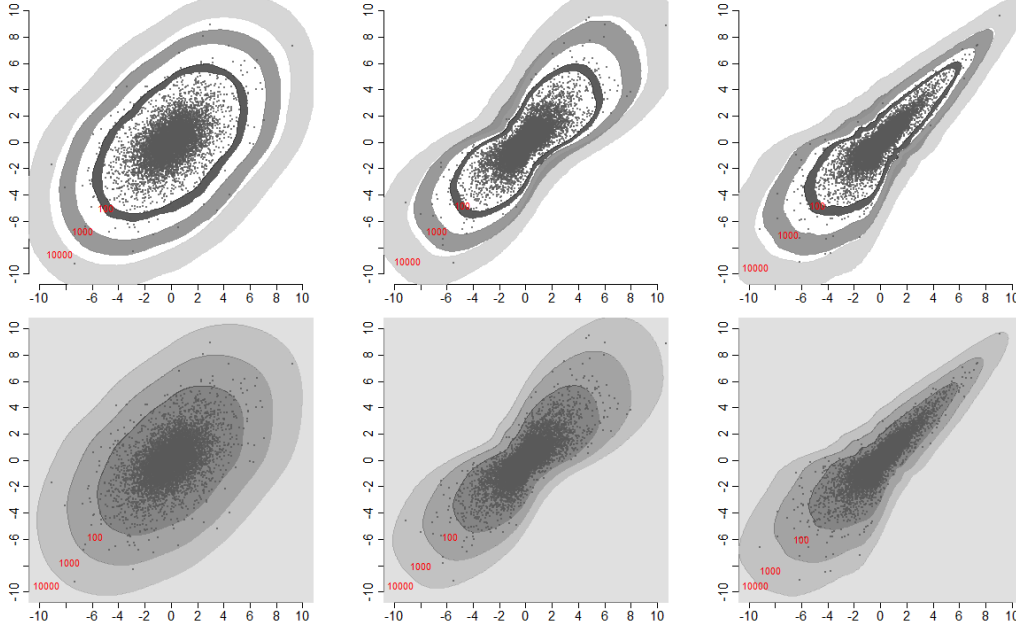


Figure 22: Top row: 0.95 prediction intervals for the boundaries $r_{\mathcal{Q}_{1-1/T}}$ of the canonical return sets with associated return period T displayed in red. Bottom row: Posterior mean of the return sets with associated return period (red) defined by the angle-wise posterior mean of $r_{\mathcal{Q}_{1-1/T}}$. Every return set contains all lighter-grey sets. Columns from left to right: Bivariate Laplace, normal, and max-stable logistic distributions in Laplace margins.

D.5 Estimation of extremal coefficients

Figure 23 displays boxplots of the means of the samples from the posterior distribution of α_1 obtained from both estimation procedures on each of the 600 samples. Table 3 presents a coverage study of the 0.95 credible intervals for α_1 .

Instances of transformed $r_{\mathcal{G}_T}$ are displayed in Figure 24. As can be observed, the transformation does

Bivariate distribution	Laplace		Normal		Max-stable	
n	1000	10000	1000	10000	1000	10000
Coverage for $\alpha_{ 1}$, Method 1	1.00	1.00	1.00	1.00	0.80	0.64
Coverage for $\alpha_{ 1}$, Method 2	1.00	1.00	1.00	1.00	0.73	0.49

Table 3: Coverage study of the 0.95 credible intervals from the posterior distribution of $\alpha_{|1}$ under both estimation methods for the bivariate Laplace, normal, and max-stable logistic distributions.

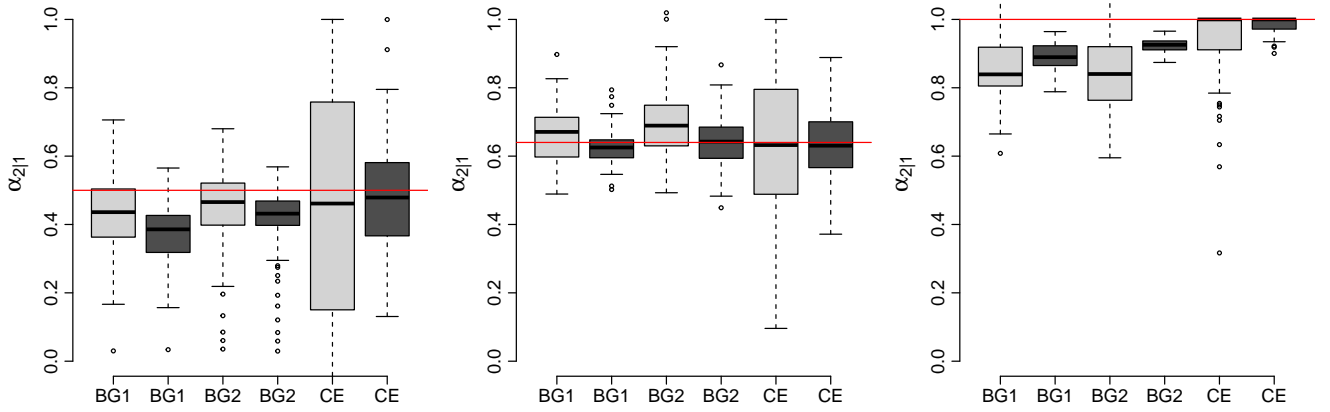


Figure 23: Boxplots of 100 means of realisations from the posterior of $\alpha_{2|1}$. Columns from left to right: Output of M_3 fitted on draws from the bivariate Laplace, Gaussian, and logistic distributions in Laplace margins. Within panels, 1: method 1 and n_1 , 2: method 2 and n_1 , 1: method 1 and n_2 , 2: method 2 and n_2 . The true values of $\alpha_{|1}$ are given by the red line.

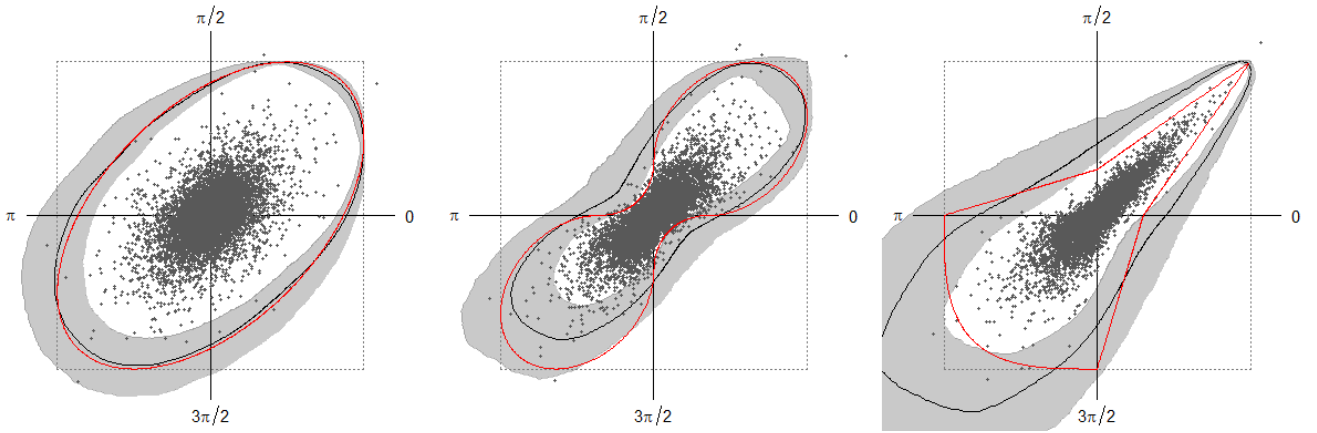


Figure 24: Posterior mean (black line) and associated 0.95 prediction bands (grey) for the transformed posterior distribution r_{G_T} of the bivariate Laplace (left), normal (centre), and max-stable logistic (right) distributions with true limit set (red line).

not lead to a posterior $r_{\mathcal{G}_T}$ that respects the limit boundary conditions everywhere, but it is better-behaved in the angular region between the angles $\mathbf{w}^{(1)}$ and $\mathbf{w}^{(2)}$. The improvement in the estimation of η through this transformation procedure is observed in the results of the simulation study. Figure 25 contains boxplots of the posterior means and 0.95 prediction intervals for η resulting from $\partial\mathcal{G}$ and $\partial\mathcal{G}_T$. Table 4 presents a coverage study of the 0.95 credible intervals for η . We argue that our model, especially under the consideration of the transformed $\partial\mathcal{G}_T$, can provide meaningful estimates of η .

Bivariate distribution	Laplace		Normal		Max-stable logistic	
n	1000	10000	1000	10000	1000	10000
Coverage for η , Method 1	0.93	0.97	1.00	0.98	0.95	0.85
Coverage for η , Method 2	0.95	0.96	1.00	1.00	0.99	0.67

Table 4: Coverage study of the 0.95 credible intervals from the posterior distribution of η under both estimation methods for the bivariate Laplace, normal, and max-stable logistic distributions.

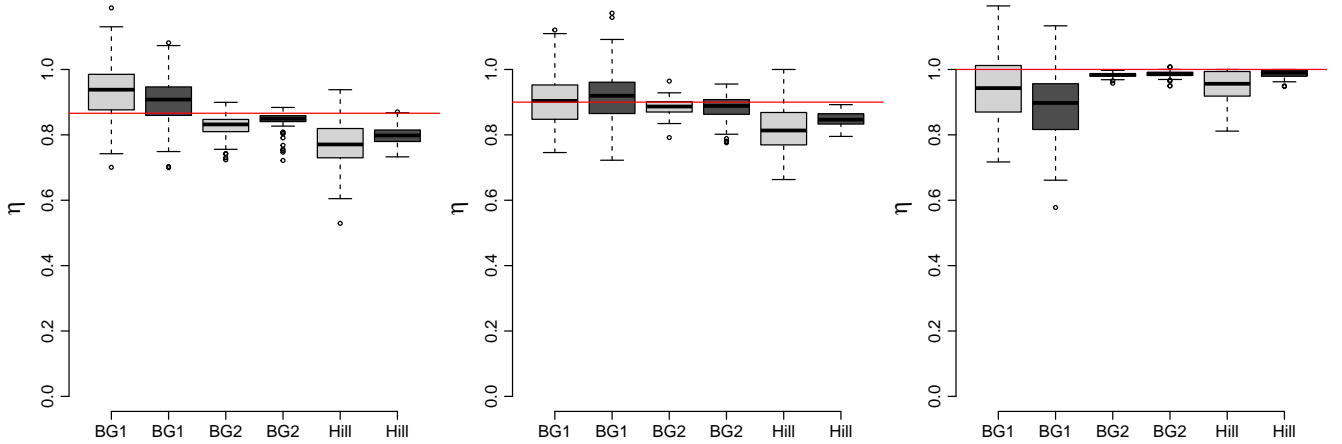
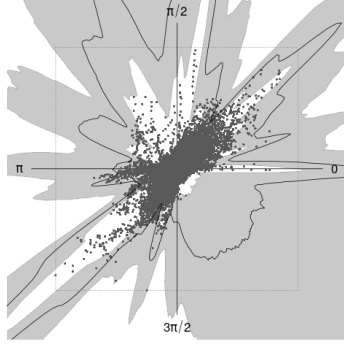


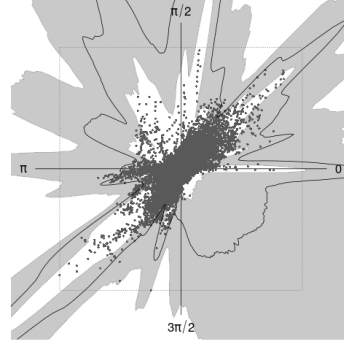
Figure 25: Boxplots of 100 means of posterior predictive samples for η . Panels from left to right: Draws from the bivariate Laplace, Gaussian, and logistic distributions in Laplace margins. Within panels, 1: method 1, 2: method 2. The true values of η are given by the red line.

E Supplementary material E

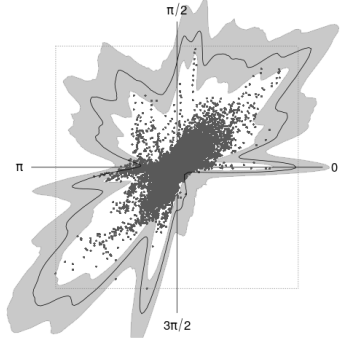
E.1 Posterior model fits on river data



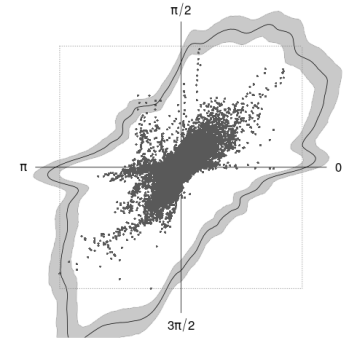
(a) M_1 , exc. only



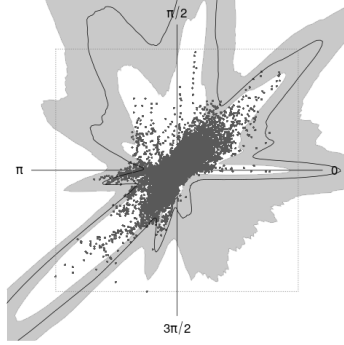
(b) M_1 , all angles



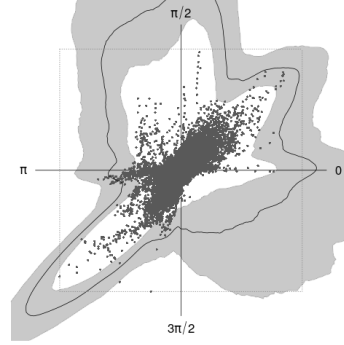
(c) M_2 , exc. only



(d) M_2 , all angles

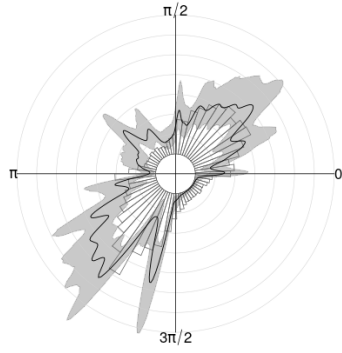


(e) M_3 , exc. only

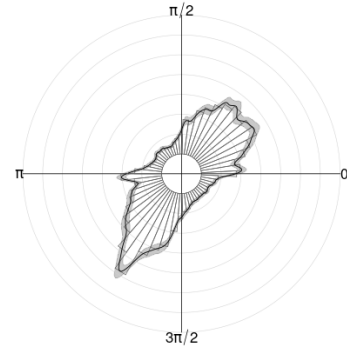


(f) M_3 , all angles

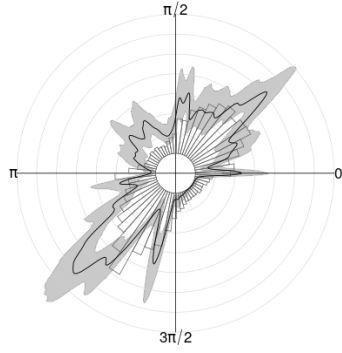
Figure 26: Posterior estimates of the unit level set $g_{\mathcal{G}}(\mathbf{x}) = 1$ for the river flow dataset. The black line corresponds to the posterior mean, with the 0.95 prediction interval shaded in grey. Black points are the original data in Laplace margins scaled by $\log(n/2)$. Dashed border line is the unit box. M_1 , M_2 , and M_3 define the angle density kernel, as described in section 3.3.



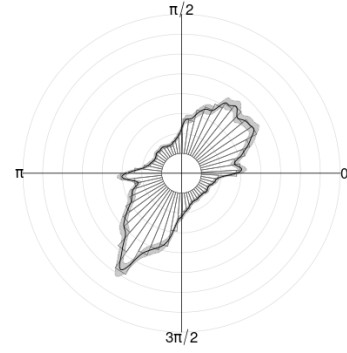
(a) M_1 , exc. only



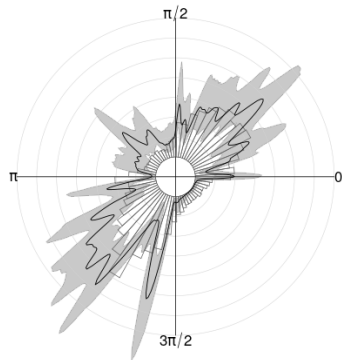
(b) M_1 , all angles



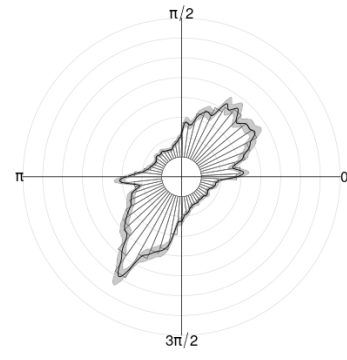
(c) M_2 , exc. only



(d) M_2 , all angles



(e) M_3 , exc. only



(f) M_3 , all angles

Figure 27: Posterior estimates of the mean angle density for the river flow dataset. The empirical density of angles is given by the underlying histogram. M_1 , M_2 , and M_3 define the angle density kernel, as described in section 3.3.

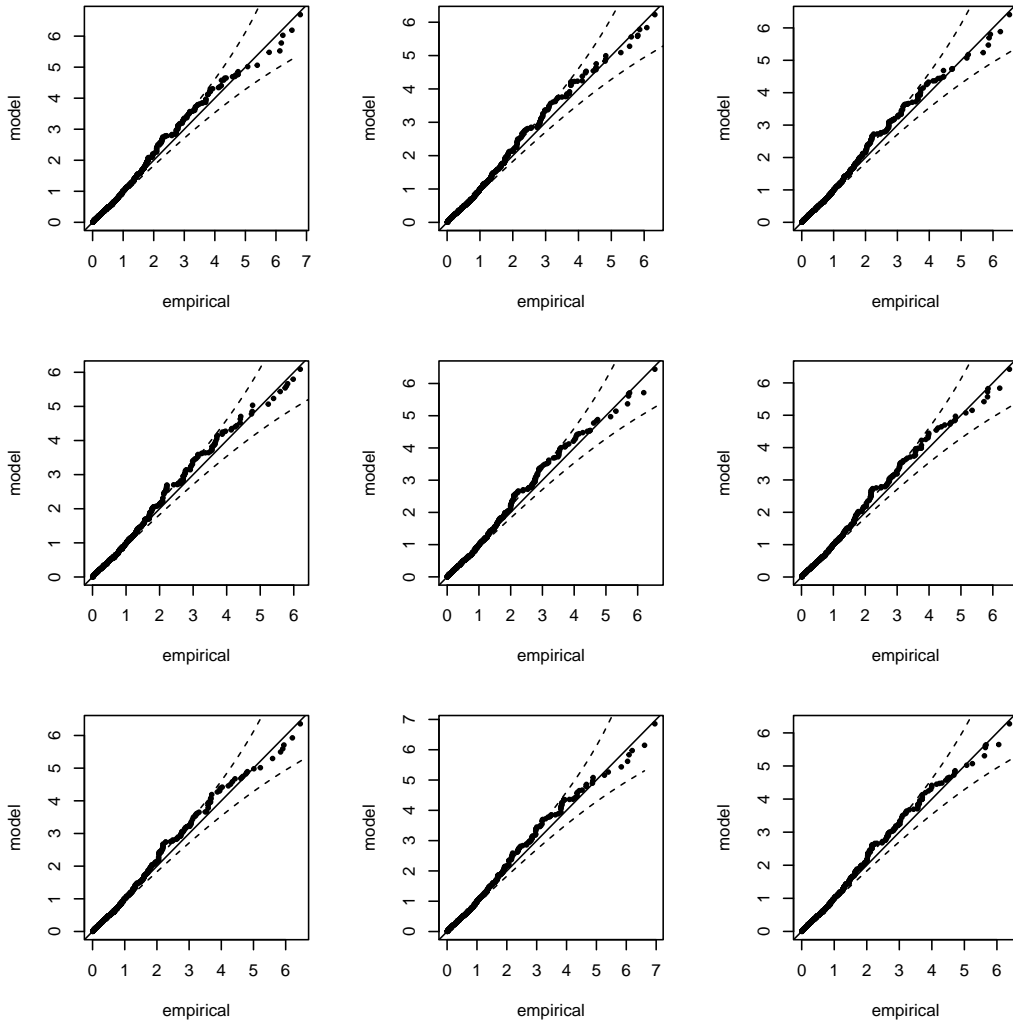


Figure 28: QQ plots for the Thames tributary river flow dataset exceedance model for 9 sampled posterior thresholds $r_{Q_q}(\mathbf{w})$, with 95% confidence intervals.

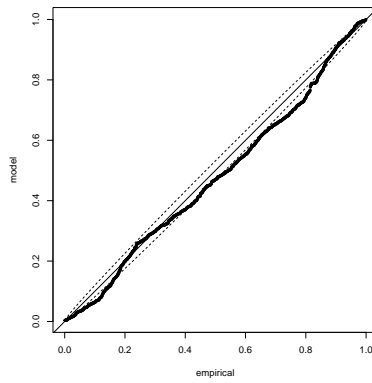


Figure 29: PP plots for the Thames tributary river flow dataset exceedance model, with 95% confidence intervals.

E.2 Posterior model fits on wave data

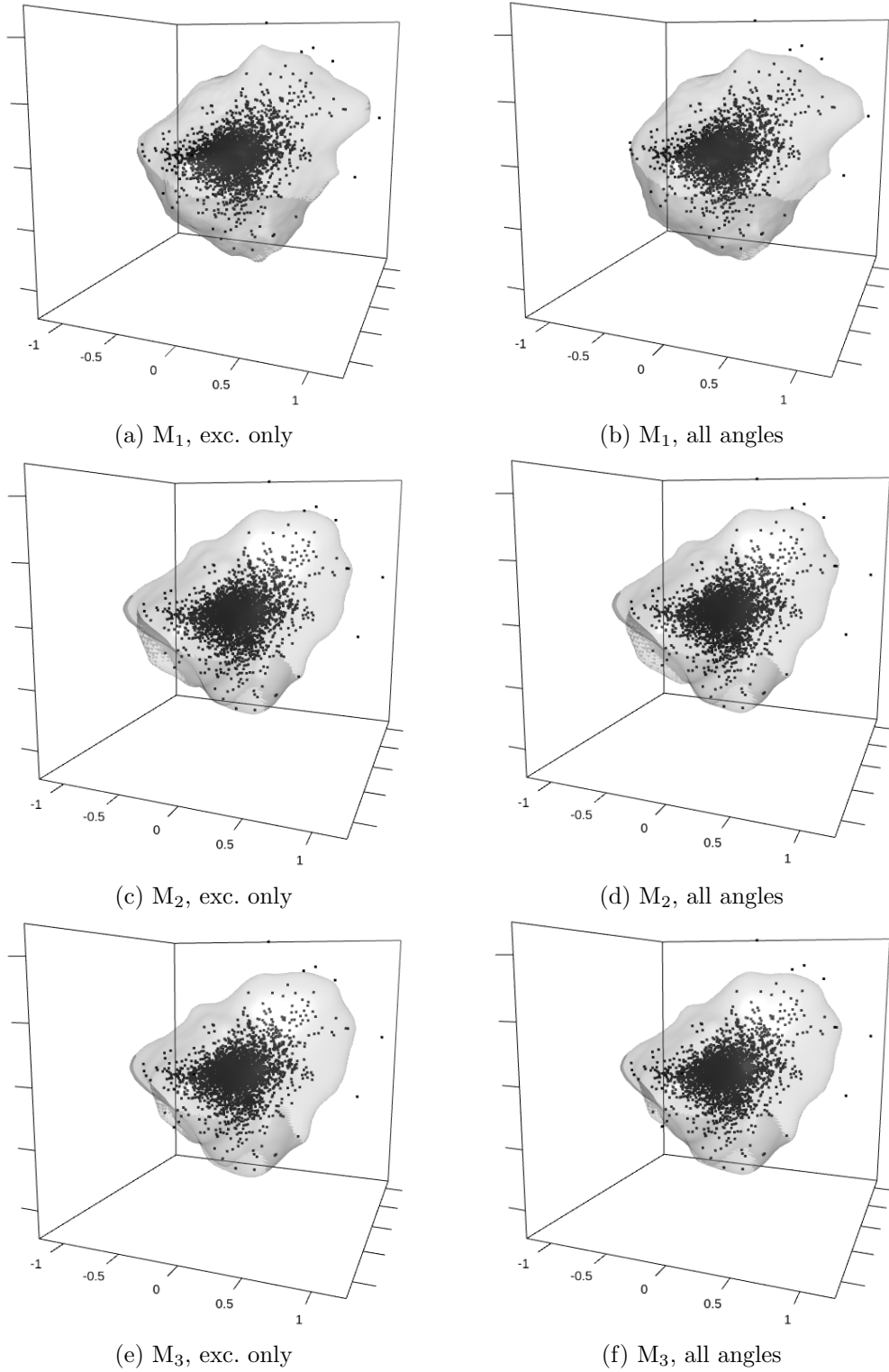


Figure 30: Posterior mean estimates of the unit level set $g_{\mathcal{G}}(\mathbf{x}) = 1$ for the wave dataset. Black points are the original data in Laplace margins scaled by $\log(n/2)$. M_1 , M_2 , and M_3 define the angle density kernel, as described in section 3.3.

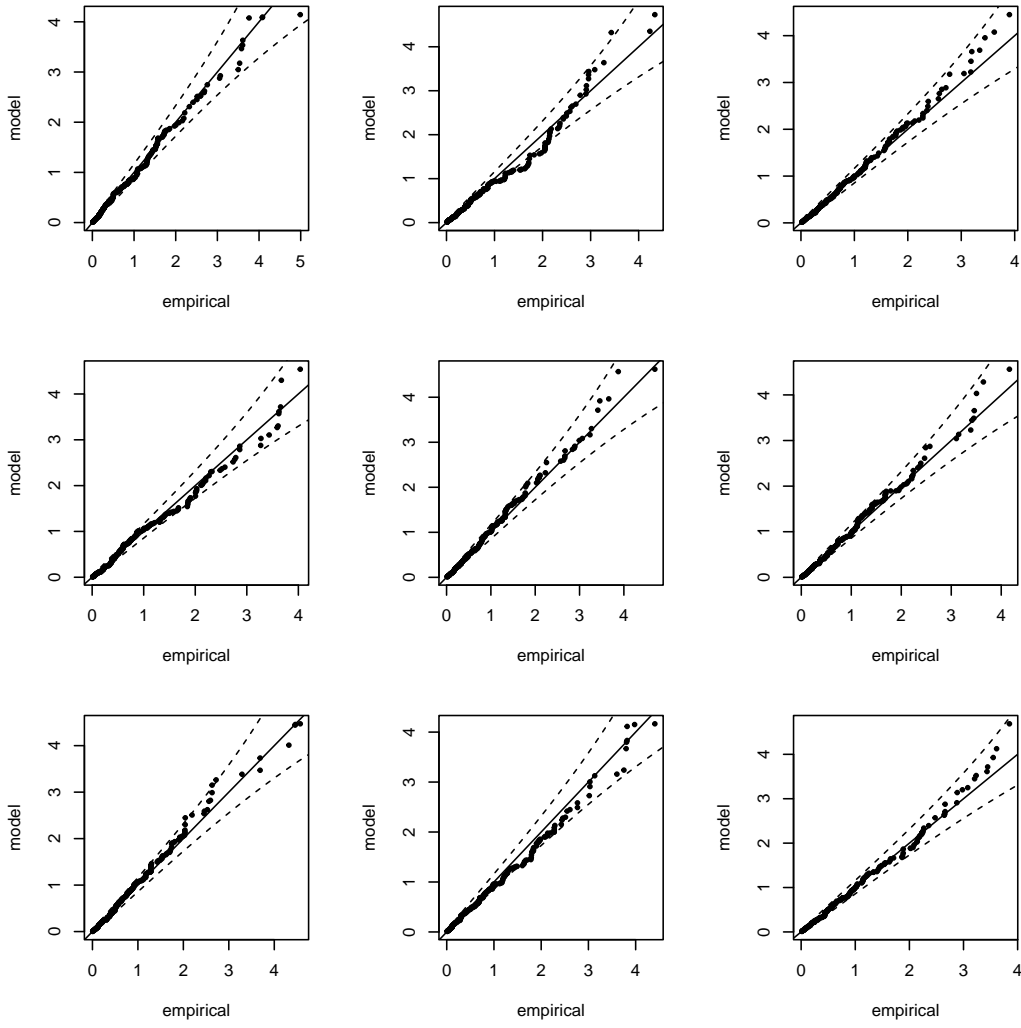


Figure 31: QQ plots for the Newlyn wave dataset exceedance model for 9 sampled posterior thresholds $r_{Q_q}(\mathbf{w})$, with 95% confidence intervals.

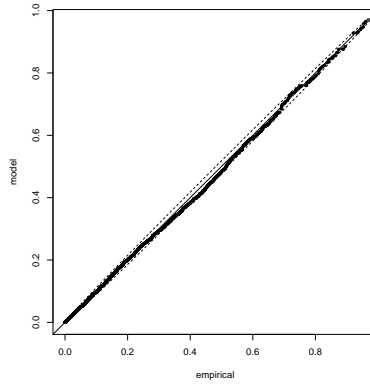


Figure 32: PP plots for the Newlyn wave dataset angle model for 9 sampled posterior thresholds $r_{Q_q}(\mathbf{w})$, with 95% confidence intervals.